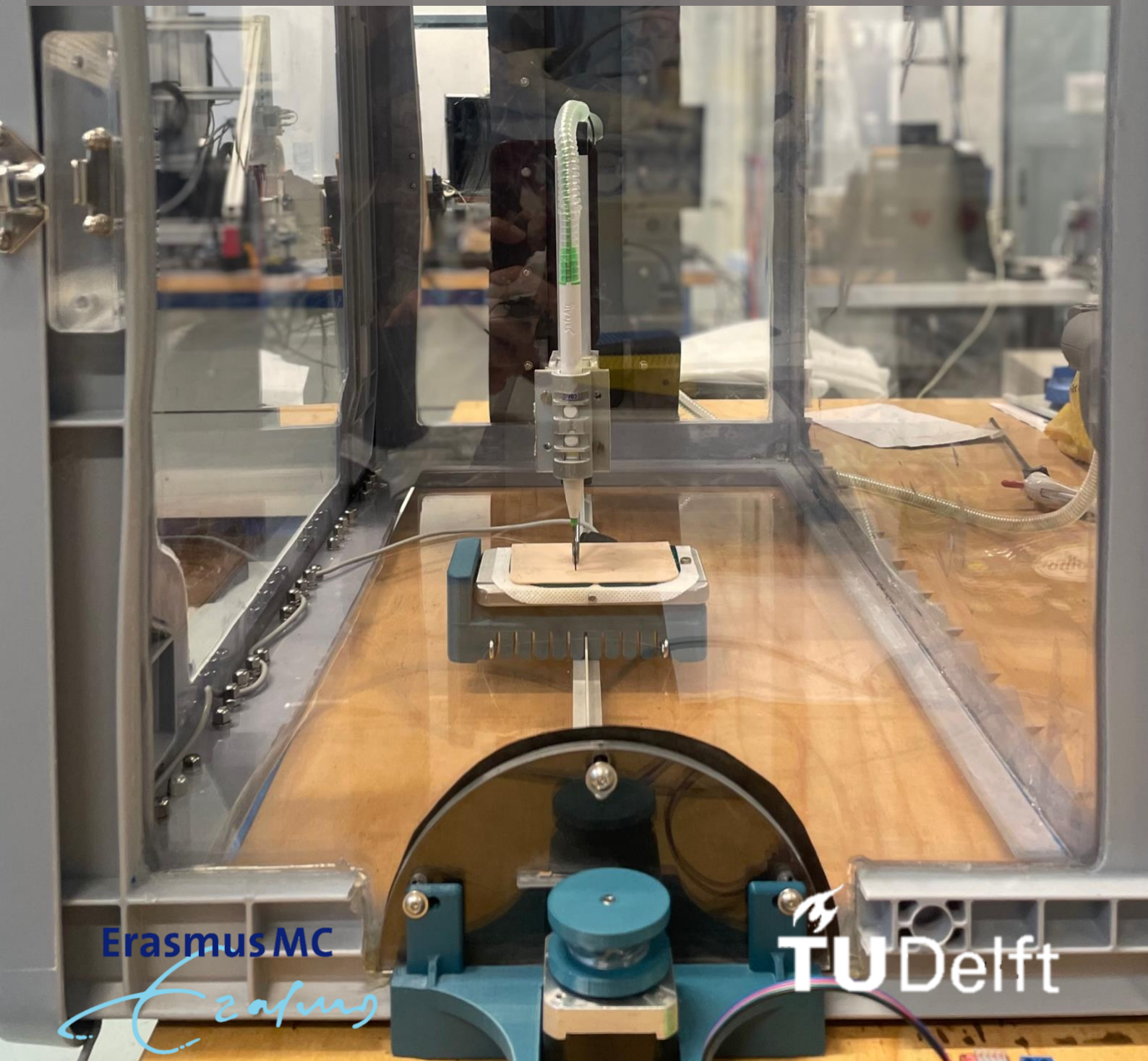




Aerosol production via electro and plasma devices:
In-vitro PlasmaJet and ERBE tissue effects and aerosol
production affecting factors evaluation

Defne Unal



Aerosol production via electro and plasma devices: In-vitro, PlasmaJet and ERBE tissue effects and aerosol production affecting factors evaluation

Master Thesis

By

Defne Unal

In partial fulfilment of the requirements for the degree of

Master of Science
in BioMedical engineering
Medical Devices (track)

At the Delft University of Technology
To be defended publicly on the 29th of August, 2023 at 1:45 PM

Student number: 5539412

Thesis committee: dr. ir. Arjo J. Loeve,
dr. ir. Nick J. van de Berg,

TU Delft, Dept. BioMechanical Engineering
TU Delft, Dept. BioMechanical Engineering



Preface

This master's thesis is the representation of a collaborative effort between the Delft University of Technology and the Erasmus MC. During this project, I have enriched my biomedical knowledge and gained invaluable insights in the realm of medical design, prototyping, experimenting, and analysis. Undertaking this assignment has provided me necessary skills to navigate complex problems and confront obstacles while leading a project independently.

I wouldn't be able to complete this thesis without the help and support of others. Therefore, I would like to express my sincere gratitude to my supervisors Arjo Loeve and Nick van de Berg for granting me this opportunity, for their valuable feedback and guidance, their trust in me, and their quick replies to my spamming emails. I would like to thank the 3ME workshop for always being patient and responsive to my never-ending questions, for lending additional parts, and for helping me to print my test setup parts. Additionally, I would like to thank Ziad Ashqar, Zeynep Ileri, and Ines Menezes for being the best study buddies and for their valuable friendship. I would like to thank the MISIT department, especially Anna Graell Collado and Thomas Anker for their assistance during the entire process and for providing such a joyful and comfortable working environment. I would like to thank Ataberk Ozsoy for his mental support and for making me smile especially during the most challenging aspects of the project. Lastly, I am grateful for my family that always supported and believed in me during this journey.

I am looking forward to the public defense on 29th August 2023 at 1:45 PM.

Defne Unal

Delft, August 20, 2023

Abstract

Surgical aerosols in other words plumes are produced during thermal tissue destruction in medical operations. The cellular debris in the form of particulate matter may contain viruses and harmful chemical compounds which can lead to an infectious transmission in case of inhalation.

The goal of this study was to design and produce an experimental setup to simulate Plasmajet (PJ) and ERBE experiments with minimal airflow disturbances. Such setup can lead to defining the lowest aerosol production conditions, investigating the production-affecting factors, and evaluating tissue effects to promote a safer and healthier surgical environment for both healthcare workers and patients. A clear correlation between the aerosol production affecting factors and particle counts was established for particle sizes 0.3, 0.5, 1.0, 2.0, 5.0, and 10.0 μm .

The results of the experiments showed that among all experimental conditions, the PJ coagulation mode with fast operation yielded the lowest aerosol counts. In cutting mode, the lowest aerosol counts were also produced by PJ with fast operation speed. However, between speed and aerosol counts, no statistically significant correlation was found.

Upon analyzing the correlation between aerosol counts and tissue effects, it was determined that, for ERBE device, higher aerosol counts were associated with darker tissue effects. In the case of the PJ device, this relationship persisted in the cutting mode, whereas no connection between tissue effect and particle counts was observed in the coagulation mode.

Further investigation on the toxicity of the produced particulate matter and establishment of a clear minimal aerosol intake is recommended. Until then, preventive measures such as implementing local exhaust ventilation and using surgical N95 masks are strongly advised to minimize aerosol inhalation.

Nomenclature

Airway: Part of the respiratory tract through which air passes during breathing.

Arduino UNO: An open-source microcontroller board based on the microcontroller ATmega328P.

CNC shield: An Arduino extension to provide the necessary power to drive stepper motors and contribute to CNC machine operation.

Gas chromatography: An analytical technique applicable to gas, liquid, and solid samples by injecting the sample into a mobile phase to separate and analyze compounds.

Local exhaust ventilation (LEV): A system designed to reduce airborne contaminants by capturing the emission at the source.

Maillard reaction: A chemical reaction between amino acids and reducing sugars that gives a browned food, such as grilling or searing

Oropharyngeal wall: The middle part of the throat, behind the mouth.

Pathogen: An organism causing disease to its host.

Pulmonary parenchyma: A large collection of thin-walled alveoli forming a gas-exchanging unit.

Tissue fragments: A small piece or part of the tissue separated from the whole.

Ultra-performance liquid chromatography (UPLC): A technique used to separate and identify different constituents of a compound.

Universal Gcode Sender (UGS): A self-contained Java application that includes all external dependencies to motion control via Arduino.

Volatile organic compound: A large group of chemicals that are emitted into the air from products or processes. Some are known to be highly toxic.

Table of Contents

1	<i>Introduction</i>	1
1.1	Surgical aerosols.....	1
1.2	Study objective	2
1.3	Research question	3
1.4	Thesis outline	3
2	<i>Background on surgical smoke and experimental hypothesis</i>	4
2.1	Aerosol production affecting factors	4
2.1.1	Findings and the research gap	4
2.2	Aerosol measurement affecting factors.....	4
2.2.1	Findings and the research gap.....	5
2.3	Hypothesis based on background information.....	5
3	<i>Design and production of the test setup</i>	6
3.1	Design requirements	6
3.2	Final design and production	7
3.2.1	Experimental box and particle counter	7
3.2.2	Automation.....	7
3.2.3	Test setup components and ERBE setup.....	9
3.2.4	ERBE device	9
3.2.5	Test setup components and PJ Setup	11
3.2.6	PJ Device.....	11
4	<i>Aerosol production via electro and plasma devices: Experimental methods</i>	12
4.1	Introduction.....	12
4.2	Experimental requirements	12
4.3	Materials and methods.....	13
4.3.1	Experimental conditions.....	13
4.3.2	Experimental protocol.....	14
4.3.3	Analysis protocol	15
5	<i>Aerosol production via electro and plasma devices: Results</i>	16
5.1	ERBE results	17
5.2	PJ results.....	20
5.3	Comparative results	23
5.4	Tissue effects	23
6	<i>Discussion and recommendations</i>	25
7	<i>Conclusion</i>	28

<i>Bibliography</i>	29
<i>Appendix A – Design methodology, and design evaluation</i>	32
A.1 Background design	32
A.2 Design methodology.....	32
A.3 Design evaluation	34
<i>Appendix B – Experimental protocol</i>	35
B.1 List of Materials	35
B.2 Step-by-step protocol	35
<i>Appendix C – List randomization</i>	37
<i>Appendix D – Tissue effects</i>	39
D.1 ERBE experiments:.....	39
D.2 PJ Experiments:	41
D.3 Brightness values and particle counts of ERBE experiments:	44
D.4 Brightness values and particle counts of PJ experiments:	45
<i>Appendix E – Experimental data</i>	46
E.1 ERBE data of each repetition	46
E.2 PJ data of each repetition.....	48
<i>Appendix F – Technical drawings</i>	50
<i>Appendix G – Arduino and Gcode settings</i>	74

1

Introduction

1.1 Surgical aerosols

Surgical smoke, also called surgical aerosols or plumes, are airborne particles that are produced during thermal tissue destruction in medical operations. These particles can be dispersed in the operation area, and they are created with the use of medical devices such as plasma, electrocautery or electrosurgery, or with instruments such as ultrasonic scalpels, saws, or drills. Aerosols compose of 95% water vapor and 5% particulate matter with particle sizes $<5\mu\text{m}$ [1-3]. The cellular debris in the form of particulate matter may contain volatile organic compounds, blood and tissue fragments, bacteria, infectious pathogens, viruses, and harmful chemical compounds. Inhalation or skin absorption of airborne particles carries infectious transmission risks to healthcare workers and patients [4].

The potential hazards of surgical smoke are directly influenced by the particle size which determines the deposition of particles in the respiratory tract as shown in Figure 1.1. Aerosols with a diameter of $<5\mu\text{m}$ tend to be deposited on oropharyngeal walls while aerosols with a diameter of 2 to $5\mu\text{m}$ are delivered to airways and aerosols with a diameter between 0.8 to $3\mu\text{m}$ are able to reach pulmonary parenchyma [5]. Exposure to these particles can cause blood disorders, asthma, neurological effects, HPV and HIV transmission, coma, cardiac arrhythmias, cancer, and many more (see Figure 1.1) [4-7].

This study focuses on surgical aerosol production during electro and plasma surgeries, specifically on ERBE and PlasmaJet (PJ) devices. Electrosurgical devices use high-frequency electric currents (ohmic heating) for tissue lesion destruction [8,9] while plasma surgeries deliver neutral argon plasma, a highly energized gas, to the tissue to create kinetic and thermal tissue effects [10,11].

Electro and plasma surgical devices can be used in both minimally invasive and open surgeries. The establishment of electro and plasma surgery was revolutionary compared to the surgeries via traditional methods of scalpels and clips. The confronted difficulties during the use of traditional methods were bleeding control, difficulties in repeating the application, damage to surrounding tissues, and infection risk [12].

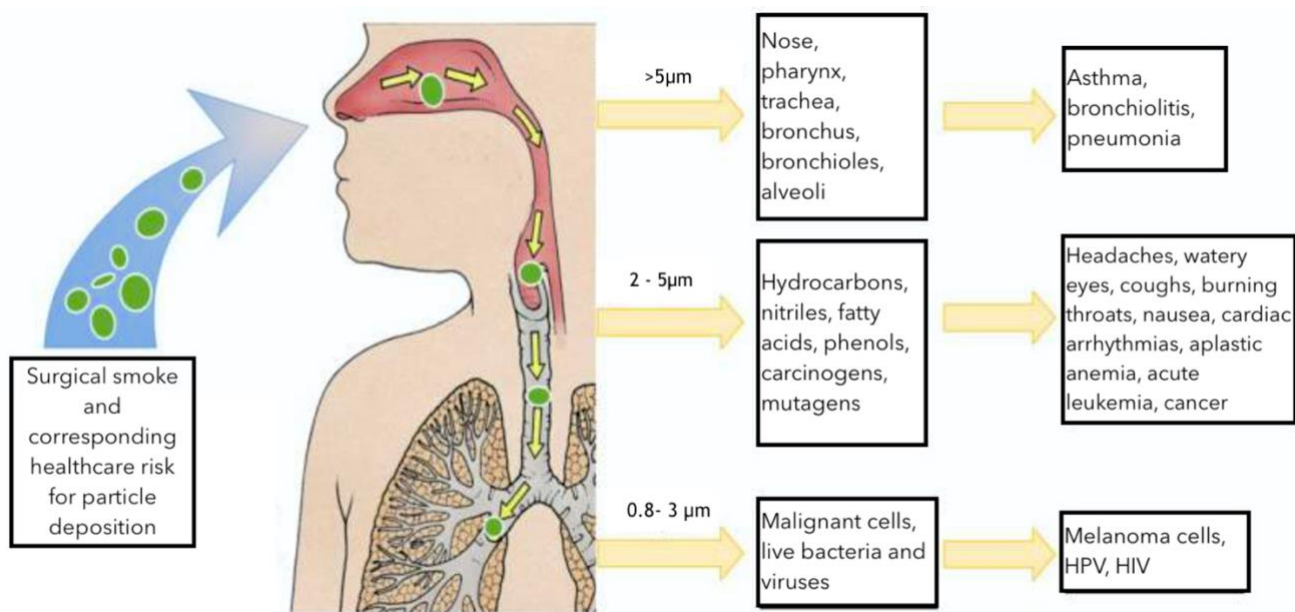


Figure 1.1 – The deposition of aerosols in the respiratory tract based on the particle size, and their corresponding health hazards. Adapted from [4].

Electro and plasma surgeries, on the other hand, provide precise tissue removal and operation on hard-to-reach areas. Compared to traditional methods, these devices can limit surrounding area damage, scarring, and bleeding [13-15]. Plasma surgeries are also able to provide non-contact tissue removal with minimized risk of damaging underlying organs [16]. However, it should be noted that electro and plasma surgical devices create thermal damage and produce surgical smoke. The safety of which is inadequately studied, and they are comparatively expensive in contrast to traditional methods of scalpels and clips [17].

The use of protection from the produced surgical smoke is essential to ensure safe operating conditions. The protectants such as surgical masks, smoke evacuation and ventilation systems, aspiration, and filtering systems have proved their effectiveness in aerosol elimination. However, these smoke protectors do not achieve 100% capture efficiency and analysis of production reductive factors is necessary [4,18].

A solution to reduce produced aerosols from electro and plasma surgeries could be the evaluation of aerosol production affecting factors by comparing different types of surgical devices, operation speed, exposure time, and mode.

1.2 Study objective

According to the conducted literature prior to this thesis, the prior findings provided the needed background information. The research gap based on the literature study showed, “Evaluation of aerosol production affecting factors, such as different kinds of surgical devices, operation speed, exposure time and mode, during electro and plasma surgeries is necessary to assess and provide guidance on safe and effective surgical practices. To define the safest and most effective operational environment, the interrelation between tissue effects and aerosol production needs to be analyzed.”

The ultimate goal of this study is to design and produce an experimental setup that complies with the design requirements to simulate PJ/ERBE experiments with minimal airflow disturbances to achieve lower aerosol production under similar tissue effects and to promote a safer and healthier surgical environment for both healthcare workers and patients.

1.3 Research question

The thesis process is divided into two parts. The first goal is to find an answer to the research question, “How aerosol production of PJ and ERBE operations are influenced by aerosol production-affecting factors such as speed, exposure time, and mode, that were normalized to the cutting length of the tissue?”

The goal of the second part of the thesis is to find an answer to the research question, “Which medical device, PJ or ERBE produces lower aerosol concentration for similar experimental conditions and tissue effects during resection, ablation or coagulation of the tissue sample?”

1.4 Thesis outline

This thesis project is a collaborative effort between the Erasmus MC and the Delft University of Technology, that provides an overview of a year-long worth MSc graduation project, including literature research and an internship, see Figure 1.2. Findings and the identification of the research gap from the literature review is covered in [Chapter 2](#). The internship phase is mainly covered in [Appendix A](#), and the thesis study is covered in the remaining Chapters.

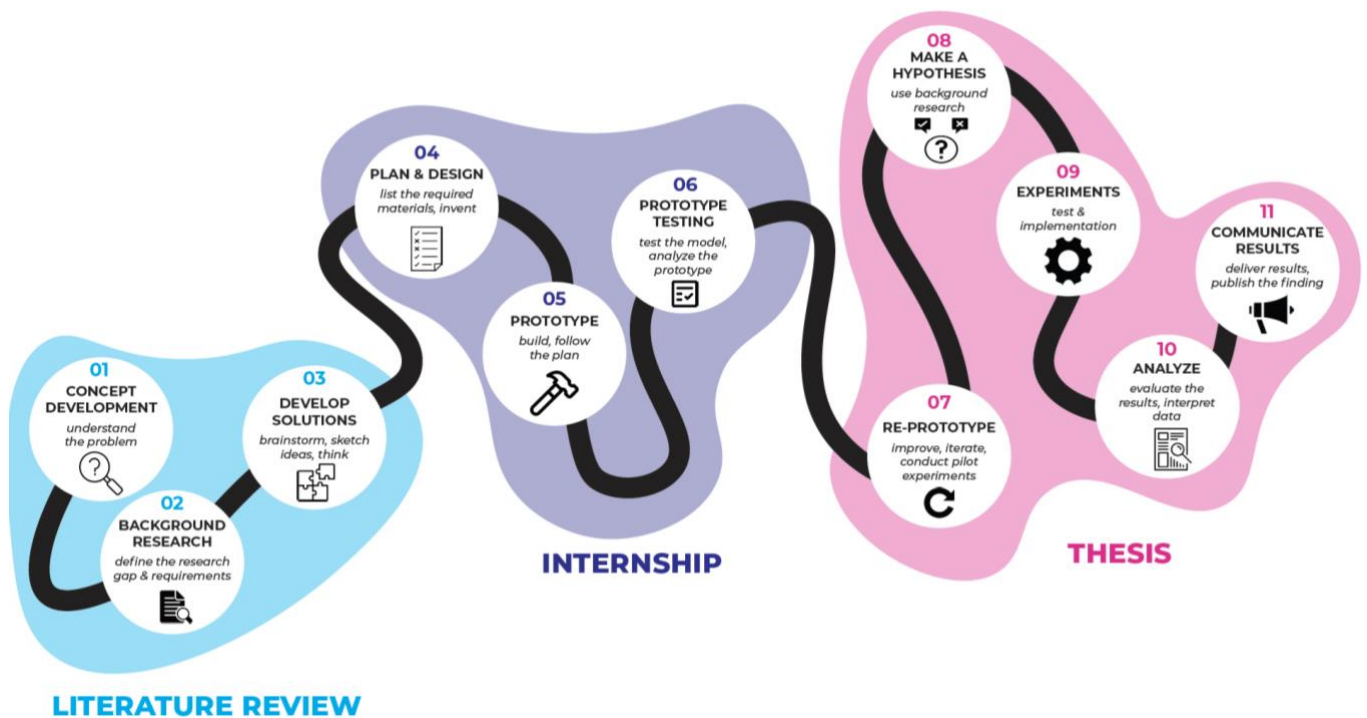


Figure 1.2 – The process model of the thesis project encompasses several phases, including background research, design, production, experiment, and analysis. These phases cover the literature review, internship, and thesis period.

2

Background on surgical smoke and experimental hypothesis

2.1 Aerosol production affecting factors

Surgical aerosol production during resection, ablation, and coagulation of soft tissues is affected by the surgical device's mode, power, wavelength, surgical device model, procedure, exposure time, tissue type, and surgical equipment material. However, the surgical device settings that PJ and ERBE do not comprise, such as wavelength and surgical equipment material are deemed to be outside of the scope of the thesis.

2.1.1 Findings and the research gap

According to the background research, the relevant literature did not provide any aerosol-related comparative studies between electro and plasma surgical devices (i.e., ERBE and PJ). Moreover, the evaluation of aerosol production affecting factors such as operation speed, exposure time, and modes (i.e., cut, coagulation, and ablation) was also not evaluated in any of the literature included in the literature review. Therefore, the literature research aided in the identification of the research gap and provided a study objective (see [Chapter 1.2](#)).

According to the literature review [19], it was concluded that device mode and type, and surgical exposure times affect aerosol production [20]. Moreover, when the tissue types were compared, the studies discovered variations in aerosol production rates attributed to differences in tissue properties, such as fat rate, thickness, and density [21-24].

2.2 Aerosol measurement affecting factors

The quantification of produced surgical aerosols is affected by several parameters: the experimental approach, the use of smoke suction and evacuation systems, and particle counting distance from the aerosol generation source. The graduation project experiments were conducted under the use of operating room ventilation systems. To eliminate the suspended particles and prevent potential hazards of aerosols

during the experiments; the experimental box was cleaned with a vacuum cleaner that was used as local exhaust ventilation (LEV) system.

2.2.1 Findings and the research gap

According to the literature review [19], high-efficiency particulate air filters (HEPA) and ultra-low penetration air (ULPA) filters can eliminate over 99.99% of the particles larger than 0.3 μm and 0.12 μm respectively [25,26]. Moreover, the use of handpiece-integrated LEV resulted in 88% lower aerosol counts compared to non-ventilated experiments [27].

The literature study revealed noteworthy variations in particle counting measurements at different distances from the source of aerosol generation. Under identical surgical conditions, aerosol counts of close-up measurements (at 30 cm) exhibited approximately 300 times higher counts than distant measurements (at 200 cm) [24]. Despite the significance of distance-related dispersion of aerosols, the studies reviewed were deficient in providing explicit information regarding the distances from the aerosol generation source. Ideally, the measurement distance should align with the spatial proximity between the aerosol generation source and the individual's breathing zone [2,22].

2.3 Hypothesis based on background information

The thesis process is divided into two parts. The first goal is to find an answer to the research question, "How aerosol production of PJ and ERBE operations are influenced by aerosol production-affecting factors, such as speed, exposure time, and mode, that were normalized to the cutting length of the tissue?"

The second goal is to find an answer to the research question, "Which medical device, PJ or ERBE produces lower aerosol concentration for similar experimental conditions and tissue effects during resection, ablation or coagulation of the tissue sample?"

The experimental hypotheses are based on pilot experiments and previous studies of TU Delft on PlasmaJet and ERBE aerosol production in 2020, see [Appendix A](#). Based on the research questions, four hypotheses were formulated. H1: coagulation mode results in lower aerosol counts than cutting mode. H2: faster operation speed results in lower aerosol counts. H3: larger and darker tissue burn results in higher particle counts. H4: PJ results in lower aerosol counts than ERBE under similar tissue effects.

3

Design and production of the test setup

This chapter outlines the design requirements and production of a closed container set-up for in-vitro electro and plasma treatments in order to count aerosols. The detailed version of the experimental setup improvements, evaluation of design requirements, step-by-step solutions, and background information on the previous setup made during the internship period can be found in [Appendix A](#).

The experimental setup described in [Chapter 3.2](#) utilized letter labeling corresponding to specific setup parts in Figures 3.1 to 3.7. Technical drawings of the laser cut parts, setup components, and information on off-the-shelf parts can be found in [Appendix F](#) and [Appendix H](#) respectively.

3.1 Design requirements

Table 3.1 – Design requirements for the experimental test setup

Criteria	Description	Reason
Minimized leakage	No visually perceptible leakage	To prevent air-flow disturbances that could impact aerosol count accuracy
Height	40 cm distance between the particle counter and aerosol generation source	To achieve relevant particle counts as in daily clinical practices
Balance	Balanced medical device weight with a counterweight	To achieve uniformed pulling motion of the tissue sample holder

Automatic execution	A repeatable functioning system to pull the tissue sample holder automatically with a 10-sec duration for a 5 cm cut	To perform remote, automated, and repeatable tissue sample operation
Cleanability	Limited edges/ridges of the setup components and the experimental box	To facilitate easy cleaning after each experimental run
User friendly	Visible particle counter screen and adjustable test setup components	To have a practical test setup and easy to adjust experimental conditions

3.2 Final design and production

3.2.1 Experimental box and particle counter

The experiment box for the PJ and ERBE experiments was produced, see Figure 3.1. The setup components were inserted into a polypropylene (PP) 80x60x40 cm experimental box (a) with 6mm thick polycarbonate (PC) plates (b) as the faces of the PP box ([Appendix H](#)). The faces were attached with Loctite 406 super glue and the voids between the plates and the edges of the box were filled with Bison Polymax sealant ([Appendix H](#)). To insert the test setup components with the least airflow disturbances, three entrance holes were laser cut on the PC plates, and the holes were sealed with rubber sheets and covered with plates (c). The lid of the box was fixated to the box with hinges (d) and clamps (e) which enabled locking during the experiments ([Appendix H](#)). To limit airflow disturbances during the measurements, the contact surface between the lid and the box was sealed with 4-6 mm D-profile rubber sealant (f) ([Appendix H](#)). The Fluke 985 particle counter (g) ([Appendix H](#)) was placed into the holder (h) and the nozzle was inserted into the box through the entrance hole (c) to count aerosols during experiments.

3.2.2 Automation

As shown in Figure 3.2, to generate an automated pulling motion, a stepper motor (i) ([Appendix H](#)) was used. The rotation of the motor was translated into a linear pulling motion with a 3D-printed motor mount (i). All of the 3D-printed sketches were printed at the TU Delft 3ME workshop using PLA. The stepper motor was fixated to its holder (j) and it was bolted to the experimental box. The stepper motor was connected to an Arduino Uno with a CNC shield (k) ([Appendix H](#)) and linked to both a computer and a power source (l).

A grbl code was coded on the Arduino IDE program to control the stepper motor and sent to Universal Gcode Sender (UGS) (m) to automate the turning motion. The UGS program allows a simple machine controller to control jogging duration, speed, and turning direction. Further information on step size calculations, Arduino code, and UGS settings can be found in [Appendix G](#).

The stepper motor mount (i) was coiled with a fishing line and threaded through the two metal hooks (n) of the tissue sample holder (o) to establish an interlock, as shown in Figures 3.3 and 3.6. The tissue sample holder (o) was placed on a guiding rail (p) to retain a linear motion during experiments. To perform the experiments, the monopolar return pad (q) and tissue sample (r) were fixated on the tissue sample holder (o).

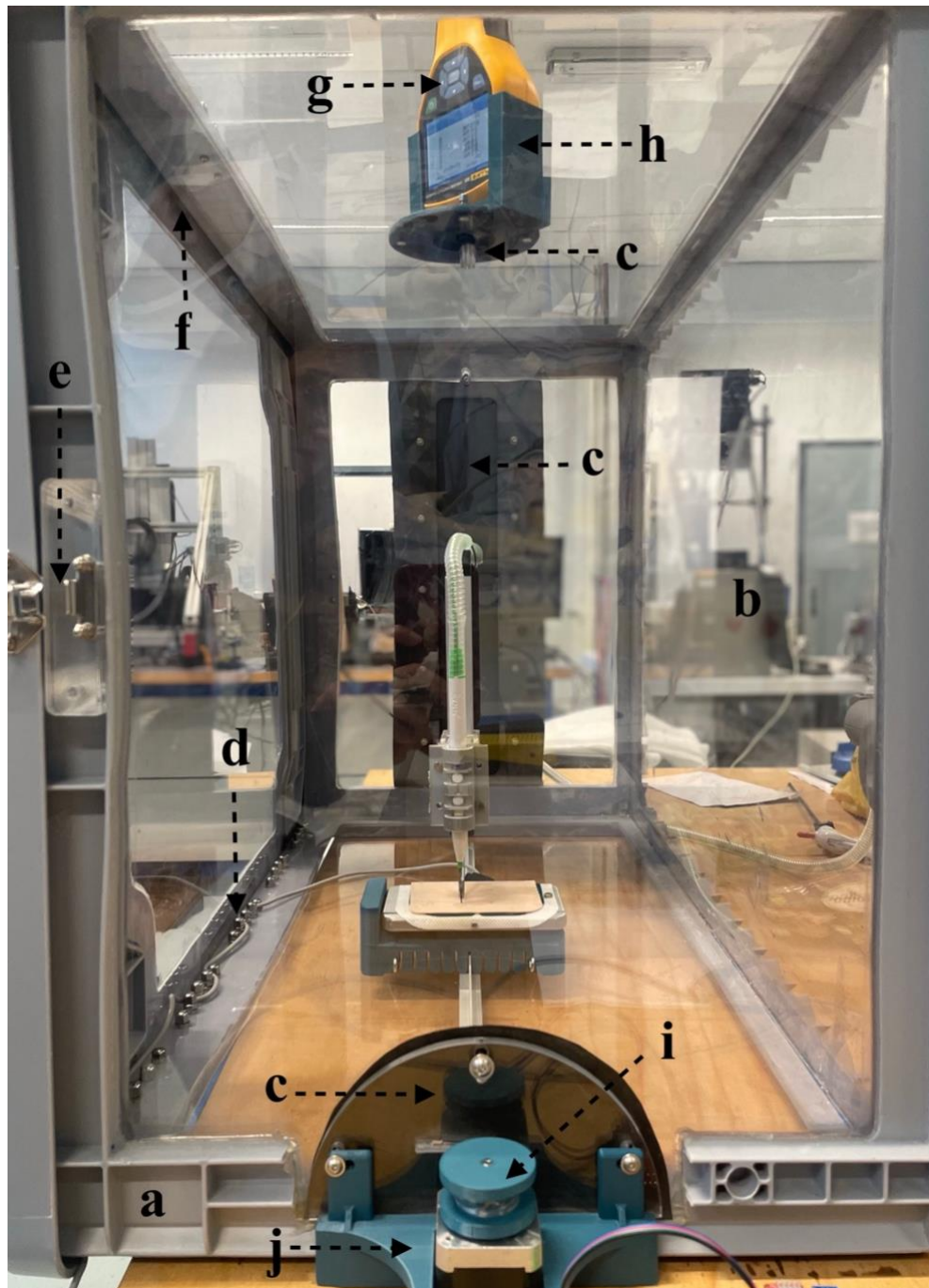


Figure 3.1 – Frontal experimental setup view that consisted of; a PP box (a) with PP plates (b), test setup entrance covers (c), hinges (d) to attach the lid, clamps (e) to lock/unlock the box, and D-profile rubber sealant (f) to seal the contact surface of the lid. The particle counter (g) is inserted into the holder (h), and the stepper motor with the mount (i) is fixated to the stepper motor holder (j). The stepper motor setup is further explained in Figure 3.2.

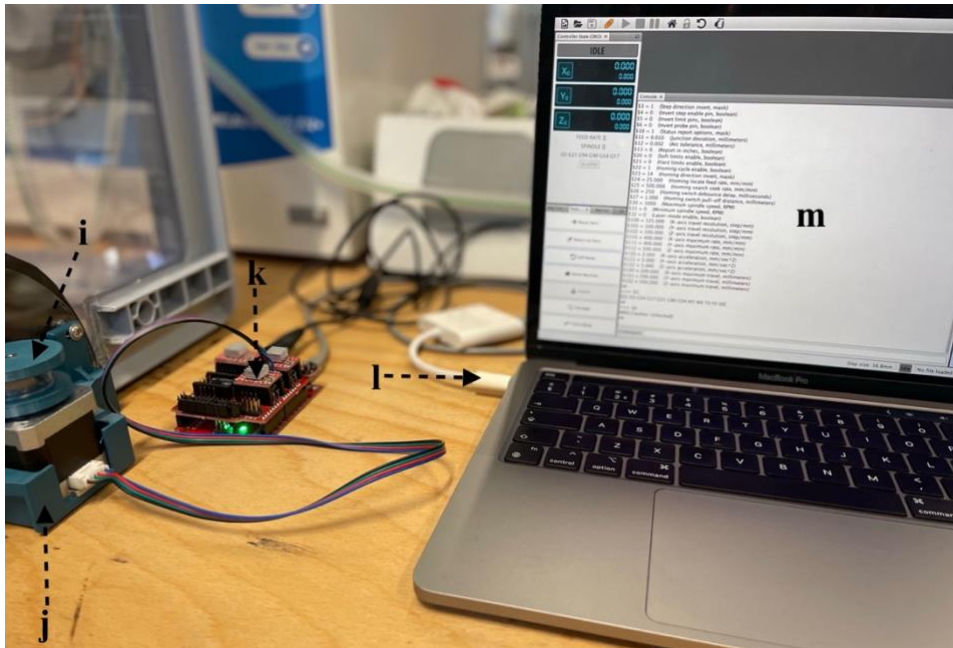


Figure 3.2 – External experimental setup view that consisted of a stepper motor with the mount (i) that is fixated to the stepper motor holder (j). The stepper motor is connected to the Arduino Uno with a CNC shield (k) extension, and linked to a power source and a computer (l). The UGS program on the computer (m) allows the establishment and control of the motor motion.

3.2.3 Test setup components and ERBE setup

As shown in Figure 3.3, a metal hook (u) was fixated on the support arm (t) to sustain and adjust the distance between the device handpiece and the tissue sample. The ERBE handpiece (s) was clamped to the support arm (t) to carry the device during the experiments. The handpiece is attached to the support arm with the 3D-printed ERBE attachment parts (v) (ERBE support arm clamp, ERBE T-bar, and ERBE ring) that were assembled on each other.

The weight of the ERBE handpiece on the tissue sample can prevent the automated tissue sample control. Therefore, as shown in Figure 3.4, the weight of the device’s handpiece was balanced with a counterweight (w) by hanging it on the support arm (t). The support arm was inserted into the support arm holder (x) and bolted to the box.

3.2.4 ERBE device

The ERBE handpiece (s) and the monopolar return electrode (q) were plugged into the ERBE generator’s (y) cut/coag and neutral electrode sockets respectively and the experimental settings such as mode and power controlled via the generator, see Figure 3.5. The experiments were conducted with minimal airflow disturbances and automated control. Therefore, an ERBE footswitch (z) was also connected to the ERBE generator (y) to cut and coagulate the tissue.

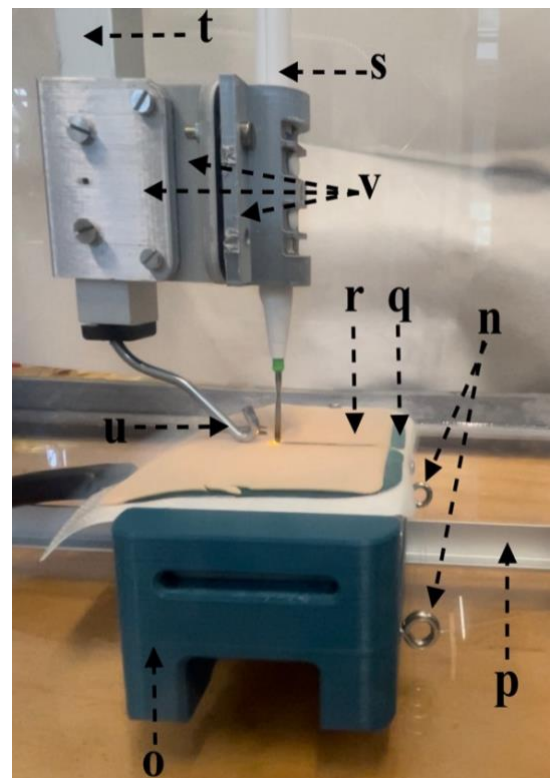


Figure 3.3 – Close up ERBE experimental setup view with metal hooks (n), tissue sample holder (o), guiding rail (p), return pad (q), tissue sample (r), ERBE handpiece (s), support arm (t), metal hook (u), and ERBE attachment parts (v).



Figure 3.4 – Back view of the experimental setup that consisted of, a PP box (a), test setup entrance covers (c), clamps (e) to lock/unlock the box, the support arm (t) with a counterweight (w), and the support arm holder (x) that is bolted to the box.



Figure 3.5 – The ERBE generator (y) with the insertions of the neutral electrode and ERBE handpiece cord. A footswitch (z) was also connected to the back of the system to control the ERBE handpiece from outside the box.

3.2.5 Test setup components and PJ Setup

As shown in Figure 3.6, a metal hook (u) was fixated on the support arm (t) to sustain and adjust the distance between the device handpiece and the tissue sample. The PJ handpiece, (aa) was clamped to the support arm (t) with the 3D-printed PJ attachment parts (ab) (PJ support arm clamp, PJ shaft support, and PJ tri-top) to carry the device during the experiments. The parts were assembled on each other.

The weight of the PJ handpiece on the tissue sample can prevent the automated tissue sample control. Therefore, as shown in Figure 3.4, the weight of the device's handpiece was balanced with a counterweight (w) by hanging it on the support arm (t).

3.2.6 PJ Device

The PJ handpiece (aa) was plugged into the PJ generator's (ac) handpiece socket (ad). The experimental settings such as mode and power were controlled via the generator, see Figure 3.7.

The experiments were conducted with minimal airflow disturbances and automated controlling. Therefore, as a PJ switch, 2 microswitches (ae) (one for cut and one for coagulation) were connected to the extended wires of the PJ handpiece and fixated into their 3D-printed holders to perform cut and coagulation from the outside of the box, as shown in Figure 3.8.

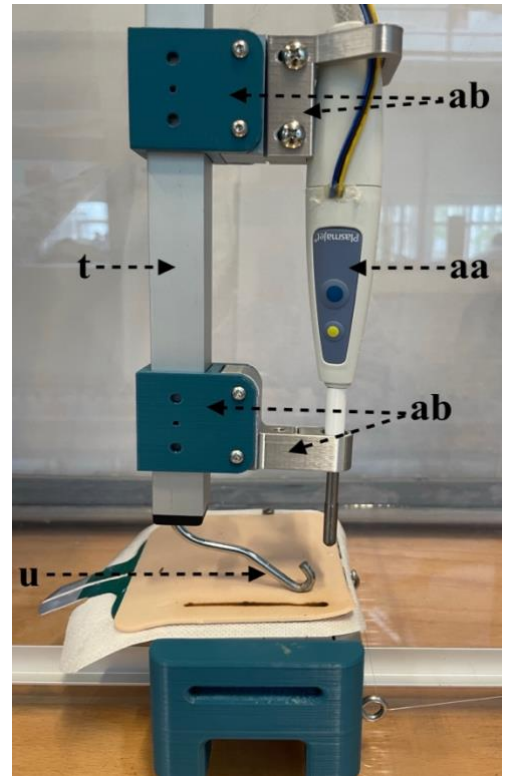


Figure 3.6 – Close up PJ experimental setup with the same tissue sample setup as shown in Figure 3.3 for ERBE experiments. The PJ setup modifications included the replacement of the PJ handpiece (aa) and PJ attachment parts (ab) to clamp the device to the support arm (t).

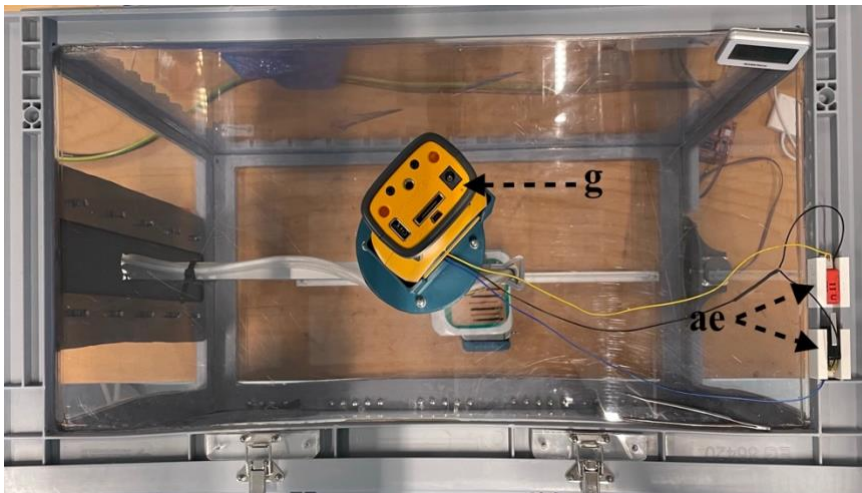


Figure 3.8 – Top view of the experimental setup that consisted of the particle counter (g) and 2 microswitches (ae) that are fixated into their 3D-printed holders.



Figure 3.7 – The PJ generator (ac) with the PJ handpiece cord plugged into its socket (ad).

4

Aerosol production via electro and plasma devices: Experimental methods

4.1 Introduction

Based on the formulated hypothesis in [Chapter 2.3](#), the experimental requirements were defined as shown in Table 4.1. This chapter includes the experimental requirements, experimental conditions, methods, and analysis protocols. A full list of materials and step-by-step experimental protocol can be found in [Appendix B](#).

4.2 Experimental requirements

Table 4.1 Requirements for the PJ and ERBE experiments

Criteria	Description	Reason
Consistency	Consistent cut and coloring of the tissue sample under the same conditions	To achieve similar tissue effects
Realistic	The experimental variables that comply with the clinical protocols used in daily practices	To achieve relevant results to those obtained from an electro or plasma surgery
Time efficiency	Each experimental run within 10 minutes (3 minute operation run, 2 minute notation of the results, and 5 minute cleaning and preperation process) .	To fit into the time constraints of the study. (The medical devices were borrowed for a limited time)

4.3 Materials and methods

The particles were counted with a particle counter ([Appendix H](#)) in an experimental box with minimal airflow disturbances (see [Chapter 3](#)), for six different particle sizes; 0.3, 0.5, 1.0, 2.0, 5.0, and 10.0 μm at a flow of 0.1 cfm (cubic foot per minute also equivalent of 2.83 l/m). The experiments were conducted at the Delft University of Technology. To minimize potential risks and animal suffering, the use of animal tissue at TU Delft is prohibited. Therefore, as a meat simulant, plant-based ham ([Appendix H](#)) was used to conduct experiments.

4.3.1 Experimental conditions

The dependent variables of the experiments were aerosol counts and particle sizes while the independent variables were device mode and operation speed. Four different conditions for each device were selected, as shown in Table 4.2. For both PJ and ERBE devices, the mode was alternated between cut and coagulation while the speed changed between fast (0.5 cm/s for 10 s exposure) and slow (0.25 cm/s for 20 s exposure).

The experimental condition codes in Table 4.2 references the independent test variables using the template [device] [mode] [speed] to identify the experimental conditions while recording the test runs. For example, the “E1F” code refers to the *ERBE device* with *cutting mode* under *fast operation* with a speed of 0.5 cm/s for 10 s. For each experimental condition, 10 repetitions were made with a total of 80 experimental runs.

The constant variables of the experiment were tissue type (meat simulant), cutting distance (5cm), particle counter distance to the aerosol source (40cm), particle counter type (Fluke 985), and particle counting duration (3x60s).

Other effective variables were temperature, humidity, residual aerosols, and tissue sample properties. These variables were observed during the experiments and to lower their influence on the results, a randomized block design was created using a list randomizer (see [Appendix C](#)). The randomized lists were independently created for both of the devices. Each list consisted of 4 experimental conditions with 10 repetitions for a total of 40 randomized experiments, and a total of 2 sets of 40 experiments, as shown in [Appendix C](#).

Table 4.2 Experimental setting combinations for PJ and ERBE devices. The experiment condition codes refer to the independent variables of the experimental condition. For example, the ‘E1F’ code refers to the ERBE device using the cutting mode with a faster operational speed of 0.5 cm/s for 10s.

Tested setting combinations and experimental codes of ERBE and PJ ECs									
Dependent variable:		Aerosol counts and sizes							
Experiment condition codes:		E1F	E1S	E3F	E3S	P1F	P1S	P3F	P3S
Device	ERBE	E	E	E	E				
	PJ					P	P	P	P
Mode	Cut	1	1			1	1		
	Coag			3	3			3	3
<i>Sub-settings of the mode</i>									
	Power setting* 30	+	+	+	+	+		+	
	20								+
	10						+		
Sub Mode	Effect1	+	+						

	Soft			+	+				
	Ultra					+	+		+
	Distance to tissue								
	Direct contact		+	+	+	+			
	2 mm (cut)					+	+		
	25 mm (coag)								+
									+
Speed	0.5 cm/s for 10 s exposure		F		F		F		F
	0.25 cm/s for 20 s exposure			S		S		S	S

**The power settings on the table are written as displayed on the device screen regardless of the unit. For the ERBE device, the power was in SI units (Watt), and for the PJ device, the power was demonstrated as power level with no unit indication.*

4.3.2 Experimental protocol

A detailed step-by-step version of the experimental protocol with a full list of materials can be found in [Appendix B](#).

Automation method

The stepper motor was fastened onto the Arduino CNC shield and linked to a computer and a power source. The UGS app on the computer was paired with the Arduino CNC shield. The turning speed and duration of the stepper motor were set according to the experimental conditions. At the start of the M1, on the UGS platform, the X+ button was pressed to pull the tissue sample for the selected experimental conditions. The motor was operated for 10 sec and 20 depending on the operation speed for a linear 5 cm cut. In case of an emergency, immediately press the disconnect button on the UGS program to stop the stepper motor functioning and disconnect Arduino from the platform.

Operation method

The medical device handpiece and the footswitch were connected to the generator. The desired device power and mode were selected. The animal tissue was fastened on the tissue sample holder and placed on the guiding rail and the distance between the handpiece tip and the tissue was adjusted with a spacer. The particle counter was placed into its holder and the box was closed and locked. Following each operation, the position of the tissue sample holder was adjusted on the guiding rail.

Particle counting method

The Fluke 985 particle counter was programmed for 3 measurements for 60 seconds for a total of 3 minutes. The base measurements (M0) counted for residual aerosols. The particles generated during the operation were recorded in the next minute M1. Following the operation, for the last count at M2, the particle counts were recorded for another minute after the settlement of aerosols. After each experimental run, the particle counter was filtered with the manufacturer's filter to clean the existing aerosols in the device.

Cleaning method

After the experimental run, the particle counter was removed from the holder and the vacuum hose was inserted into the particle counter entrance to vacuum residual aerosol for a minute without causing aerosol emission. Then, the box was opened, the tissue sample was removed and the inside of the box was vacuumed for another minute while cleaning inside the box, the device's handpiece, and test setup components with disinfectant wipes.

4.3.3 Analysis protocol

Data analysis

In each experiment, the number of particles was noted for M0, M1, and M2 measurements for each particle size (0.3, 0.5, 1.0, 2.0, 5.0, and 10.0 μm) at a sampling flow rate of 0.1 cfm (2.83 l/m). The total number of produced particles of each run was obtained by adding together the number of particles produced in M1 and M2; then subtracting the base level counts (M0) two times from the total. This calculation allowed the separation of baseline aerosols from the newly produced aerosol counts.

The number of aerosol particles was normalized to the operation length on the tissue. The tissue operation length was measured in pixels and converted into mm. The particle counts of each particle size (0.3, 0.5, 1.0, 2.0, 5.0, and 10.0 μm) and the total number of particles were divided by the operation length, and the results were achieved in the units of [particles/cfm/mm] for each particle size. This calculation assumes the same number of particles were produced throughout the 5cm cut.

Following the count summation, base level extraction, and length normalization; the statistical analyses were performed with 3-way ANOVA using MATLAB (MATLAB 2020/2021, The MathWorks Inc.) on eight experimental conditions (see Table 4.2) with ten repetitions to compare the effects of three independent factors; device, mode, and speed. The effects were considered significant $p < 0.05$.

Tissue effect analysis

The correlation between the total particle counts and the tissue effects was examined in MATLAB. The images of the tissue samples were imported into MATLAB and transformed into black-and-white images. The surface scans and black-and-white versions of experimental tissues can be found in [Appendix D](#). For optimal accuracy, a trial and error approach was used to determine a threshold level, ultimately setting it as 0.52. The mean brightness was computed in MATLAB for the seven selected areas (20mm cutting length 5mm destruction width), one area for each experimental run on the tissue. If the cut does not fit within the 7 selected areas, a separate region of interest with a separate code was defined for the cut.

The brightness of the selected areas was quantified on a scale from 0 to 1 where 0 corresponds to black and 1 to white. The damaged and cut-through experimental tissues were categorized as the most extensive level of tissue destruction and represented in the color black. Therefore, pixel growth was applied to cut-through tissue scans using Adobe Photoshop (Adobe Creative Cloud, 2022) to colorize the selected areas in black. The brightness data was used to create plots that illustrate brightness versus particle count [particle/cfm/mm] to demonstrate the interrelation between tissue effects and particle counts.

5

Aerosol production via electro and plasma devices: Results

In this section, the ERBE and PJ particle counts were evaluated after being normalized to length. Table 5.2 and 5.3 represents the mean numbers and standard deviations of counted particles per sample flow rate per millimeter. The mean of each particle size and the total number of particles of each condition can be found in Figures 5.1 to 5.5. For more detailed information on the particle counts per repetition, see [Appendix E](#).

In Table 5.1, a separate three-way ANOVA was performed for each column and put together as shown in Table 5.1. Significant effects were found on the device and mode ($p < 0.05$) for all particle sizes and also for the total number of particles. The effect of the speed in all cases was not statistically significant for speed ($p > 0.05$). The interactions of independent factors were also evaluated and the interactions were not statistically significant for all particle sizes (see Table 5.1).

Table 5.1 – The p-values to define the effects of independent factors (device, speed, and mode) and their interactions on the particle counts [particles/cfm/mm] for each particle sizes and for the total number of particles. The effects were considered significant when $p < 0.05$ and the significant values are marked in bold.

	Particle size						Total number of particles
	0.3 μ m	0.5 μ m	1.0 μ m	2.0 μ m	5.0 μ m	10 μ m	
Device	p<0.001	p<0.001	p<0.001	p<0.001	p<0.05	p<0.001	p<0.05
Speed	p=0.07	p=0.07	p=0.24	p=0.21	p<0.001	p<0.05	p=0.05
Mode	p<0.001	p<0.001	p<0.001	p<0.05	p<0.001	p<0.001	p<0.001
Device:Speed	p<0.001	p<0.05	p=0.90	p=0.27	p<0.001	p<0.001	p<0.05
Device:Mode	p<0.001	p<0.001	p=0.41	p=0.42	p=0.31	p<0.05	p<0.001
Speed:Mode	p=0.50	p=0.27	p=0.33	p<0.05	p<0.05	p<0.05	p=0.88
Device:Speed:Mode	p=0.28	p<0.05	p=0.35	p<0.05	p<0.001	p<0.001	p<0.05

5.1 ERBE results

The means and standard deviations of ERBE aerosol counts [particles/cfm/mm] are shown in Table 5.2. The results indicate that the ERBE coagulation mode produced lower aerosol counts compared to the ERBE cutting mode. However, the impact of operation speed on aerosol counts was not consistent. In cutting mode, higher aerosol counts were generated under fast operation speed, whereas in coagulation mode, higher aerosol counts were generated under slow operation speed.

Table 5.2 – The means and standard deviations of aerosol counts [particles/cfm/mm] over 10 repetitions for ERBE device's experimental conditions and each particle sizes and in total number of particles

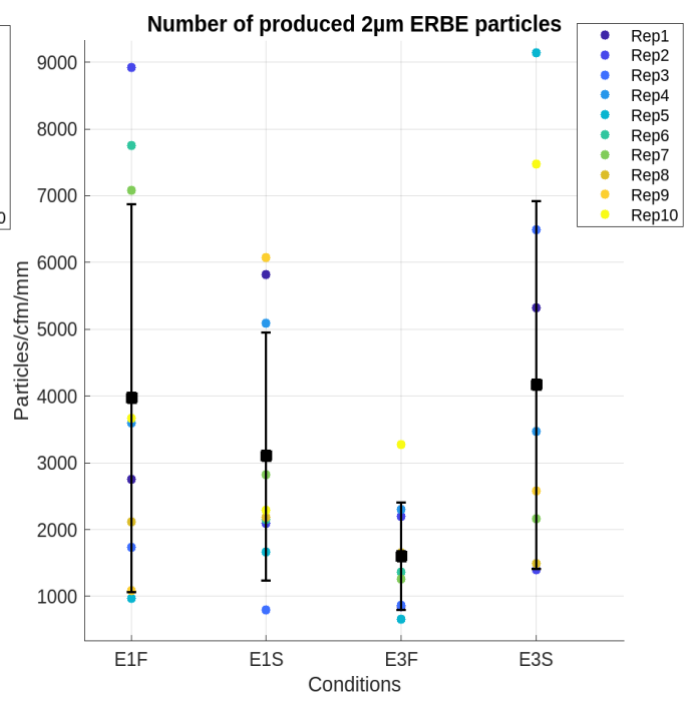
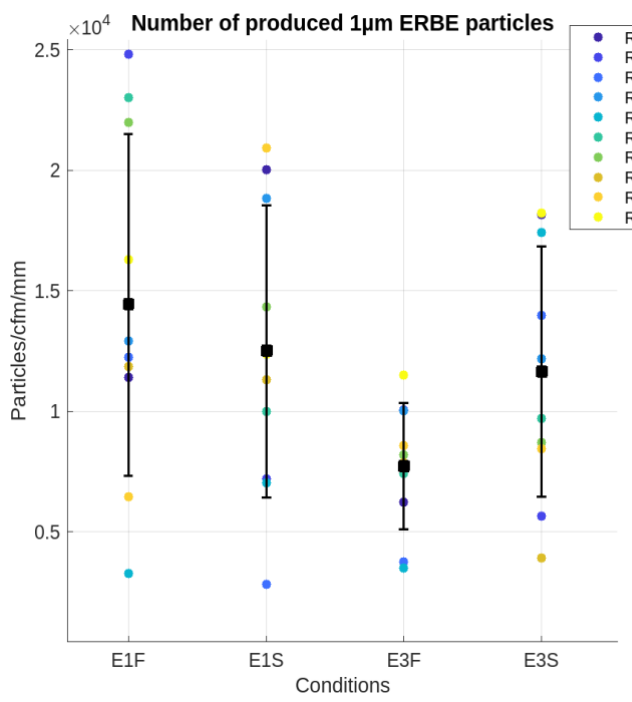
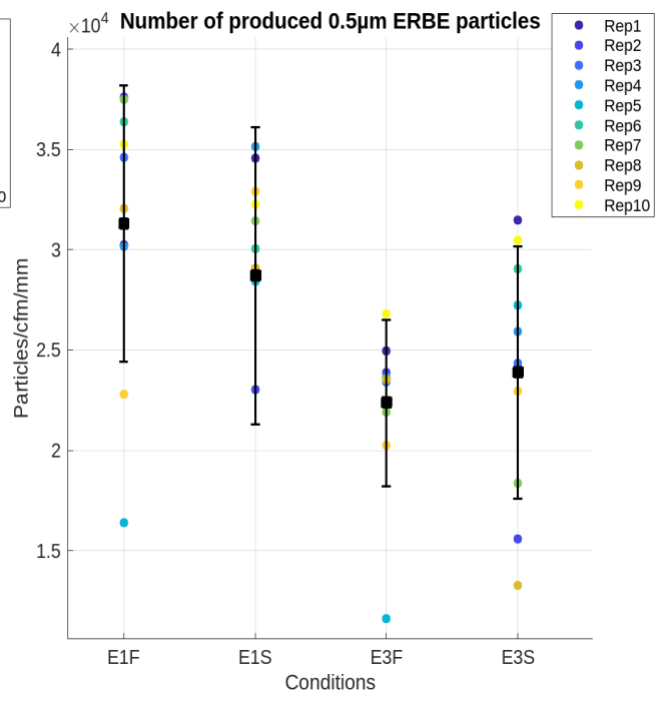
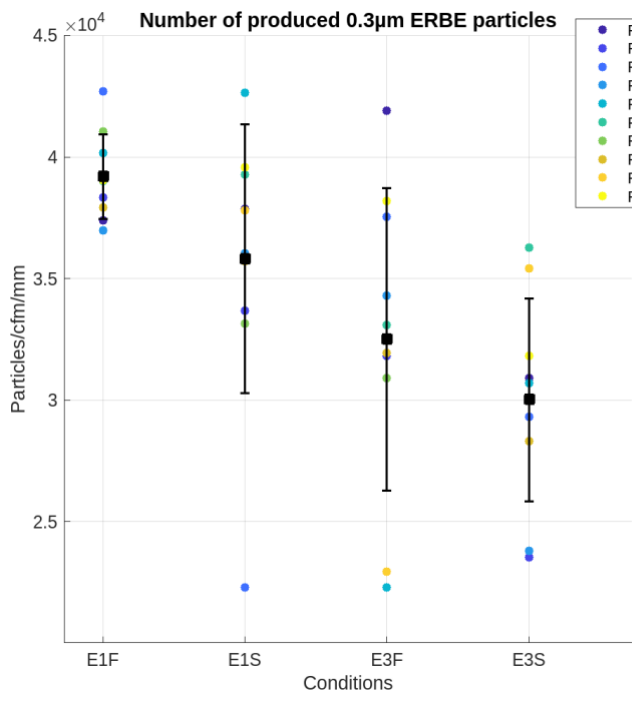
Exp. Code	0.3µm	0.5µm	1.0µm	2.0µm	5.0µm	10.0µm	Total number of particles
	Mean ± SD	Mean ± SD	Mean ± SD	Mean ± SD	Mean ± SD	Mean ± SD	Mean ± SD
E1F	39178±1378,4	31302±6890,5	14422±7090,7	3968±2903,0	60±15,3	8±2,8	88938±16253,3
E1S	35809±5532,1	28707±7399,1	12482±6062,1	3099±1856,8	116±34,1	19±6,5	80232±18429,5
E3F	32493±6227,8	22365±4145,6	7717±2624,0	1598±804,9	8±2,7	0,9±0,7	64181±11542,3
E3S	30010±4174,8	23871±4174,8	11637±5196,7	4168±2752,8	7±3,2	0,7±0,6	69695±15222,9

The particles were counted at a flow rate of 0.1 cfm (2.83l/m), and the base level measurements were subtracted from both measurements (M1+M2-2M0). The particle counts were normalized to length to achieve the counts in the units of [n/cfm/mm]. The experimental codes refer to the independent factors of the test run, see Chapter 4.3. For example, the code 'E1F' refers to the ERBE cutting mode under fast operation.

As illustrated in Figure 5.1, across all modes and speeds, the number of smaller ERBE particles exceeded the number of larger particles. The condition 'E1F' resulted in the highest particle counts in total. However, there was a deviation for the particle sizes of 5.0 and 10.0 µm, where the highest number of particles was observed in the 'E1S'.

The lowest number of particles were produced from the condition 'E3F'. However, there was a deviation for the particle sizes 0.3, 5.0, and 10.0 µm, where the lowest number of particles was produced from the condition 'E3S'.

Statistical analysis indicated a significant effect of the mode on all particle sizes and also for the total number of particles ($p < 0.05$). A higher number of particles were consistently produced from the cutting modes 'E1F' and 'E1S' compared to the coagulation mode 'E3F' and 'E3S'. However, the effect of the operation speed was not statistically significant ($p > 0.05$) except for the particle sizes 5.0 and 10.0µm. The number of 5.0 and 10.0µm particles was statistically significant ($p < 0.05$) and up to 50 times higher in ERBE cutting than particle counts in ERBE coagulation mode.



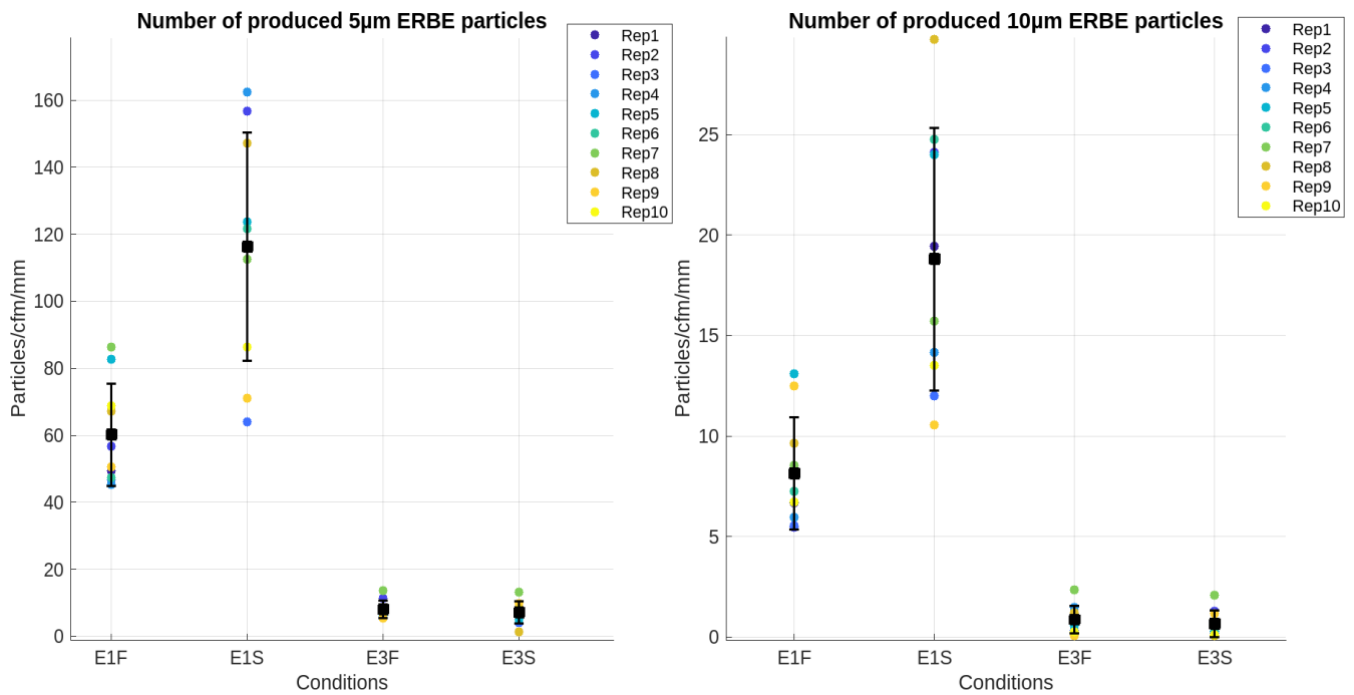


Figure 5.1 – Scatter plots with error bars of particle counts [particles/cfm/mm] across all ERBE experimental runs $n=10$ and conditions (E1F, E1S, E3F, E3S) for each particle size. Note that the y-axis of each sub-figure was scaled depending on the maximum number of particles for each particle size.

Figure 5.2 illustrates the mean particle counts [particles/cfm/mm] of each ERBE experimental condition over 10 repetitions. The particle counts and displayed numbers on the y-axis are in the log scale and the $10.0\ \mu\text{m}$ counts of the experimental conditions ‘E3F’ and ‘E3S’ were infinitesimal and resulted in negative counts in the log scale. The particle counts of $10.0\ \mu\text{m}$ ERBE particles can be found in Figure 5.1 and more detailed information on the particle count comparison between repetition of all ERBE conditions can be found in [Appendix E](#).

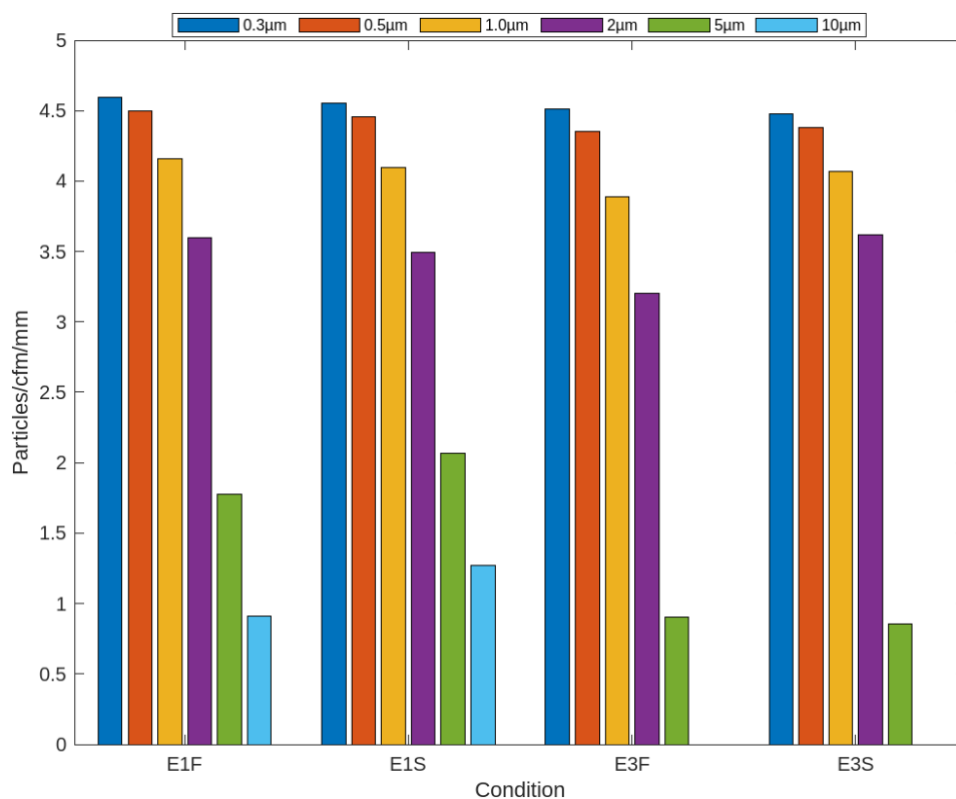


Figure 5.2 – The mean particle counts [particles/cfm/mm] of $n=10$ across all ERBE experimental conditions for each particle size. Note that, the displayed particle counts on the y-axis are also in the log scale and the 10.0 μm counts of the experimental conditions ‘E3F’ and ‘E3S’ were not able to be displayed in the log scale plot. See Figure 5.1 for 10.0 μm ‘E3F’ and ‘E3S’ particle counts.

5.2 PJ results

The means and standard deviations of PJ aerosol counts [particles/cfm/mm] are shown in Table 5.3. The results indicate that the PJ coagulation mode produced lower aerosol counts compared to the PJ cutting mode for each particle size and in total. Moreover, the results showed that faster operation results in lower aerosol counts for each particle size and for the total except for 5.0 μm particles of cutting mode.

Table 5.3 – The means and standard deviations of aerosol counts [particles/cfm/mm] over 10 repetitions for PJ device's experimental conditions and each particle sizes and in total number of particles

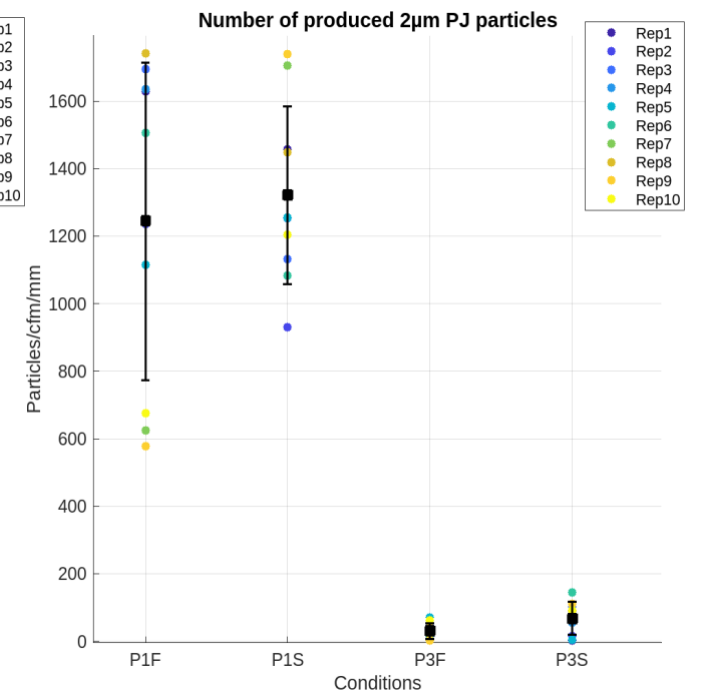
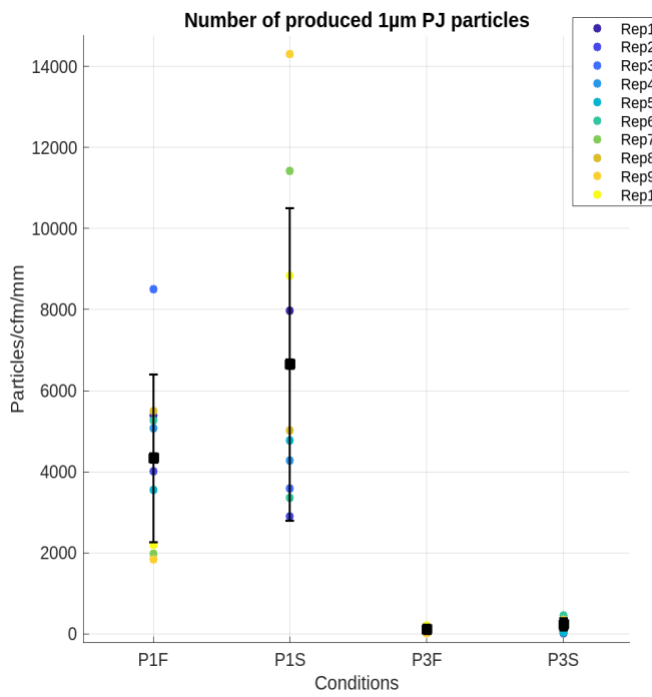
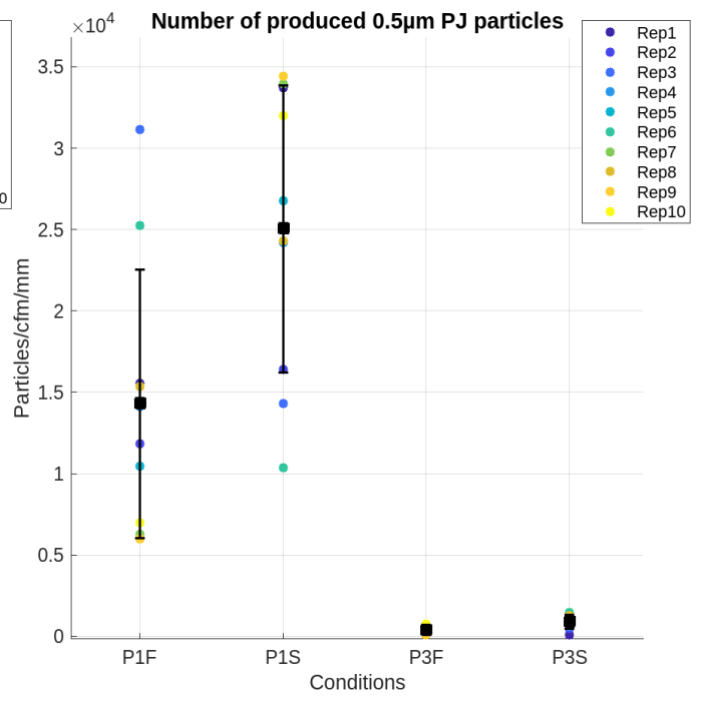
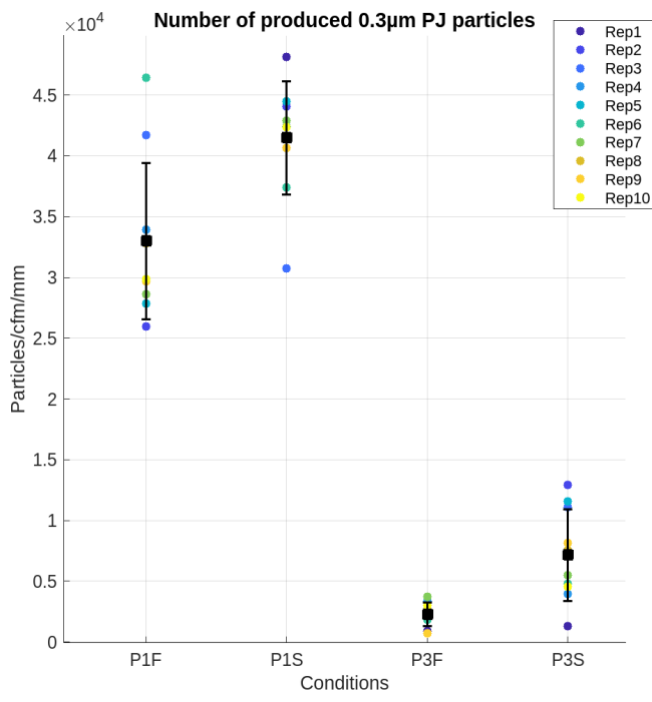
Exp. Code	0.3 μm	0.5 μm	1.0 μm	2.0 μm	5.0 μm	10.0 μm	Total number of particles
	Mean \pm SD	Mean \pm SD	Mean \pm SD	Mean \pm SD	Mean \pm SD	Mean \pm SD	Mean \pm SD
P1F	32991 \pm 6439,2	14294 \pm 8257,5	4328 \pm 2069,3	1244 \pm 469,8	77 \pm 31,6	10 \pm 5,1	52945 \pm 16375,0
P1S	41474 \pm 4682,3	25045 \pm 8824,7	6645 \pm 72,7	1321 \pm 263,8	73 \pm 10,9	8 \pm 2,7	74565 \pm 15381,4
P3F	2274 \pm 978,3	354 \pm 223,1	97 \pm 72,6	30 \pm 24,0	1,2 \pm 0,8	0,1 \pm 0,2	2756 \pm 1149,0
P3S	7139 \pm 3787,7	903 \pm 420,5	226 \pm 149,6	69 \pm 48,5	3,8 \pm 2,4	0,5 \pm 0,3	8341,7 \pm 3891,6

The particles were counted at a flow rate of 0.1 cfm (2.83l/m), and the base level measurements were subtracted from both measurements (M1+M2-2M0). The particle counts were normalized to length to achieve the counts in the units of [n/cfm/mm]. The experimental codes refer to the independent factors of the test run, see Chapter 4.3. For example, the code ‘P1F’ refers to the PJ cutting mode under fast operation.

As illustrated in Figure 5.3, across all modes and speeds, the number of smaller PJ particles exceeded the number of larger particles. The condition ‘P1S’ (slow-cutting mode) resulted in the highest total particle counts. However, there was a deviation observed for the particle sizes of 5.0 and 10.0 μm , where the highest number of particles was observed in the ‘P1F’ (fast-cutting mode).

The lowest number of particles were produced from the condition ‘P3F’ (fast-coagulation mode) for all particle sizes. The statistical analysis indicated a significant effect of the mode on all particle sizes and also for the total number of particles ($p < 0.05$). A higher number of particles consistently produced from the cutting mode ‘P1F’ and ‘P1S’ compared to the coagulation mode ‘P3F’ and ‘P3S’. The particle counts were up to 50 times higher in PJ cutting than the particle counts in PJ coagulation mode.

When the operation speed between different conditions was evaluated, although a higher total number of particles were produced from slower operations, the effect of the operation speed was not statistically significant ($p > 0.05$) except for the particle sizes 5.0 and 10.0 μm ($p < 0.05$).



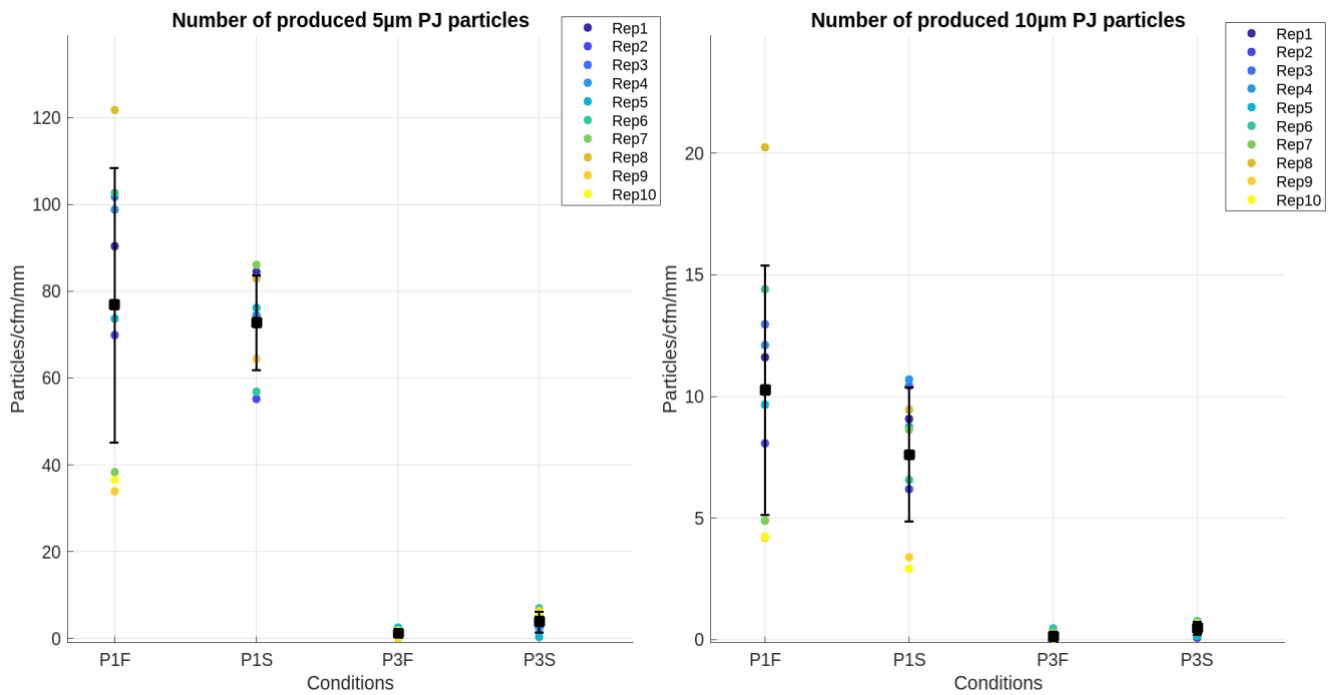


Figure 5.3 – Scatter plots with error bars of particle counts [particles/cfm/mm] across all PJ experimental runs $n=10$ and conditions (P1F, P1S, P3F, P3S) for each particle size. Note that the y-axis of each sub-figure was scaled depending on the maximum number of particles for each particle size.

Figure 5.4 illustrates the mean particle counts [particles/cfm/mm] for each PJ experimental condition over 10 repetitions. The particle counts and the displayed numbers on the y-axis are in the log scale. The 10.0 μm particle counts of the experimental conditions ‘P3F’ and ‘P3S’ were infinitesimal and resulted in negative counts in the log scale. The particle counts of 10.0 μm PJ particles can be found in Figure 5.3. More detailed information on the particle count comparison between repetition of all PJ conditions can be found in [Appendix E](#).

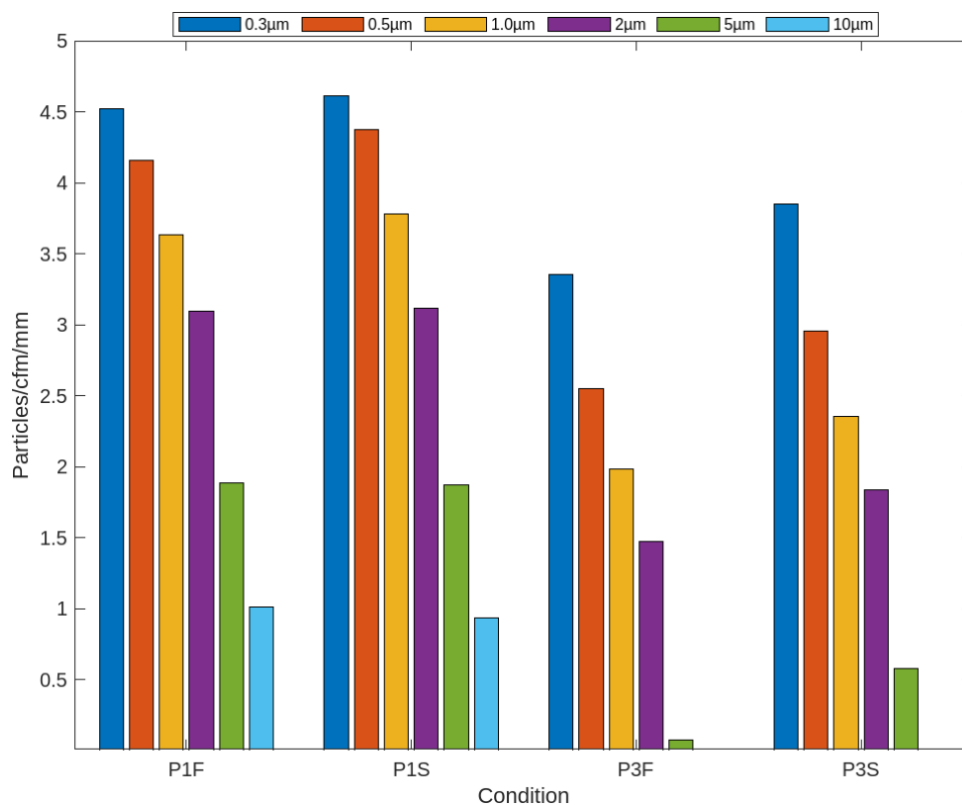


Figure 5.4 – The mean particle counts [particles/cfm/mm] of n=10 across all PJ experimental conditions for each particle size. Note that, the displayed particle counts on the y-axis are also in the log scale and the 10.0 μm counts of the experimental conditions ‘P3F’ and ‘P3S’ were not able to be displayed in the log scale plot. See Figure 5.3 for 10.0 μm ‘P3F’ and ‘P3S’ particle counts.

5.3 Comparative results

The means of the total number of produced particles [particles/cfm/mm] of all ERBE and PJ experimental conditions with standard deviation error bars are shown in Figure 5.5.

According to 3-way ANOVA, the device type and the mode has a significant effect (p<0.05) on the total number of particle counts. There is a clear trend of a higher number of particle counts on ERBE compared to PJ and cutting mode compared to coagulation. Moreover, the interactions of device, mode, and speed were also statistically significant (p<0.05) except for the interaction of speed and mode (p=0.88).

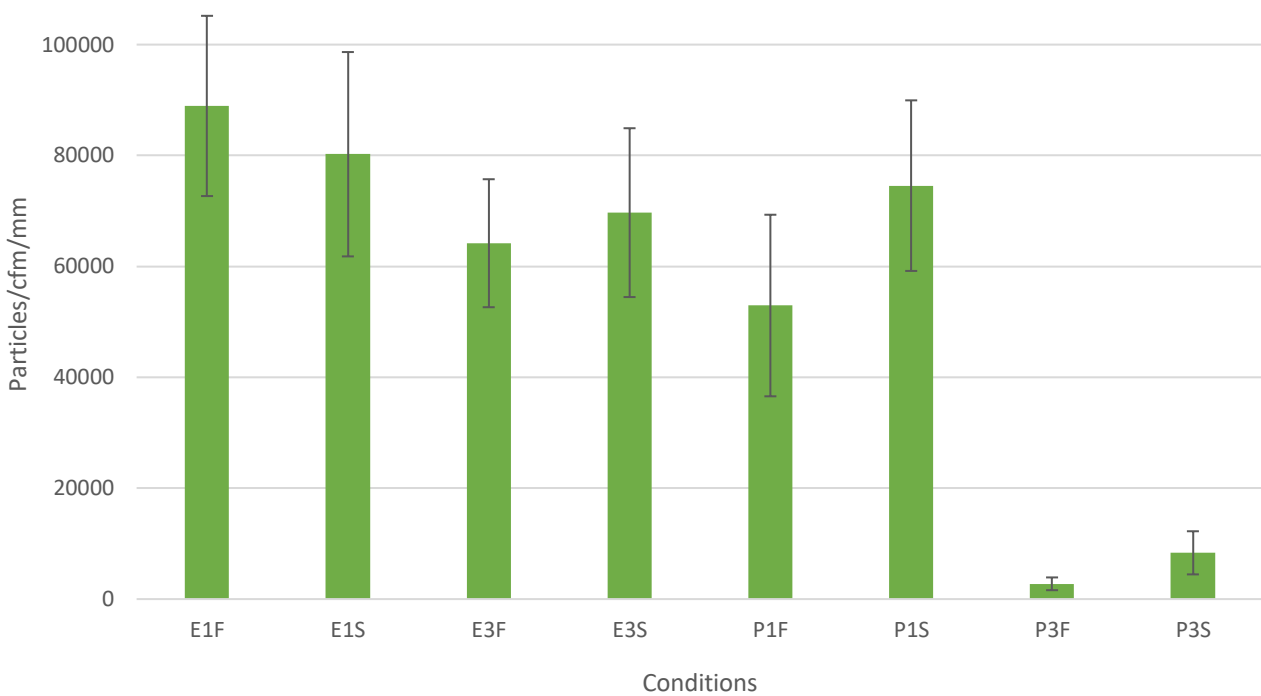


Figure 5.5 – The means of the total number of aerosol counts [particles/cfm/mm] of all ERBE and PJ experimental conditions with standard deviation error bars.

5.4 Tissue effects

The surface scans and black-and-white versions of experimental tissue samples can be found in [Appendix D](#). The brightness of the selected areas was scaled from 0 to 1; where 0 represents black and 1 represents white. During the analysis of the tissue effects, the statistical significance of the device type and mode (p<0.05) were considered (see Table 5.1). Based on the statistical significance, the independent factors were grouped as “E1”, “E3”, “P1”, and “P3”. The brightness values of the experimental conditions can be found in Table 5.4. The interrelation between the tissue effects and particle counts [particles/cfm/mm] was investigated and presented in Figure 5.6.

Brightness values [0 to 1]	
Exp. Code	Mean ± SD
E1	0,63±0,12
E3	0,79±0,07
P1	0,37±0,10
P3	0,53±0,17

Table 5.4 – The means and standard deviations of the brightness values for the experimental conditions.

In the cutting modes (mode 3) of both ERBE and PJ devices, a correlation between the tissue effects and particle counts was observed. Lower brightness values (indicating darker tissue effects) corresponded to higher particle counts while higher brightness values (indicating brighter tissue effects) corresponded to lower particle counts.

For the ERBE device, the cutting mode resulted in higher particle counts compared to the coagulation mode. When considering the analysis of tissue effects, it was concluded that higher particle counts were associated with darker tissue effects. This correlation implies that in the ERBE device, more tissue destruction is associated with higher particle counts.

On the other hand, for the PJ device, no interrelation between the tissue effect and particle counts was found in the “P3” mode. However, the “P1” mode resulted in darker tissue effects from higher particle counts.

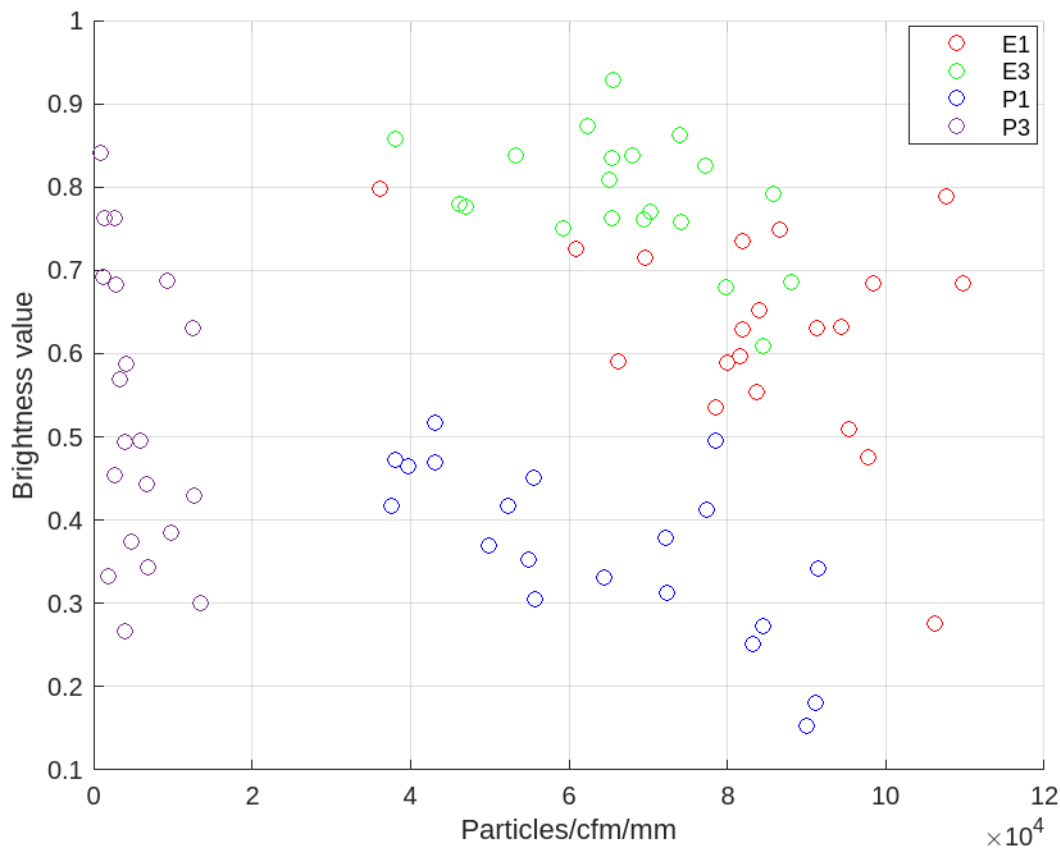


Figure 5.6 – The scatter plot overview of the relationship between the brightness values and particle counts [particles/cfm/mm] for the independent conditions E1, E3, P1, and P3. The brightness values represent the tissue effects on a scale of 0 to 1 where 0 represents black (highest tissue effects) and 1 represents white (lowest tissue effects).

6

Discussion and recommendations

The goal of this study was to investigate the influence of aerosol production affecting factors such as speed, exposure time, and mode during electro and plasma surgeries, explicitly focusing on ERBE and PJ devices. The research objectives also included comparing and deciding on which medical device ERBE or PJ generates lower aerosol counts under similar experimental conditions and tissue effects. To achieve these goals, an experimental setup was produced and evaluated based on the design requirements (see [Chapter 4.2](#) and [Appendix A.3](#)).

The analysis of particle size distribution showed that the smaller particles outnumbered larger particles across all experimental conditions. This observation can be attributed to the smaller particles remaining suspended in the air and being able to reach the particle counter while in contrast, bigger particles, such as 5.0 and 10 μm particles, tended to settle down [28]. During the experiments, Fluke 985 particle counter was able to detect particles as far as 0.3 μm . Notably, the presence of high counts from particles sized 0.3 μm showed a high probability of the existence of particles smaller than the detection limit of 0.3 μm . The hazards of ultrafine particles smaller than 0.3 μm can't be negligible. Due to its high toxicity and ability to translocate to other organs, the presence of these smaller particles (PM_{2.5}) is recommended to be evaluated in further studies [29]. Further investigation can be done by using fast mobility particle sizers since these particle counters can detect from 0.0056 to 0.56 μm [30].

The research goal was achieved and the results established a clear correlation between the aerosol production-affecting factors and particle counts for all particle sizes. As hypothesized, the coagulation mode and PJ device exhibited lower aerosol counts than the cutting mode and ERBE device respectively. However, the operation speed did not demonstrate a significant effect on aerosol production, despite slower operations of all experimental conditions generally produced higher particle counts. This might be because of the production of more aerosol particles in condition E1F than in condition E1S.

Among all experimental conditions, for all particle sizes, the “P3F” condition yielded the lowest particle counts, which did not reach the unhealthy and toxic dose (400 ppm for 15-minute exposure) [31,32]. However, the chemical composition and toxicity of the produced particles were beyond the scope of this

thesis. For the non-toxicity and healthiness level assertion, a further analysis, which can be done by ultra-performance liquid chromatography (UPLC), is recommended to clarify the particulate matter composition [33]. Given the established possibility of virus transmission through electro and plasma surgeries, it is essential to prioritize the investigation of aerosol's chemical composition and implement measures to prevent aerosol inhalation, especially in countries with high rates of virus transmission [34,35].

The second part of the research question which focused on device comparison, concluded that the PJ device yielded lower aerosol counts than the ERBE device across all modes and speeds. However, in terms of device comparison, it should be noted that this study solely focused on comparing aerosol production and the results do not provide insights into the effectiveness of these medical devices.

Comparing the features of ERBE and PJ devices revealed that PJ generated more dispersed energy to the tissue due to non-contact tissue removal, resulting in a wider tissue effect, particularly in the coagulation setting. Both devices exhibited sensitivity to the distance between the device and the tissue, requiring consistent distance adjustment throughout the experiment. However, the experiments were conducted in a no-touch environment, and even though the tissue sample was a manufactured meat simulant, the thickness throughout the tissue sample was not equal and resulted in inconsistent tissue effects.

The tissue effects of experimental conditions were compared and revealed a clear correlation in the cutting modes of both devices. However, no such correlation was observed with the "P3" condition, which exhibited the lowest aerosol counts in overall compared to other modes and devices. This obscure finding may be attributed to the Maillard reaction occurring on the meat simulant that was due to the use of argon gas. The Maillard reaction is a non-enzymatic browning process that occurs in foods, such as grilling, in the presence of heat [36]. It is possible that the reaction led to the attachment of the aerosol particles on the tissue and resulting in lower aerosol counts. Suggestively, lesion analysis of the tissue sample with gas chromatography and chemical composition analysis of the captured aerosol using UPLC can be done to further investigate these mentioned effects.

There were several limitations encountered during the experimental process. The experiments were conducted at Delft University of Technology and the use of animal tissues was not permitted. However, this restriction led to the utilization of plant-based tissue, which differs in properties such as density, thickness, and fat content compared to animal tissue. Moreover, the plant-based tissue deteriorated and changed color after a short period of time. The depth of the destruction was not measured and only the surface scans were evaluated.

Another limitation faced during the experimental process was the manual pressing of the X+ button on the UGS platform while simultaneously cutting or coagulating the tissue using the medical device. Achieving an exact duration for pressing the cut or coagulation was not feasible and resulted in deviations between repetitions of experimental conditions. During the course of the study, one additional limitation was encountered, namely the inability to attain fully airtight experimental conditions. Despite efforts to minimize airflow within the experimental box, some degree of air exchange persisted. This lack of complete airtightness may have contributed to variations in the results observed across different repetitions of the experiment.

The significant effect of the production-affecting factors was evaluated using 3-way ANOVA on MATLAB. Given the three independent factors in the experiments (device, mode, and speed), 3-way ANOVA was chosen to assess the comparison and interactions between experimental conditions. However, when the experimental data was evaluated, the data deviated from a normal distribution pattern

due to a limited number of experimental repetitions. Despite this non-normality of the data, 3-way ANOVA was still chosen as a meaningful analysis method to provide a comprehensive analysis of how the factors of interest influence the dependent variable and whether there are significant interactions.

As mentioned throughout the discussion, several recommendations can be made based on the findings discussed throughout the study. Future research should focus on examining the toxicity of the produced aerosol to determine a minimal dosage for generated aerosols during electro and plasma surgery. Furthermore, even though the Fluke 985 particle counter was primarily sensitive to particles larger than 0.3 μm , the possible presence of smaller aerosol particles ($\text{PM}_{2.5}$) should be acknowledged and evaluated in further research.

As a last recommendation, lesion analysis of the tissues operated with PJ coagulation mode, and analysis of operated tissue dept is suggested to see a clear picture of tissue effects. Lastly, regardless of the conducted further analysis, the evaluation of the aerosol measurement affecting factors showed that removing aerosols directly from the surgical environments showed its efficiency in preventing aerosol inhalation [37]. Implementing local exhaust ventilation during surgeries can reduce aerosol measurements by up to 88% [2, 22, 27]. To enhance protection further, the use of N95 surgical masks should be improved to achieve a filtering efficiency of 95% [31,38].

7

Conclusion

This study aimed to design and produce an experimental setup in order to replicate PJ and ERBE experiments with minimal airflow disturbances, aiming to create conditions that generate lower aerosol counts to provide a safer and healthier surgical environment for both healthcare workers and employees.

The findings of this study established a clear correlation between the aerosol production-affecting factors and particle counts for all particle sizes. Among the experimental conditions, the PJ device in coagulation mode with a fast operation (“P3F”) provided the lowest aerosol counts. Further research is warranted to investigate the toxicity of generated aerosols and establish a threshold for minimal aerosol intake. Additionally, for a more comprehensive understanding of tissue effects, it is recommended to conduct a lesion analysis of the affected tissue and assess the depth analysis of the resection.

Based on the current findings, when solely focused on aerosol production, the PJ device and coagulation mode consistently produced lower aerosol counts than the ERBE device and cutting mode respectively. However, until the toxicity and minimal dose of aerosols are determined, preventive measures such as the implementation of local exhaust ventilation and the use of surgical masks are strongly advised to minimize aerosol inhalation.

Bibliography

1. Tan, W., Zhu, H., Zhang, N., Dong, D., Wang, S., Ren, F., Xiang, J., Wu, R., Lv, Y. (2019). Characterization of the PM_{2.5} concentration in surgical smoke in different tissues during hemi hepatectomy and protective measures. *Environmental toxicology and pharmacology*, 72, 103248. doi.org/10.1016/j.etap.2019.103248
2. Okoshi, K., Hida, K., Kinoshita, K., Morishima, T., Nagai, Y., Tomizawa, Y., Yorozuya, K., Nishida, T., Matsumoto, H., Yamato, H. (2022). Measurement of particulate matter 2.5 in surgical smoke and its health hazards. *Surgery today*, 52(9), 1341–1347. /10.1007/s00595-022-02473-z
3. Fan, J. K., Chan, S. F., Chu, K. (2009). Surgical smoke. *Asian journal of surgery*, 32(4), 253-257. /10.1016/S1015-9584(09)60403-6.
4. Liu, Y., Song, Y., Hu, X., Yan, L., Zhu, X. (2019) Awareness of surgical smoke hazards and enhancement of surgical smoke prevention among gynecologists. *J cancer*. 10(12), 2788-2799. /10.7150/jca.31464
5. Okoshi, K., Kobayashi, K., Kinoshita, K. (2015). Health risks associated with exposure to surgical smoke for surgeons and operation room personnel. *Surgery today*, 45, 957-965, doi-org.tudelft.idm.oclc.org/10.1007/s00595-014-1085-z
6. Sanderson, C. (2012) Surgical smoke. *Journal of perioperative practice*, 22(4), 122-128. <https://doi/10.1177/175045891202200405>
7. Alp, E., Bijl, D., Bleichrodt, R., Hansson B., Voss, A. (2006) Surgical smoke and infection control. *Journal of Hospital Infection* 62 (1) 1-5
8. Balytskyy, V., Zakharash, M., Kuryk, O. (2021). The results of surgical treatment of combined anorectal diseases using radiofrequency and high-frequency electrosurgical devices. *Georgian medical news*, (318), 13–19.
9. Svider, P. F., (2018) Principles of electrosurgery. *Laryngoscopes investigate otolaryngology*. https://www.asit.org/assets/documents/Principals_in_electrosurgery.pdf
10. Weltmann, K. D., Woedtke, Th. (2017). Plasma medicine— Current state of research and medical application. *Plasma Physics and Controlled Fusion*. 59. 014031. 10.1088/0741-3335/59/1/014031.
11. Deb, S., Sahu, B., Deen, S., Newman C., Powell M. (2012). Comparison of tissue effects quantified histologically between PlasmaJet coagulator and Helica thermal coagulator. *Arch Gynecology Obstetrics* 286, 399–402 <https://doi.org/10.1007/s00404-012-2302-x>
12. Jaiswal, A., & Huang, K. G. (2017). Energy devices in gynecological laparoscopy— Archaic to modern era. *Gynecology and minimally invasive therapy*, 6(4), 147–151. <https://doi.org/10.1016/j.gmit.2017.08.002>
13. Farin, G., & Grund, K. E. (1994). The technology of argon plasma coagulation with particular regard to endoscopic applications. *Endoscopic surgery and allied technologies*, 2(1), 71–77.
14. Loh, S. A., Carlson, G. A., Chang, E. I., Huang, E., Palanker, D., Gurtner, G. C. (2009). Comparative healing of surgical incisions created by the PEAK PlasmaBlade, conventional electrosurgery, and scalpel. 124(6), 1849–1859. <https://doi.org/10.1097/PRS.0b013e3181bcee87>

15. Phelps, D.L., Saso, S., Ghaem-Maghami, S. (2020). Is ovarian cancer surgery stuck in the dark ages? A commentary piece reviewing surgical technologies. *British Journal of Cancer*. 123, 1471–1473 <https://doi.org/10.1038/s41416-020-01035-9>
16. M Volcke, A., Van Nieuwenhuysen E., Han S., Salihi R., Van Gorp T., Vergote I. (2021). Experience with PlasmaJet™ in debulking surgery in 87 patients with advanced-stage ovarian cancer. *Surgical Oncology* 123: 1109- 1114. <https://doi-org.tudelft.idm.oclc.org/10.1002/jso.26385>
17. Shah N. R. (2012). Commentary On: Surgical Smoke— A Health Hazard in the Operating Theatre: A Study to Quantify Exposure and a Survey of the Use of Smoke Extractor Systems in UK Plastic Surgery Units. *Annals of medicine and surgery*, 1, 23–24. [https://doi-org.tudelft.idm.oclc.org/10.1016/S2049-0801\(12\)70008-0](https://doi-org.tudelft.idm.oclc.org/10.1016/S2049-0801(12)70008-0)
18. Benson S.M., Novak D.A., Ogg M.J. (2013) Proper use of surgical n95 respirators and surgical masks in the operating room *Aorn Journal*; 97:457–67
19. Unal, D. (2023) Surgical aerosol measurement methods and particle concentration affecting factors in abdominal surgery: a systematic review
20. Kisch, T., Liodaki, E., Kraemer, R., Mailaender, P., Brandenburger, M., Hellwig, V., & Stang, F. H. (2015). Electrocautery Devices with Feedback Mode and Teflon-Coated Blades Create Less Surgical Smoke for a Quality Improvement in the Operating Room Theater. *Medicine*, 94(27), e1104. doi.org/10.1097/MD.0000000000001104
21. Cheng, PC., Wen, MH., Hsu, WL. et al. A study to quantify surgical plume and survey the efficiency of different local exhaust ventilations. 11, 14096 (2021). [/10.1038/s41598-021-92859-9](https://doi.org/10.1038/s41598-021-92859-9)
22. Karjalainen, M., Kontunen, A., Saari, S., Rönkkö, T., Lekkala, J., Roine, A., & Oksala, N. (2018). The characterization of surgical smoke from various tissues and its implications for occupational safety. *PloS one*, 13(4), e0195274. <https://doi.org/10.1371/journal.pone.0195274>
23. Ragde, S. F., Jørgensen, R. B., & Føreland, S. (2016). Characterization of Exposure to Ultrafine Particles from Surgical Smoke by Use of a Fast Mobility Particle Sizer. *The Annals of occupational hygiene*, 60(7), 860–874. <https://doi.org/10.1093/annhyg/mew033>
24. Wang, H. K., Mo, F., Ma, C. G., Dai, B., Shi, G. H., Zhu, Y., Zhang, H. L., & Ye, D. W. (2015). Evaluation of fine particles in surgical smoke from urologis's operating room by time and by distance. *International urology and nephrology*, 47(10), 1671–1678. <https://doi-org.tudelft.idm.oclc.org/10.1007/s11255-015-1080-3>
25. Kocher G, Sesia S., Lopez-Hilfiker F., & Schmid R. (2019) Surgical smoke: still an underestimated health hazard in the operating theatre, *European Journal of Cardio-Thoracic Surgery*, Volume 55, Issue 4, Pages 626–631, <https://doi-org.tudelft.idm.oclc.org/10.1093/ejcts/ezy356>
26. Watters D.A., Foran P., McKinley S., & Campbell G. (2022), Clearing the air on surgical plume: 57-61. <https://doi/10.1111/ans.17340>
27. Jones L. C. R., Parry M., Britton J., Tyrer J.R. (2021). Engineering controls for surgical smoke in laser medical handpieces, *Journal of Laser Applicaaions*, 33, 022007. [10.2351/7.0000360](https://doi.org/10.2351/7.0000360)
28. Graziani, F., Izzetti, R., Lardani, L., Totaro, M., & Baggiani, A. (2021). Experimental Evaluation of Aerosol Production after Dental Ultrasonic Instrumentation: An Analysis on Fine Particulate Matter

Perturbation. *International Journal of Environmental Research and Public Health*, 18(7), 3357. MDPI AG. Retrieved from <http://dx.doi.org/10.3390/ijerph18073357>

29. Schraufnagel D. E. (2020). The health effects of ultrafine particles. *Experimental & molecular medicine*, 52(3), 311–317. <https://doi.org/10.1038/s12276-020-0403-3>
30. Ragde, S. F., Jørgensen, R. B., & Føreland, S. (2016). Characterization of Exposure to Ultrafine Particles from Surgical Smoke by Use of a Fast Mobility Particle Sizer. *The Annals of occupational hygiene*, 60(7), 860–874. <https://doi.org/10.1093/annhyg/mew033>
31. Wang, H. K., Mo, F., Ma, CG. (2015). Evaluation of fine particles in surgical smoke from an urologist's operating room by time and by distance. *Int Urol Nephrol* 47, 1671–1678 <https://doi.org/10.1007/s11255-015-1080-3>
32. Shah N. R. (2012). Commentary On: "Surgical Smoke - A Health Hazard in the Operating Theatre: A Study to Quantify Exposure and a Survey of the Use of Smoke Extractor Systems in UK Plastic Surgery Units". *Annals of medicine and surgery*, 1, 23–24. [https://doi.org/10.1016/S2049-0801\(12\)70008-0](https://doi.org/10.1016/S2049-0801(12)70008-0)
33. Hahn, K. Y., Kang, D. W., Azman, Z. A. M., Kim, S. Y., & Kim, S. H. (2017). Removal of Hazardous Surgical Smoke Using a Built-in-Filter Trocar: A Study in Laparoscopic Rectal Resection. *Surgical laparoscopy, endoscopy & percutaneous techniques*, 27(5), 341–345. [/doi-org/10.1097/SLE.0000000000000459](https://doi.org/10.1097/SLE.0000000000000459)
34. Searle, T., Ali, F.R. Al-Niaimi, F. (2020), Surgical plume in dermatology: an insidious and often overlooked hazard. *Clinical and Experimental Dermatology*, 45: 841-847. <https://doi/10.1111/ced.14350>
35. Liu, G., Mugo, N. R., Brown, E. R., Mgodhi, N. M., Chirenje, Z. M., Marrazzo, J. M., Winer, R. L., Mansoor, L., Palanee-Phillips, T., Siva, S. S., Naidoo, L., Jeenarain, N., Gaffoor, Z., Nair, G. L., Selepe, P., Nakabiito, C., Mkhize, B., Mirembe, B. G., Taljaard, M., Panchia, R.; Barnabas, R. V. (2022). Prevalent human papillomavirus infection increases the risk of HIV acquisition in African women: advancing the argument for human papillomavirus immunization. 36(2), 257–265. <https://doi.org/10.1097/QAD.0000000000003004>
36. Hoskin, J.C., Dimick, P.S. (1995). Non-enzymatic browning of foods. In: Beckett, S.T. (eds) *Physico-Chemical Aspects of Food Processing*. Springer, Boston, MA. https://doi.org/10.1007/978-1-4613-1227-7_4
37. Schreiber, J., Brüggmann, D., Braun, M. (2022). The measuring aerosol spreading during countermeasures (MASC) study presents an automated system to investigate face mask efficacy and other aerosol countermeasures in varying environments. *Sci Rep* 12, 21349 <https://doi.org/10.1038/s41598-022-25210-5>
38. Canicoba A. R. B. (2022). Surgical smoke and occupational health. *Annals of translational medicine*, 10(24), 1303. <https://doi.org/10.21037/atm-22-5631>
39. Research & Compare Materials. (2009). Polycarbonate versus PMMA makeitfrom.com/compare/PC/Polymethylmethacrylate-PMMA-Acrylic

Appendix A – Design methodology, and design evaluation

A.1 Background design

In 2020, an experimental setup to evaluate the aerosol production of PJ and ERBE devices was built as shown in Figure A.1. The experimental box of the previous design consists of PMMA plates (1) with metal edges (2), the entrance holes for the support arm (3), the particle counter with a foam cast (4), a support arm (5), and a counterweight (6) to carry the weight of the medical device handpiece. Moreover, in the previous design, 3D-printed parts were produced for the experimental test setup (7) and the experimental tissue sample was also fixated on the tissue sample holder (8).

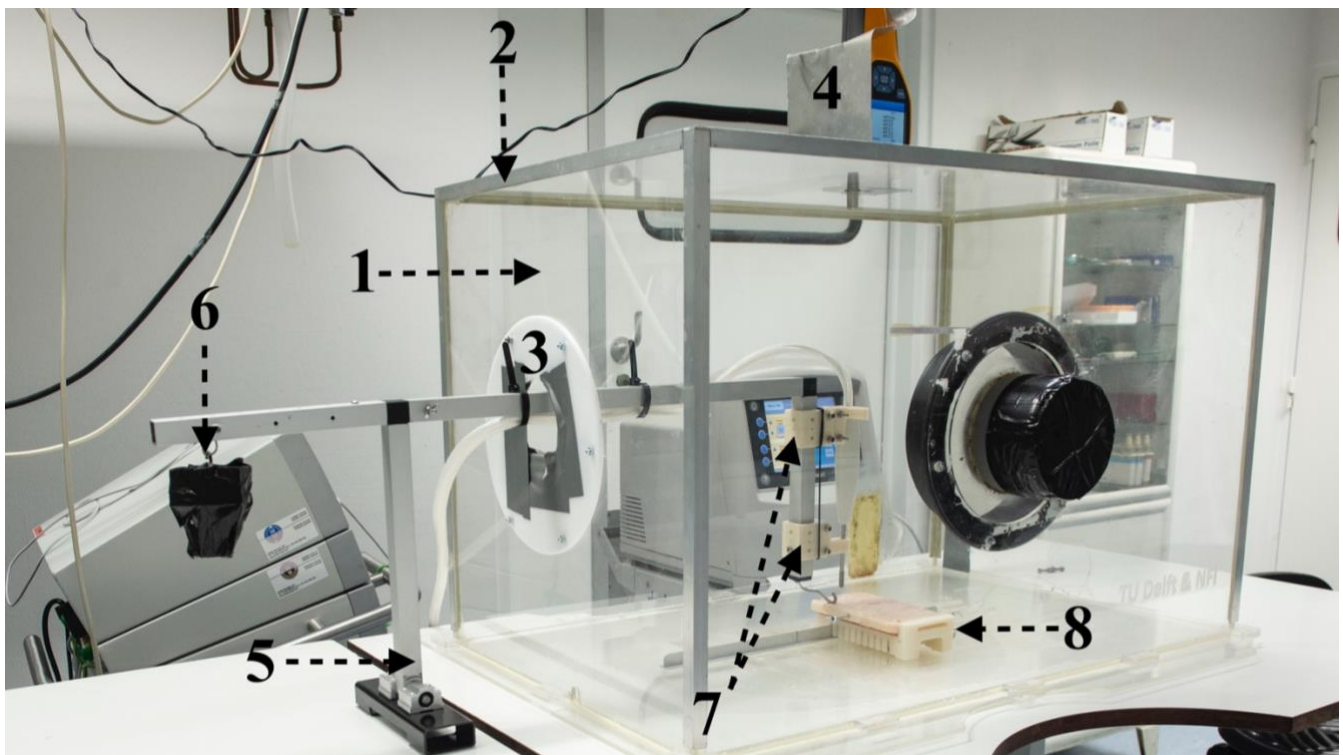


Figure A.1 – The experimental box of the previous design consists of transparent PMMA plates (1), metal box edges (2), entrance holes (3), a particle counter with a foam cast (4), a support arm (5), counterweight (6), medical device test setup (7) and tissue sample holder (8).

The preliminary design needed improvements such as enhancing the durability of the experimental box with different plate material that has higher tensile strength [39]. Additionally, there was a need for increased airflow minimization, new medical device setup parts, and the implementation of an automated tissue sample holder movement to ensure the consistency of experimental runs. The experimental box design requirements in [Chapter 4.2](#) were developed according to these guidances.

A.2 Design methodology

In order to comply with the design requirements in [Chapter 4.2](#), a new experimental box with new test setup components was produced. This section provides more in-depth details on the design methodology including the setup for evaluating the tissue effects. The experimental box design phase was covered

during the internship period. The experimental design phase was first initiated by cutting the faces of a 40 x 60 x 80 cm PP box (see Figure A.2) with a jig sawing tool and then embedding the laser-cut transparent plates into the box. Subsequently, as illustrated in Figure A.3, the entrance areas for the support arm and guiding rail were covered with rubber sheets and laser-cut cover plates (9) to minimize airflow. The particle counter holder with a rubber sheet (10) and the locks and hinges (11) were also bolted to the box and the lid for preparation of the smoke test to evaluate the airflow disturbances.

Tissue effects setup

To achieve consistent tissue surface scans and reliable mean brightness assessment on MATLAB, a two-point spotlight setup at a 45-degree angle from the tissue sample was built.

As shown in Figure A.4, a two-point spotlight setup (12) was mounted on a configuration of aluminum extrusion profiles (13) combined with connection elements. The tissue sample was placed on the gray shooting backdrop (14) and the tissues were scanned after the experiments on the tissue sample is completed. The surface scans of experimental tissue samples can be found in [Appendix D](#).

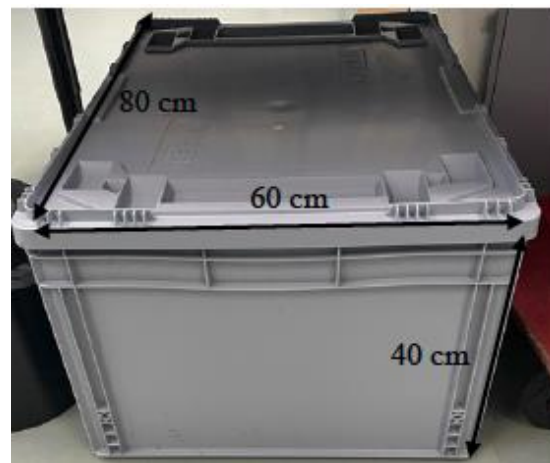


Figure A.2 – The 40x60x80 cm PP box before the faces removed



Figure A.3 – The experimental box with laser cut cover plates (9), particle counter holder with a rubber sheet (10), and the locks and hinges (11).

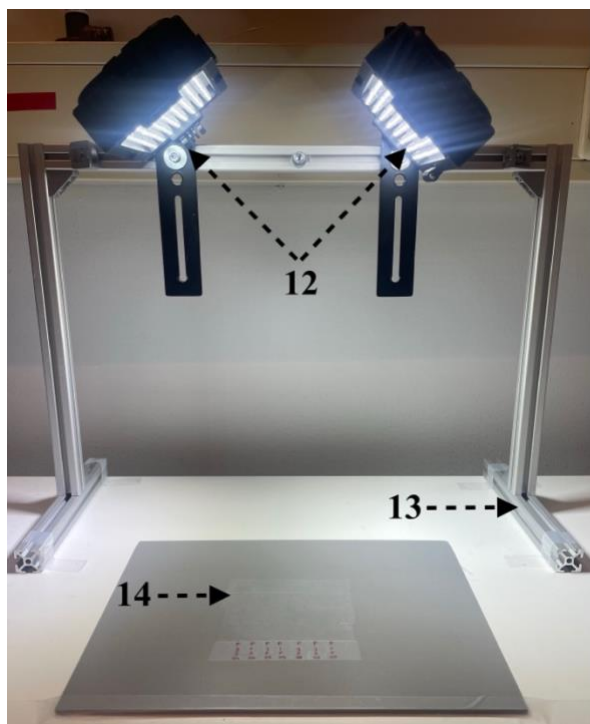


Figure A.4 – Two-point spotlight setup (12) was mounted on an aluminum extrusion profile (13). The gray shooting backdrop (14) was used as a tissue scan surface.

A.3 Design evaluation

At the end of the internship period, a smoke test was conducted to evaluate and observe visually perceptible leakage by placing a smoke bomb into the experimental box in a ceramic cup as shown in Figure A.5. The smoke test resulted in slight leakage from the locks and hinges at the top of the box. The results were considered sufficient enough to measure particle counts since the amount of produced smoke would be comparatively lower than a smoke bomb.

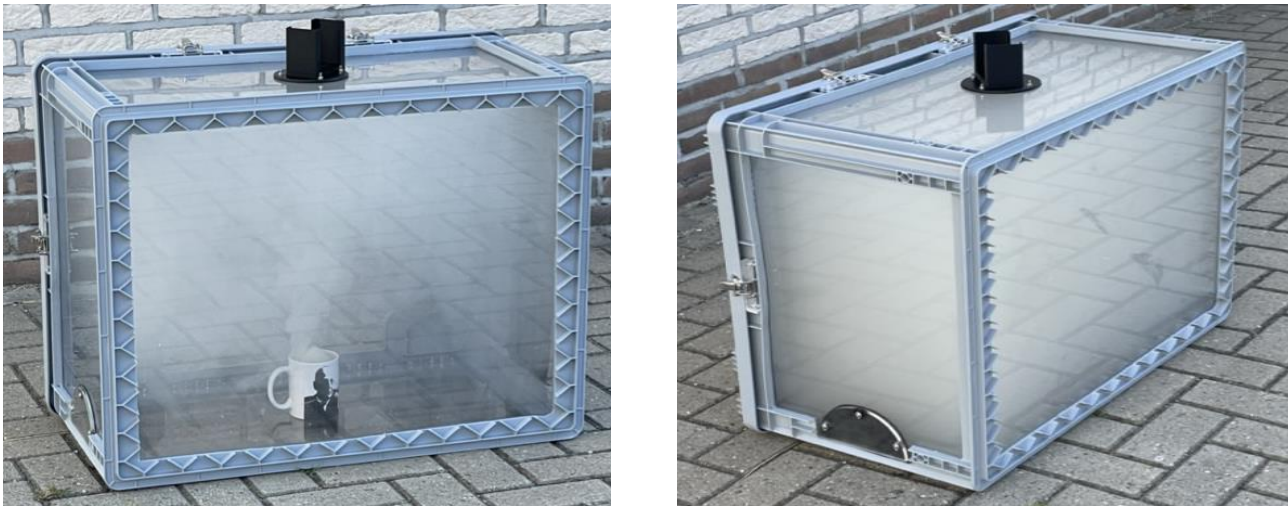


Figure A.5 – The smoke bomb was placed in a ceramic cup, and the bomb was ignited (left). A minute after, the box was filled with smoke, and the visually perceptible leakage points were observed (right).

Following the experimental box design, pilot tests were conducted to evaluate the experimental design requirements in [Chapter 3.1](#). The satisfaction rates of the experimental requirements can be found in Table A.1. Except for the leakage minimization, all criteria were satisfied.

Table A.1 – Evaluation of the experimental box design requirements for PJ and ERBE experiments. Yellow indicates an acceptable result with minor defects while green indicates a successful requirement completion.

Criteria	Description	Satisfaction
Leakage minimization	No visually perceptible leakage	Slight leakage from the top of the box. Sufficient to continue according to the supervisors.
Height	40 cm distance between the particle counter and aerosol generation source	Yes, the particle counter was placed 40 cm from the aerosol generation source.
Balance	Balanced medical device weight with a counterweight	The weight of the medical device handpiece was successfully balanced.
Automatic execution	A repeatable functioning system to pull the tissue sample holder automatically with a 10-sec duration for a 5 cm cut	A remote and automated tissue sample operation was performed with the use of a stepper motor and UGS.
Cleanability	Limited edges/ridges of the setup components and the experimental box	The experimental box was cleaned and the particles were vacuumed properly.
User friendly	Visible particle counter screen and adjustable test setup components	The particle counter screen was visible during the experiments and the setup was easy to adjust.

Appendix B – Experimental protocol

B.1 List of Materials

For detailed information on off-the-shelf parts, see [Appendix H](#).

- PJ generator
- PJ handpiece
- ICC 50 ERBE- generator
- ERBE handpiece
- Particle counter, Fluke 985
- Plant-based tissue samples
- Arduino Uno
- Arduino CNC shield
- Stepper motor
- Latex gloves
- N95 surgical masks
- Monopolar Return pad
- Microswitch
- Footswitch

B.2 Step-by-step protocol

Step 1. Take out the tissue sample from the fridge 15 min before experiments.

Step 2. Fasten the stepper motor onto the Arduino with a CNC shield and link it to a computer and a power source.

Step 3. Open the Gcode platform on a computer and set the speed with the step sizer.

Step 4. Connect the medical device to the corresponding PJ/ERBE generator.

Step 5. Connect the (PJ/ERBE) generator power cord to the power socket.

Step 6. Power the medical device generator and plug the handpiece into the generator's handpiece socket.

Extra steps for ERBE setup;

Step6.1 Plug the footswitch into the back of the ERBE generator.

Step6.2 Fixate the monopolar return pad to the tissue sample holder and plug its adapter into the ERBE neutral electrode socket.

Step 7. Set the intended experimental conditions, such as power, speed, and mode.

Step 8. Place and fixate the tissue sample onto the tissue sample holder (For PJ).

Step 8.1 Fasten the tissue sample onto the monopolar return pad (For ERBE).

Step 9. Set the handpiece distance from the tissue sample. For PJ handpiece distance adjustment, use a spacer.

Step 10. Insert the particle counter into the particle counter holder.

Step 11. Close the experimental box lid and lock the clamps.

Step 12. Conduct the measurements;

Count the aerosols continuously for 3 minutes by using Fluke 985 particle counter.

M0: Start counting the base measurement for 60 s with Fluke 985 for residual aerosols from previous tests or the room.

M1: Start counting aerosols for the 60 s.

Simultaneously, ablate, cut, or coagulate the tissue sample by stepping on the medical device's footswitch to control its handpiece.

Simultaneously, press X+ on the Gcode platform to move the experimental tissue bed with the intended speed of 0.25 cm/s and 0.5 cm/s for 20 s and 10 s respectively.

M2: Continue counting the residual aerosols for another 60 s.

Step 13. Remove the particle counter from the holder and note down the temperature, aerosol counts, and sizes.

Step 14. Open the experimental box to clean the box and the device's handpiece and vacuum the residual aerosols.

Step 15. Change the position of the experimental tissue bed on the guiding rail.

Step 16. Update the independent variables such as power, mode, speed, and surgical exposure time.

Step 17. After the experiment, filter the existing aerosols in the box with the manufacturer's filter to prevent counting the residual particles.

Step 18. Start from Step 9 to repeat the remaining experiments.

Appendix C – List randomization

Table C.1: *Randomized block experiment list of the ERBE device for the experimental conditions; EIF, E1S, E3F, and E3S with 10 repetitions.*

There were 40 items in your list. Here they are in random order:

1. E1S01
2. E1S06
3. E1S10
4. E3S08
5. E3F06
6. E3S06
7. E1S07
8. E1S04
9. E3F08
10. E3F09
11. E3S01
12. E3S04
13. E1F07
14. E1F02
15. E1S03
16. E1F10
17. E1F08
18. E1S02
19. E3S02
20. E3F05
21. E3F03
22. E1F05
23. E3F01
24. E1F09
25. E3F10
26. E1S09
27. E3S05
28. E3S10
29. E3F07
30. E3F02
31. E1F06
32. E3S07
33. E1F01
34. E3F04
35. E3S03
36. E1F03
37. E1S08
38. E1S05
39. E1F04
40. E3S09

IP: 2001:1c00:b11:3500:1096:a34c:8eaf:414

Timestamp: 2023-04-16 17:35:21 UTC

Table C.2: *Randomized block experiment list of the PJ device for the experimental conditions; P1F, P1S, P3F, and P3S with 10 repetitions.*

There were 40 items in your list. Here they are in random order:

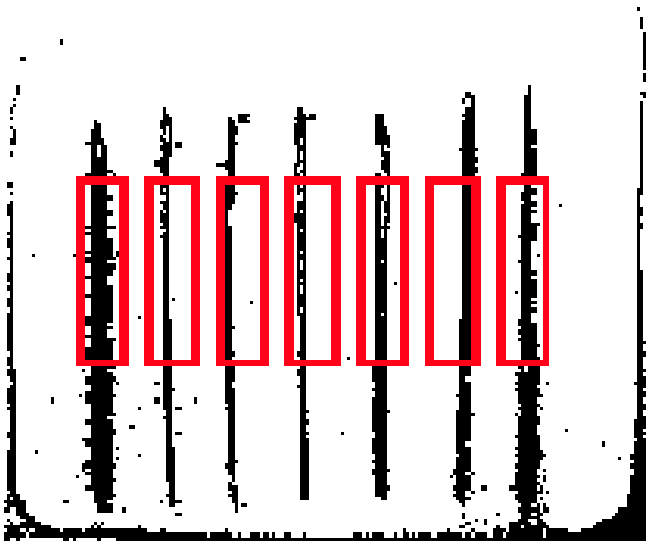
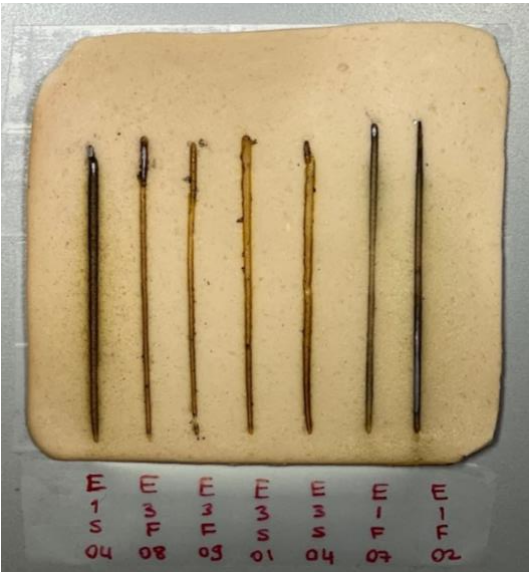
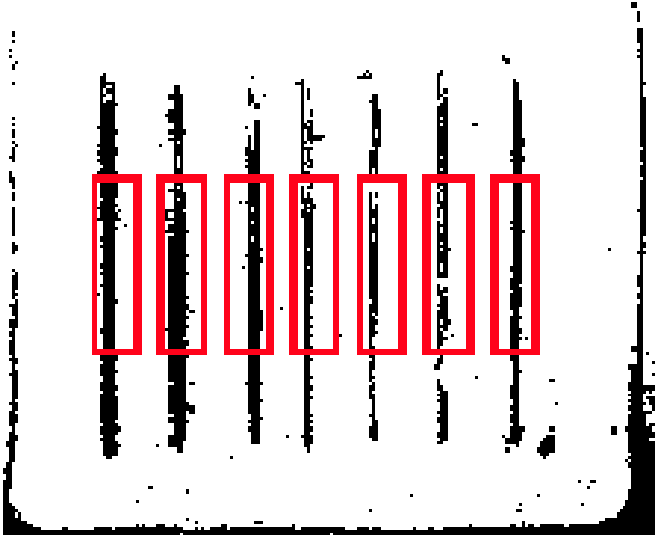
1. P1F06
2. P3F02
3. P1S05
4. P3F03
5. P1S01
6. P3S07
7. P3S10
8. P1S10
9. P1F03
10. P1S07
11. P3S05
12. P1S09
13. P3F08
14. P1F05
15. P3S08
16. P3F06
17. P3F10
18. P1S08
19. P3F07
20. P3F01
21. P3F09
22. P1S03
23. P1F02
24. P3S01
25. P1S04
26. P3S02
27. P1F01
28. P1F08
29. P3S06
30. P3F04
31. P1S02
32. P1F07
33. P1F10
34. P3S04
35. P1S06
36. P3F05
37. P1F04
38. P3S09
39. P3S03
40. P1F09

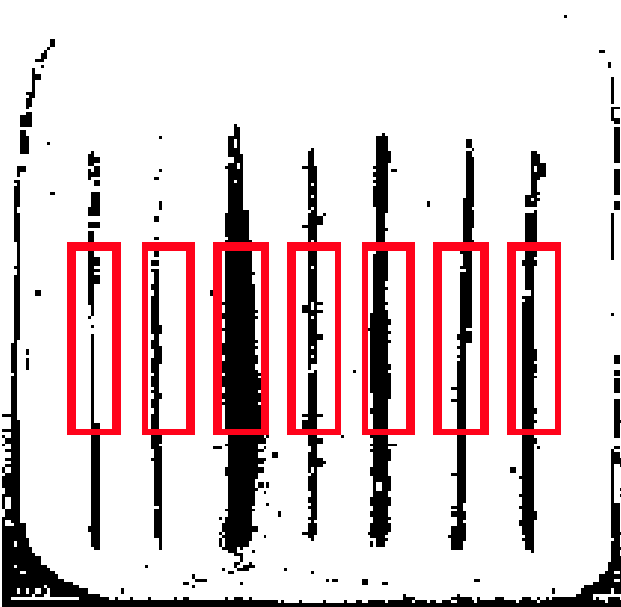
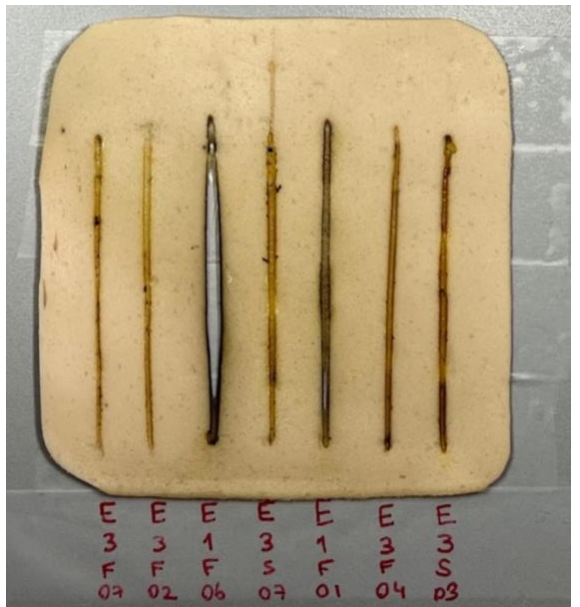
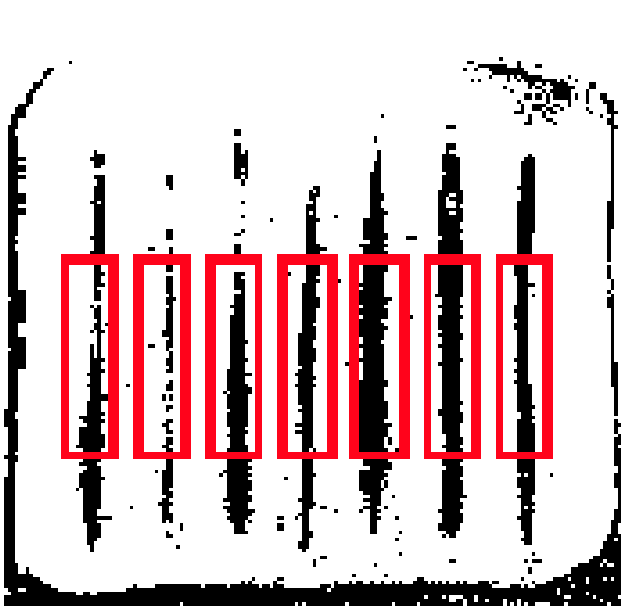
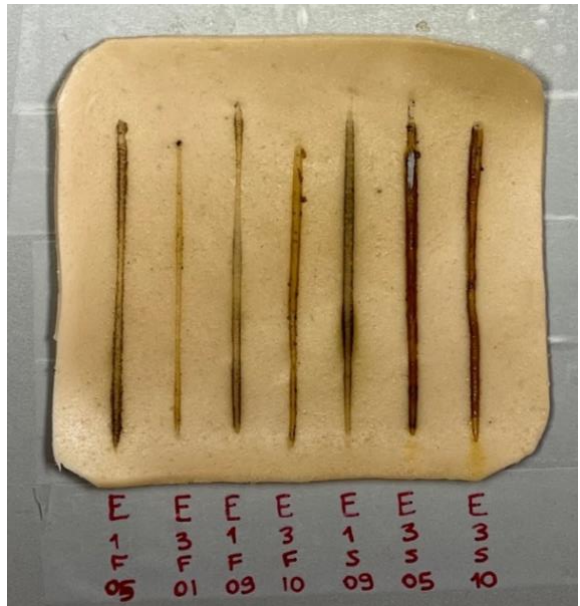
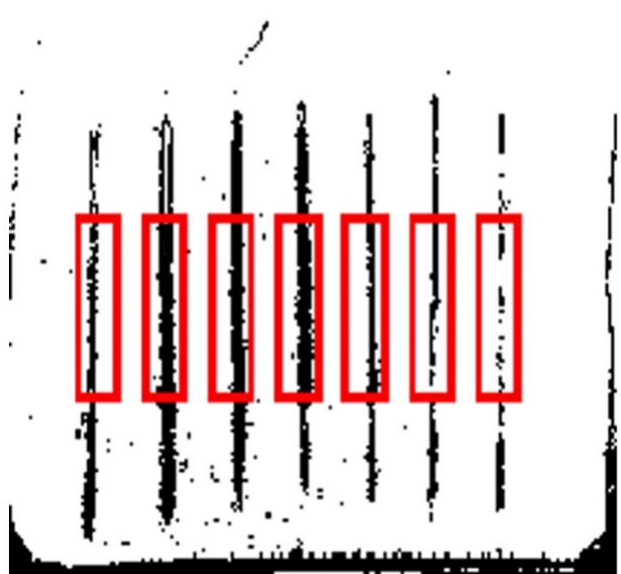
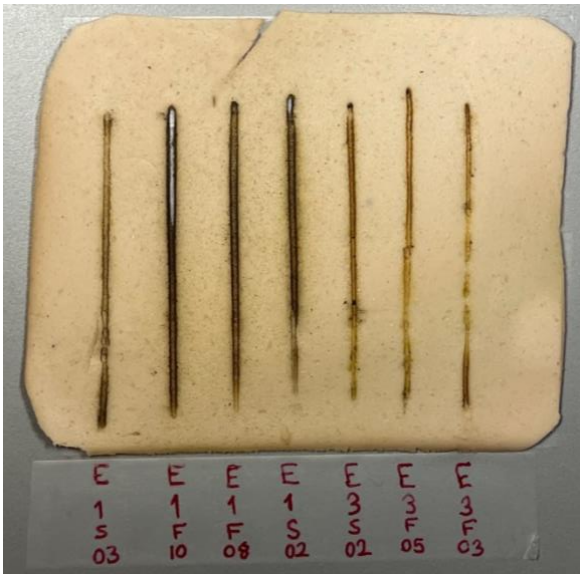
IP: 145.94.212.230

Timestamp: 2023-04-17 09:29:50 UTC

Appendix D – Tissue effects

D.1 ERBE experiments:





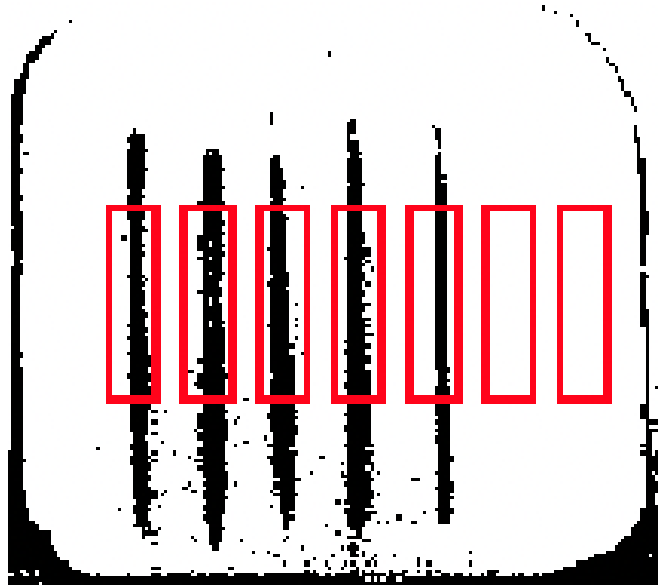
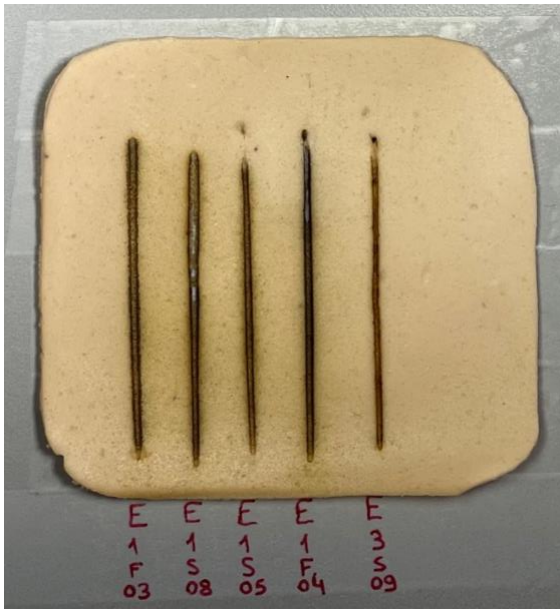
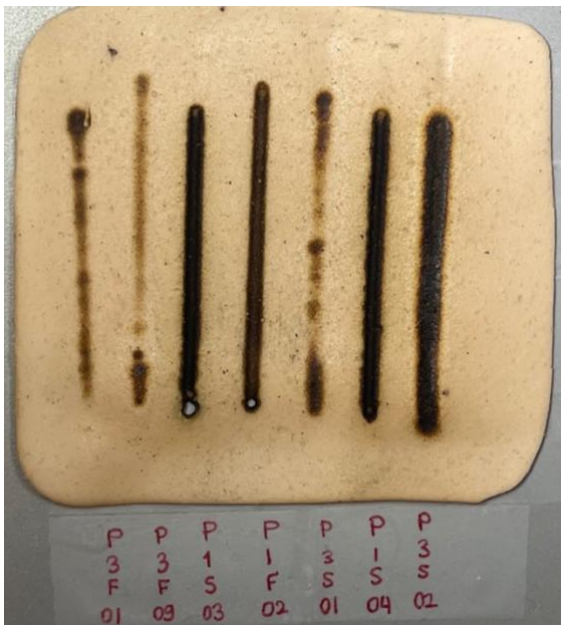
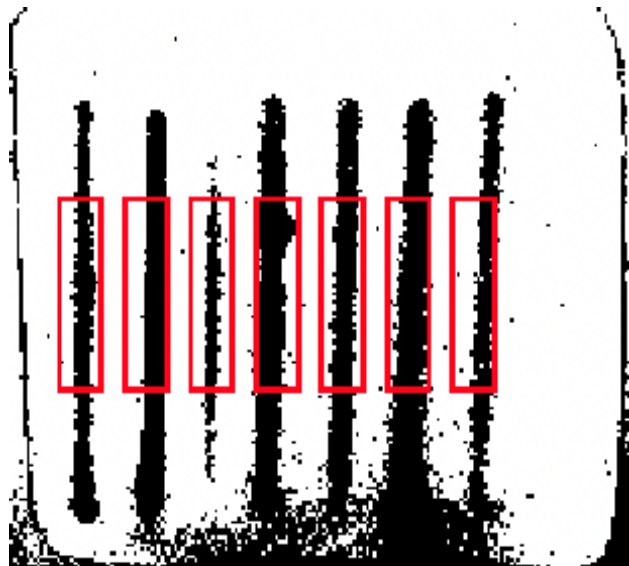
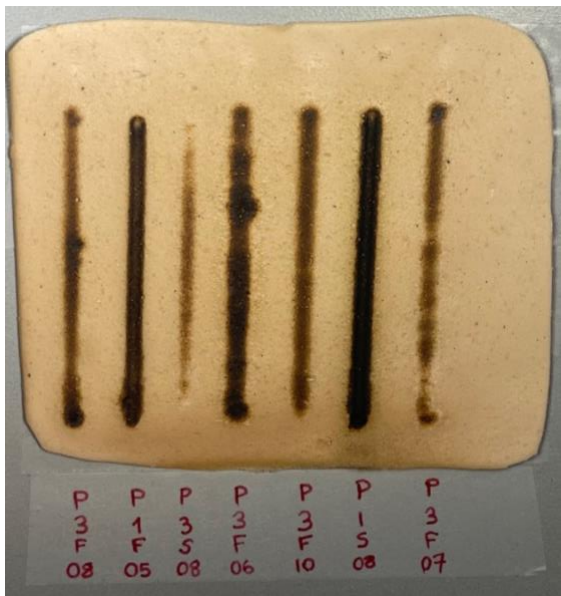
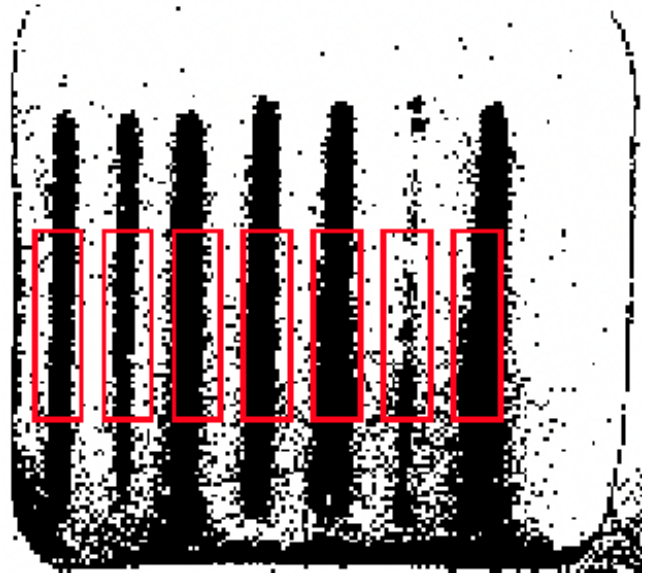
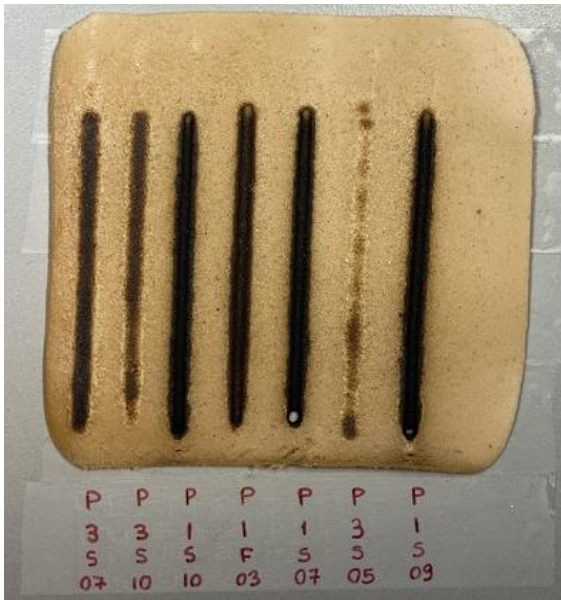


Figure D.1 – The surface scans of tissue effects (left) and MATLAB edited black-and-white versions (right) to quantify the brightness of each ERBE experimental run. The experimental order was according to the list randomization in Table C.1. Note that the cut-through areas of tissues (see experimental run, E1F06) were filled with pixel growth on Adobe Illustrator, 2022.

D.2 PJ Experiments:





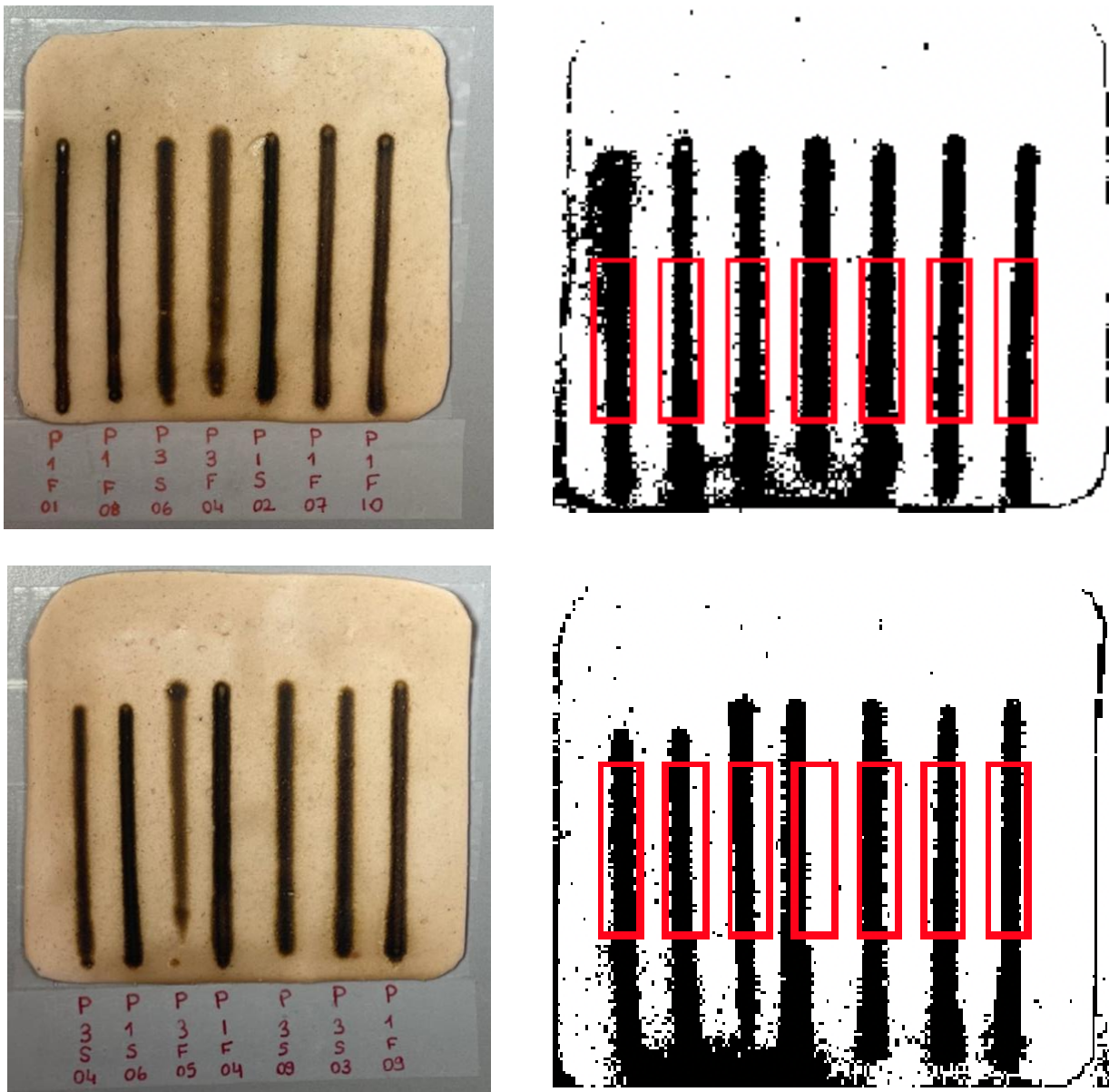


Figure D.2 – The surface scans of tissue effects (left) and MATLAB edited black-and-white versions (right) to quantify the brightness of each PJ experimental run. The order of the experimental runs was according to the list randomization in Table C.2. Note that for cuts that did not fit within the selected area, a separate region of interest with a separate MATLAB code was defined (see experimental run, P1F04 in the last image).

D.3 Brightness values and particle counts of ERBE experiments:

Table D.1 – Brightness values and particle counts of each ERBE experimental run

Condition	Brightness [0 -1]	ERBE [particles/cfm/mm]
E1F01	0.6297	81851
E1F02	0.6851	109707
E1F03	0.6313	91334
E1F04	0.5545	83713
E1F05	0.7254	60924
E1F06	0.2759	106206
E1F07	0.7894	107693
E1F08	0.6523	84035
E1F09	0.7152	69573
E1F10	0.6329	94339
E1S01	0.6841	98423
E1S02	0.5906	66169
E1S03	0.7976	36134
E1S04	0.5091	95280
E1S05	0.5896	79918
E1S06	0.5964	81623
E1S07	0.7353	81902
E1S08	0.5358	78493
E1S09	0.4753	97814
E1S10	0.7489	86562
E3F01	0.8631	73948
E3F02	0.8377	67952
E3F03	0.9291	65630
E3F04	0.7703	70313
E3F05	0.8584	38048
E3F06	0.8348	65464
E3F07	0.8737	62298
E3F08	0.8091	65014
E3F09	0.8385	53354
E3F10	0.6801	79791
E3S01	0.7921	85844
E3S02	0.7803	46212
E3S03	0.7577	74120
E3S04	0.7624	65386
E3S05	0.6088	84517
E3S06	0.8251	77185
E3S07	0.7504	59270
E3S08	0.7765	46996
E3S09	0.7618	69406
E3S10	0.6855	88010

D.4 Brightness values and particle counts of PJ experiments:

Table D.2 – Brightness values and particle counts of each PJ experimental run

Condition	Brightness [0-1]	PJ [particles/cfm/mm]
P1F01	0.3052	55780
P1F02	0.4698	43128
P1F03	0.2516	83159
P1F04	0.3521	54873
P1F05	0.5174	43060
P1F06	0.4962	78550
P1F07	0.4166	37534
P1F08	0.4502	55518
P1F09	0.4720	38100
P1F10	0.4654	39739
P1S01	0.3412	91391
P1S02	0.3313	64372
P1S03	0.3694	49828
P1S04	0.3789	72230
P1S05	0.4122	77361
P1S06	0.4177	52263
P1S07	0.1532	90075
P1S08	0.3120	72447
P1S09	0.1809	91166
P1S10	0.2721	84518
P3F01	0.6923	1212
P3F02	0.7623	2712
P3F03	0.6831	2772
P3F04	0.2670	3953
P3F05	0.4533	2734
P3F06	0.3320	1933
P3F07	0.5876	4086
P3F08	0.5690	3290
P3F09	0.8415	832
P3F10	0.4940	4032
P3S01	0.7633	1386
P3S02	0.3002	13438
P3S03	0.4295	12706
P3S04	0.3738	4805
P3S05	0.6299	12471
P3S06	0.3427	6878
P3S07	0.4435	6744
P3S08	0.6875	9221
P3S09	0.3845	9816
P3S10	0.4955	5953

Appendix E – Experimental data

E.1 ERBE data of each repetition

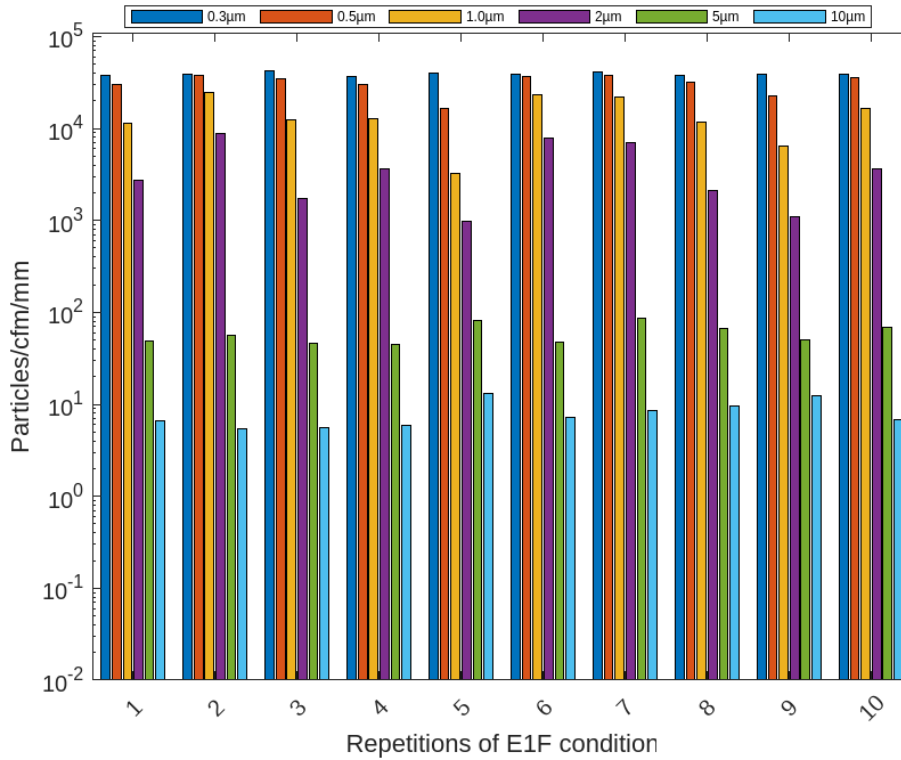


Figure E.1 – The number of aerosol particles [particles/cfm/mm] for each particle size and each repetition of the ‘E1F’ condition. Note that, the Y-axis is in the logarithmic scale.

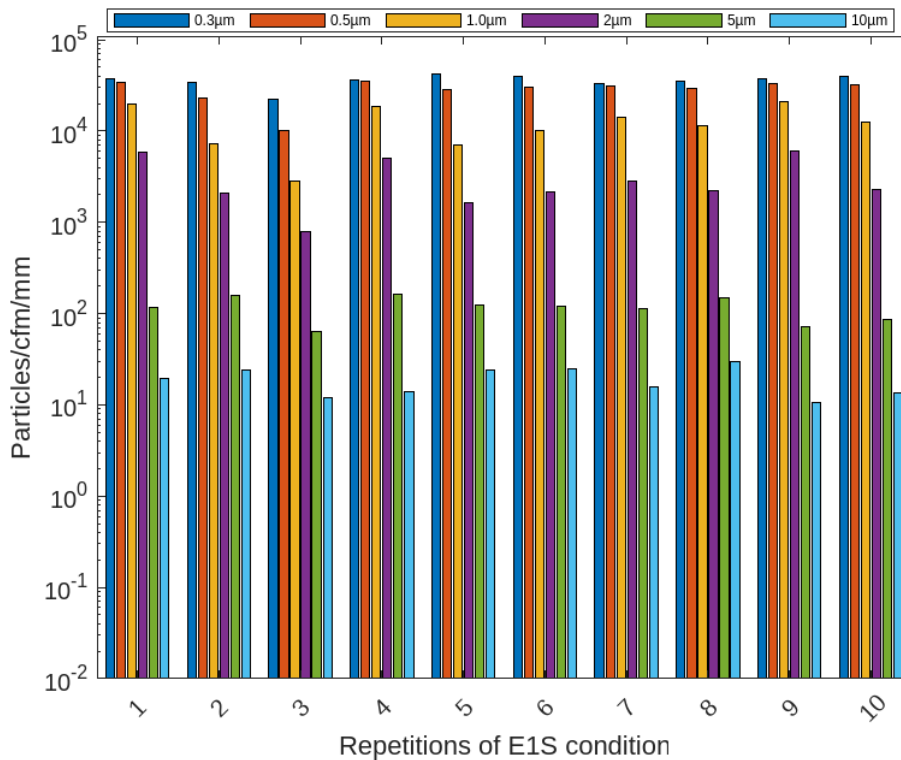


Figure E.2 – The number of aerosol particles [particles/cfm/mm] for each particle size and each repetition of the ‘E1S’ condition. Note that, the Y-axis is in the logarithmic scale.

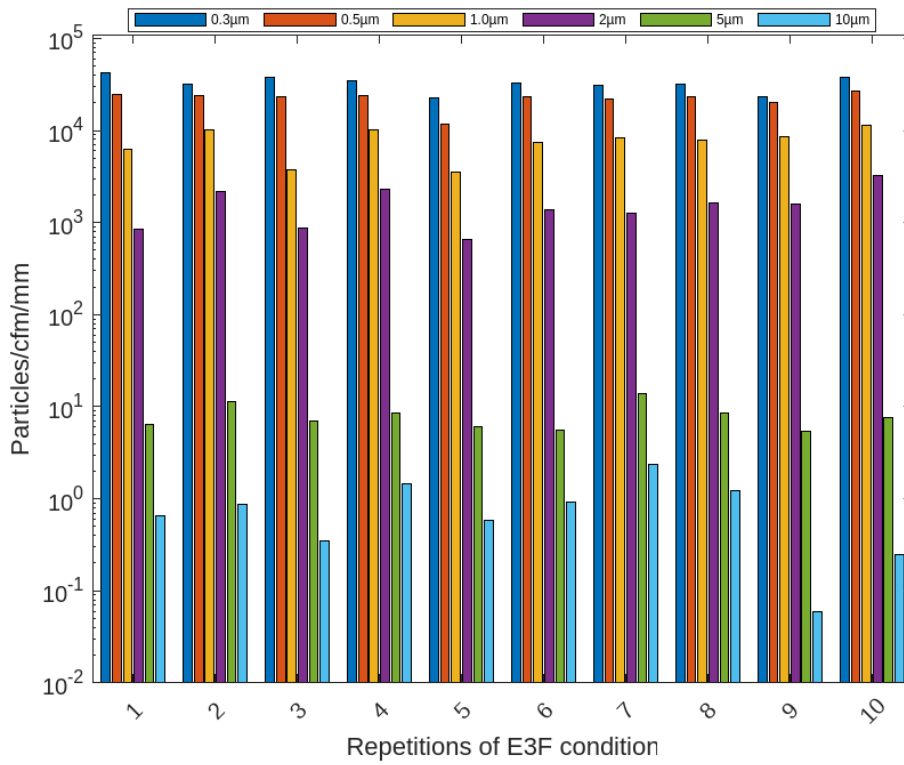


Figure E.3 – The number of aerosol particles [particles/cfm/mm] for each particle size and each repetition of the ‘E3F’ condition. Note that, the Y-axis is in the logarithmic scale.

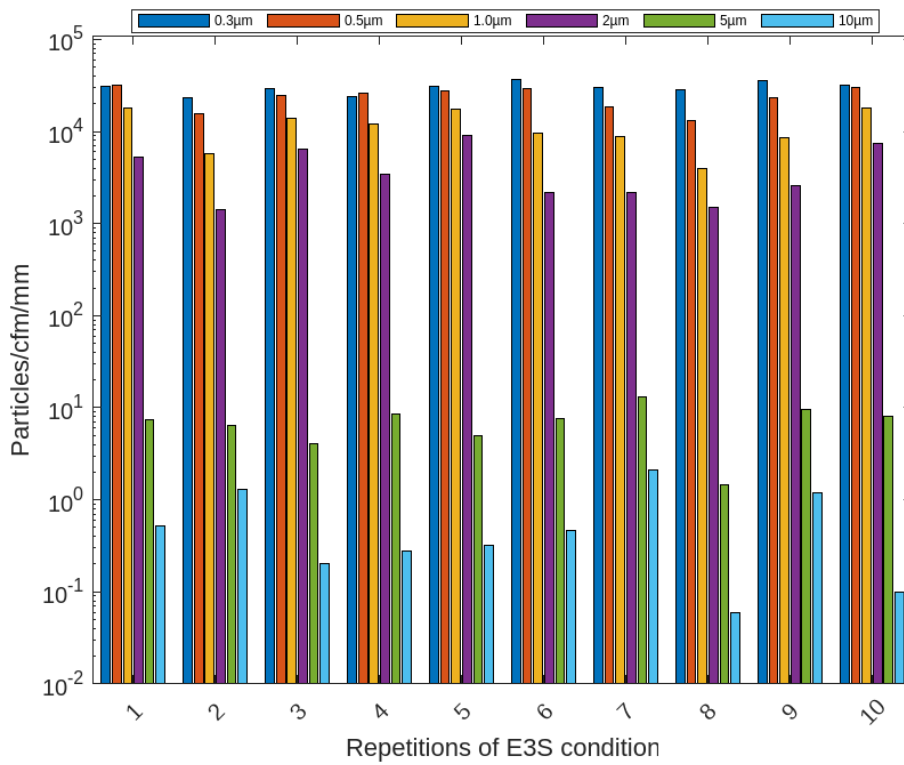


Figure E.4 – The number of aerosol particles [particles/cfm/mm] for each particle size and each repetition of the ‘E3S’ condition. Note that, the Y-axis is in the logarithmic scale.

E.2 PJ data of each repetition

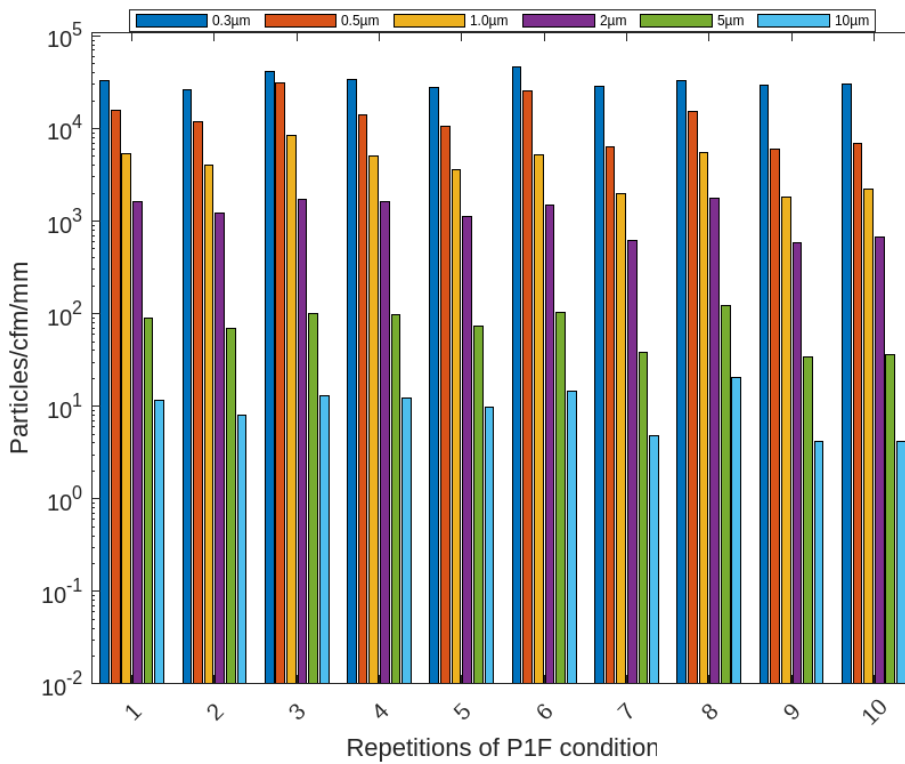


Figure E.5 – The number of aerosol particles [particles/cfm/mm] for each particle size and each repetition of the ‘P1F’ condition. Note that, the Y-axis is in the logarithmic scale.

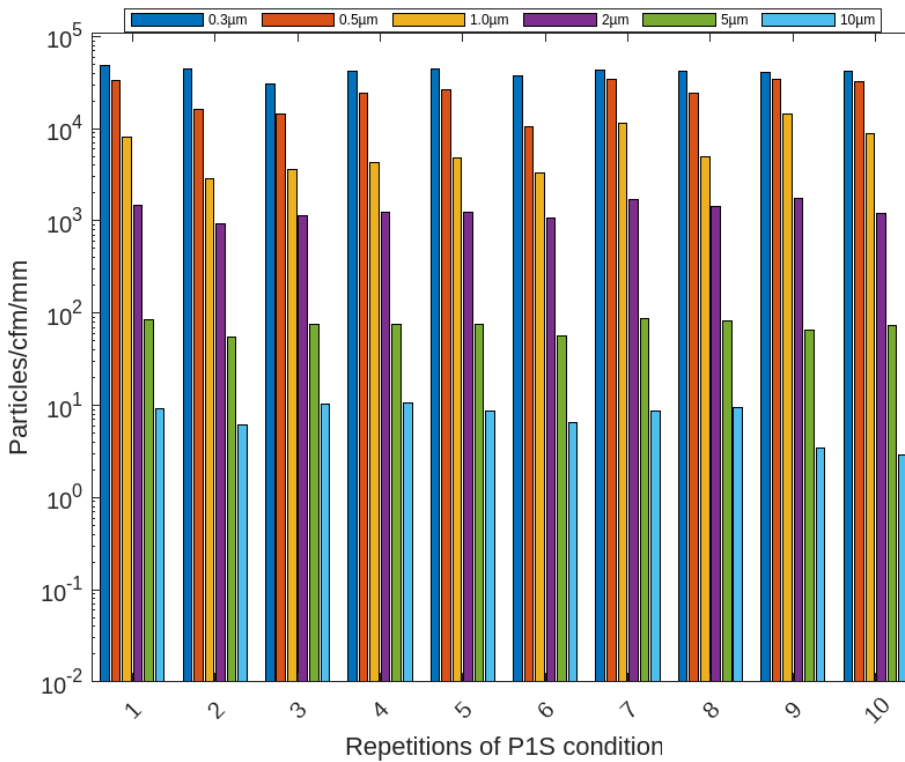


Figure E.6 – The number of aerosol particles [particles/cfm/mm] for each particle size and each repetition of the ‘P1S’ condition. Note that, the Y-axis is in the logarithmic scale.

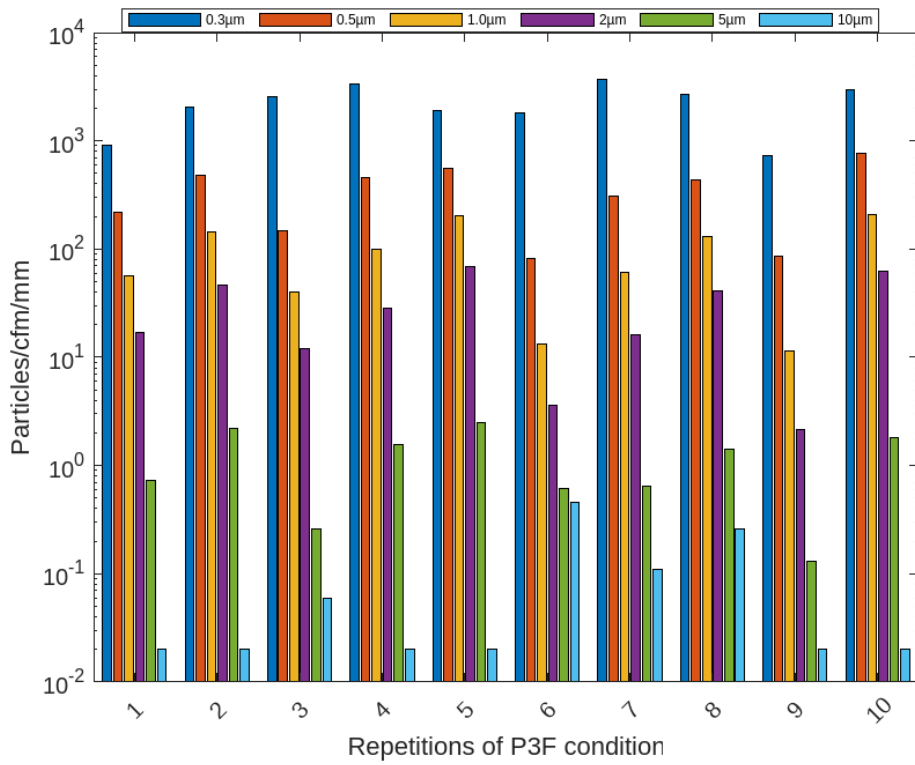


Figure E.7 – The number of aerosol particles [particles/cfm/mm] for each particle size and each repetition of the ‘P3F’ condition. Note that, the Y-axis is in the logarithmic scale.

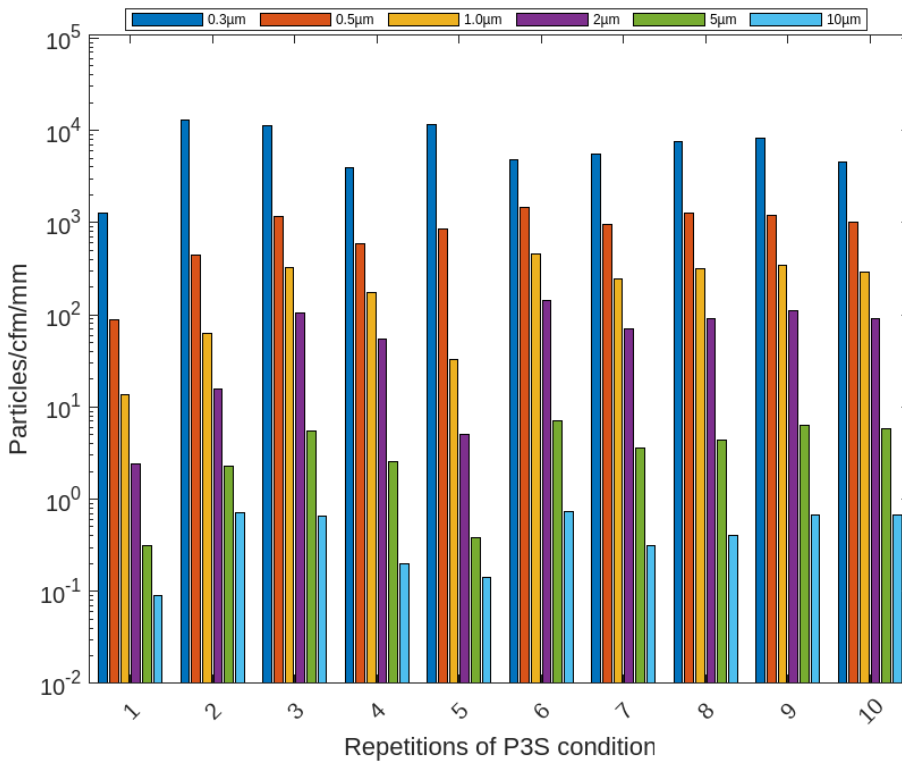
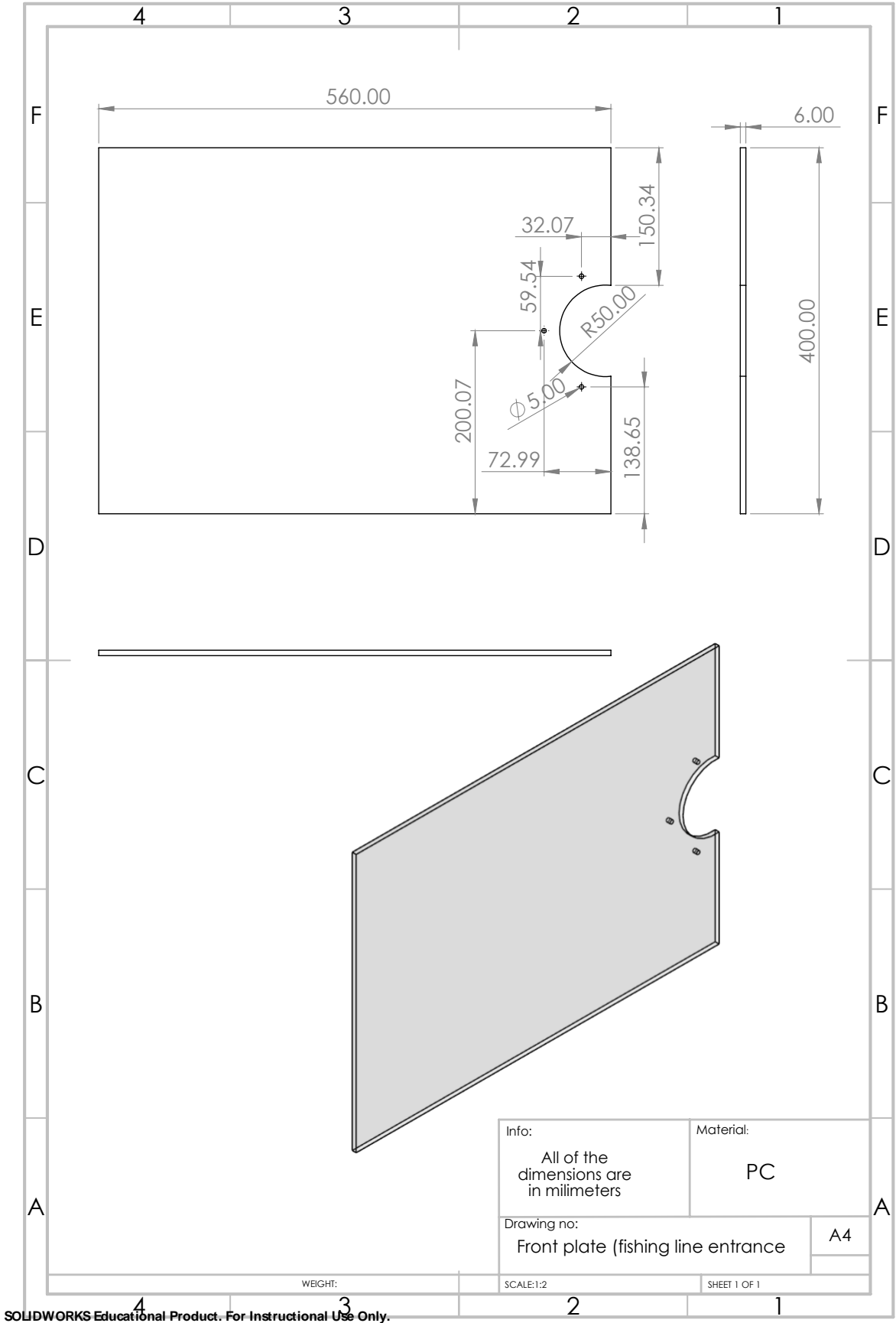
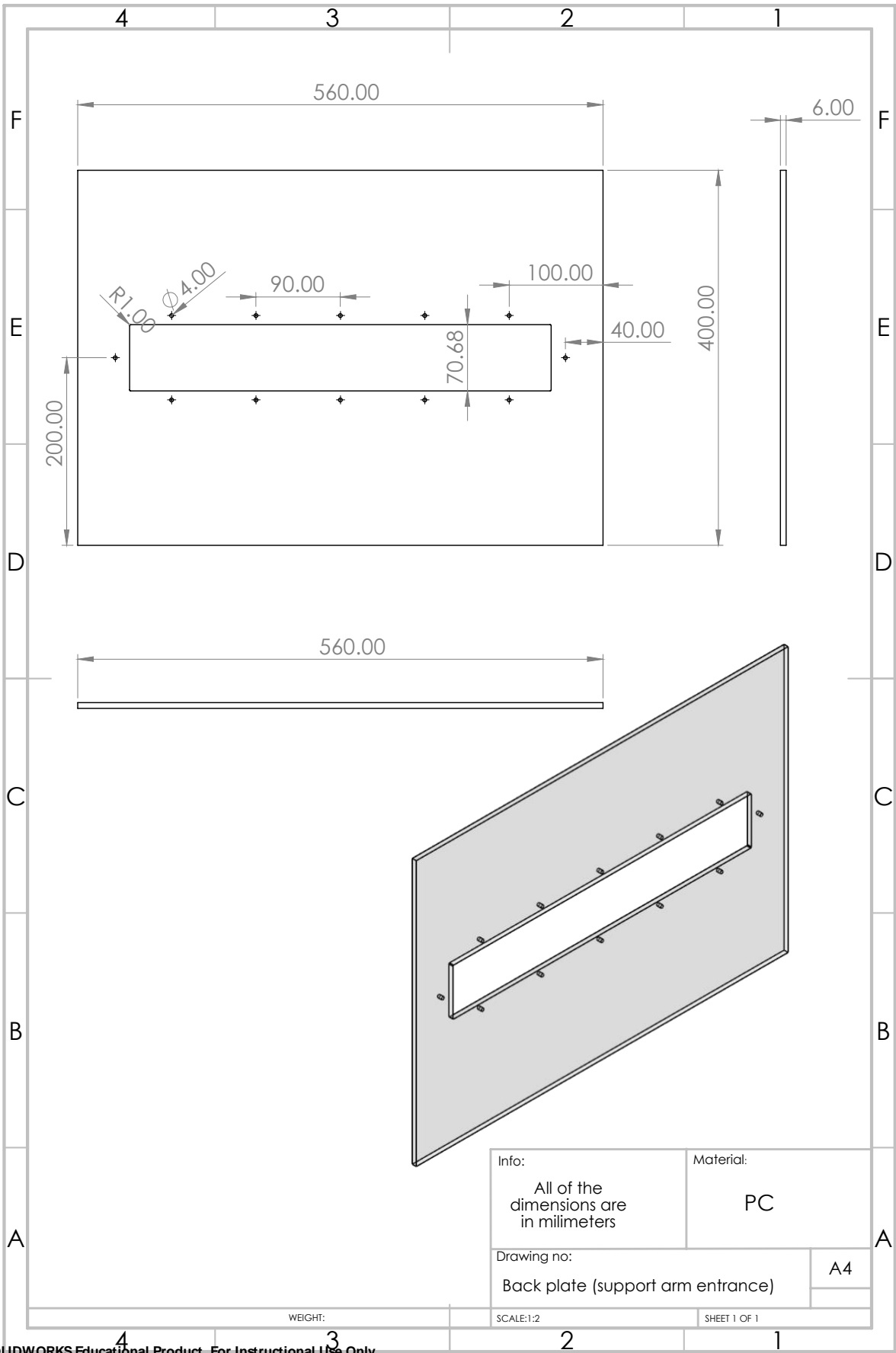


Figure E.8 – The number of aerosol particles [particles/cfm/mm] for each particle size and each repetition of the ‘P3S’ condition. Note that, the Y-axis is in the logarithmic scale.

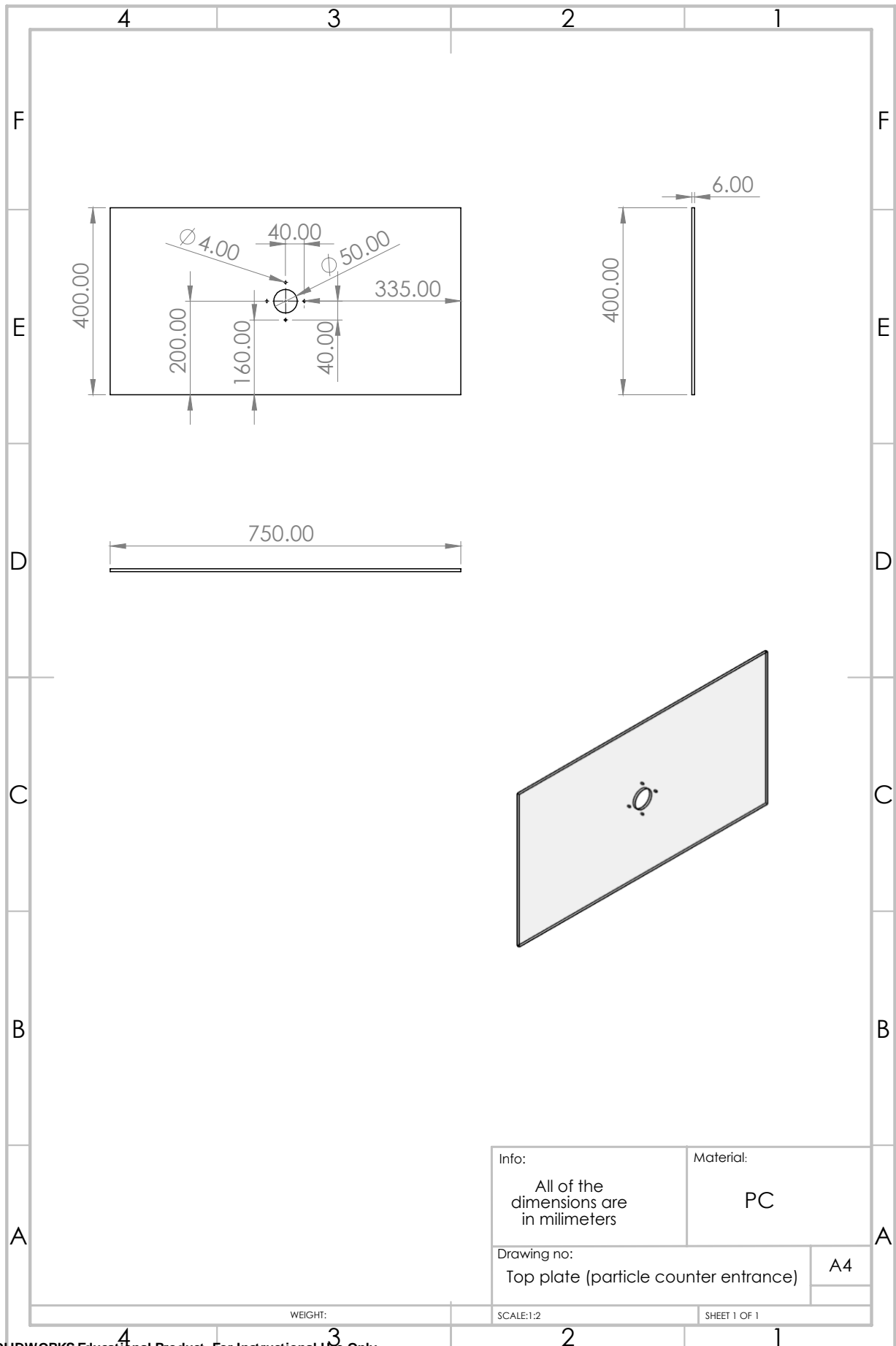
Appendix F – Technical drawings

Experimental box plates

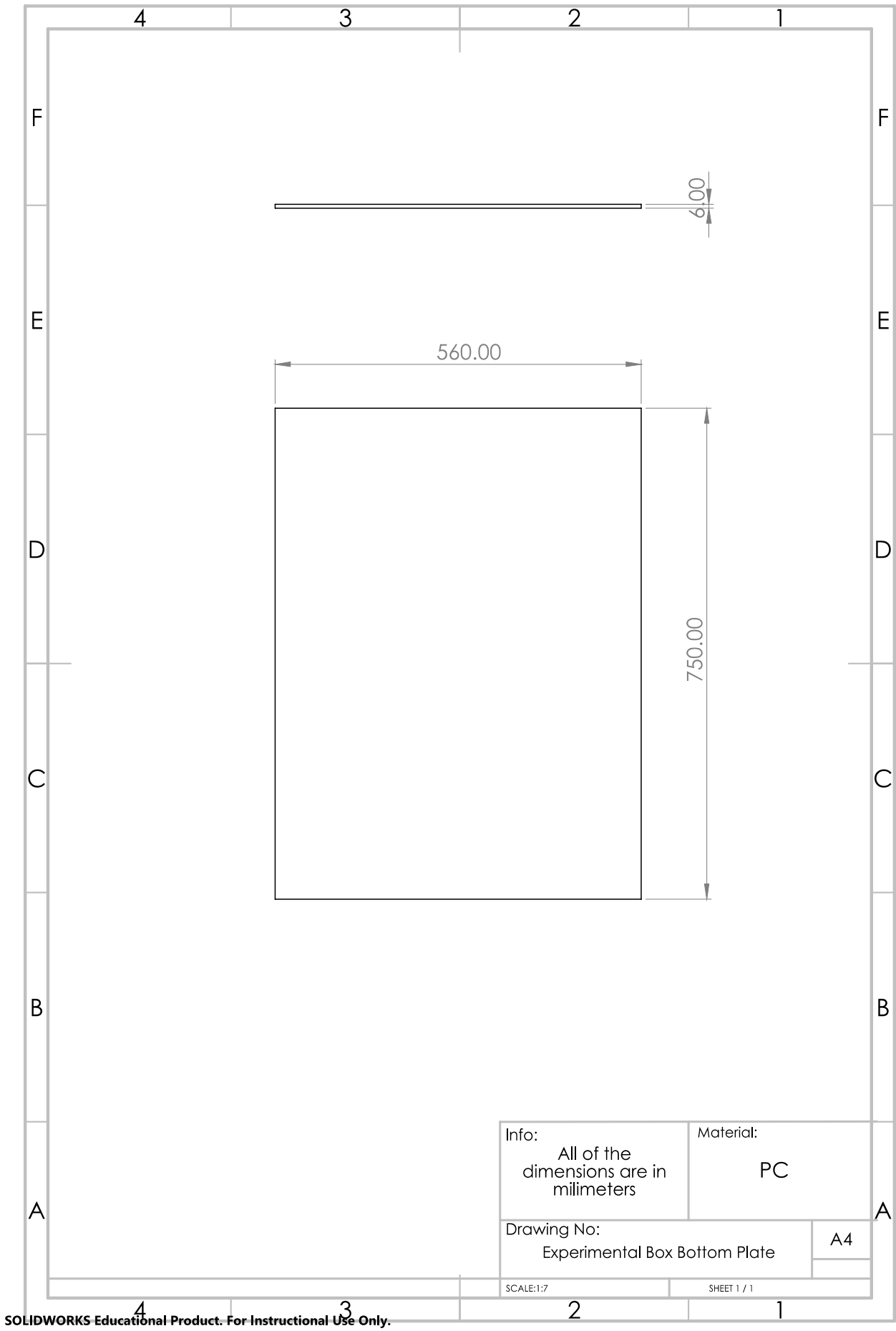


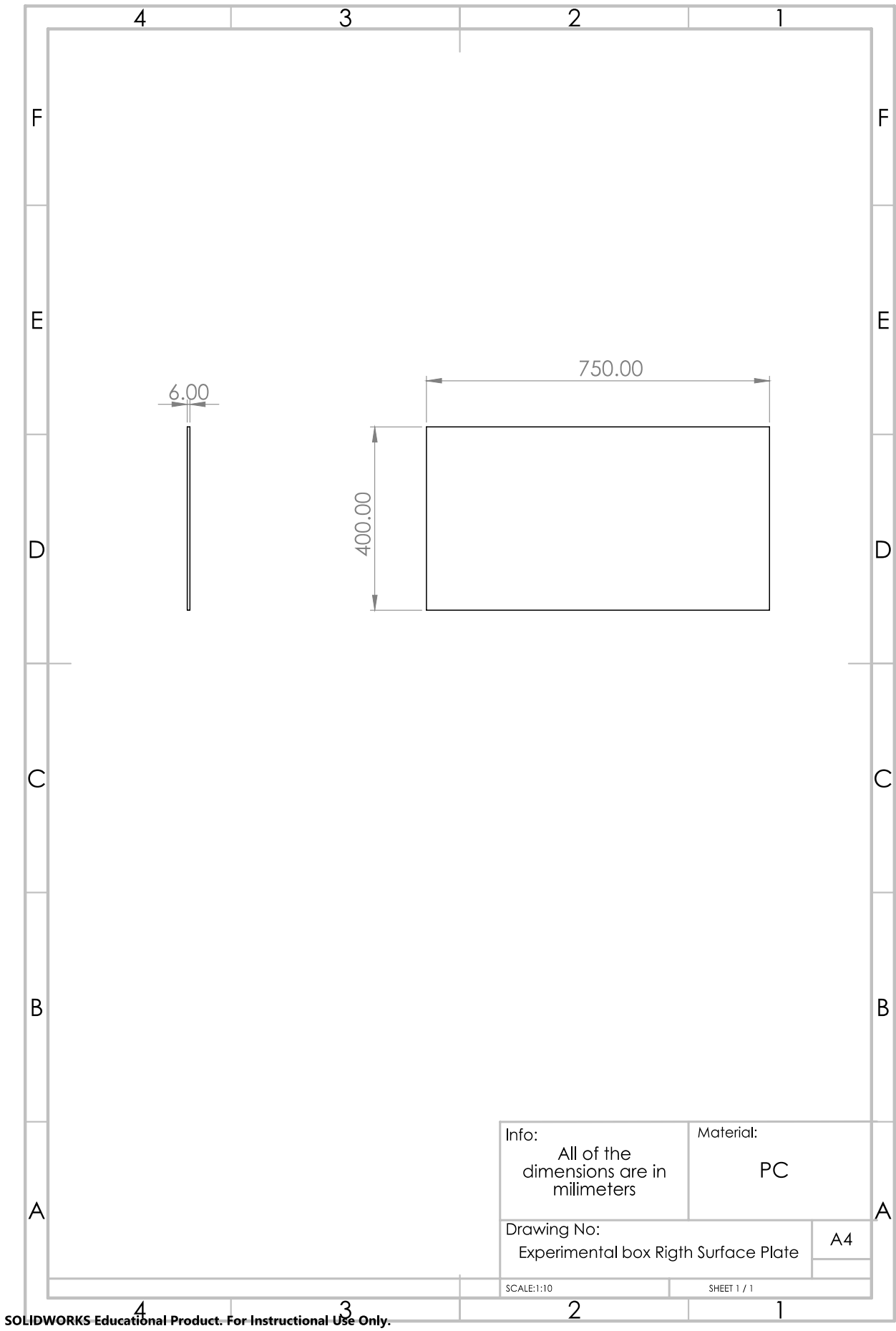


SOLIDWORKS Educational Product. For Instructional Use Only.

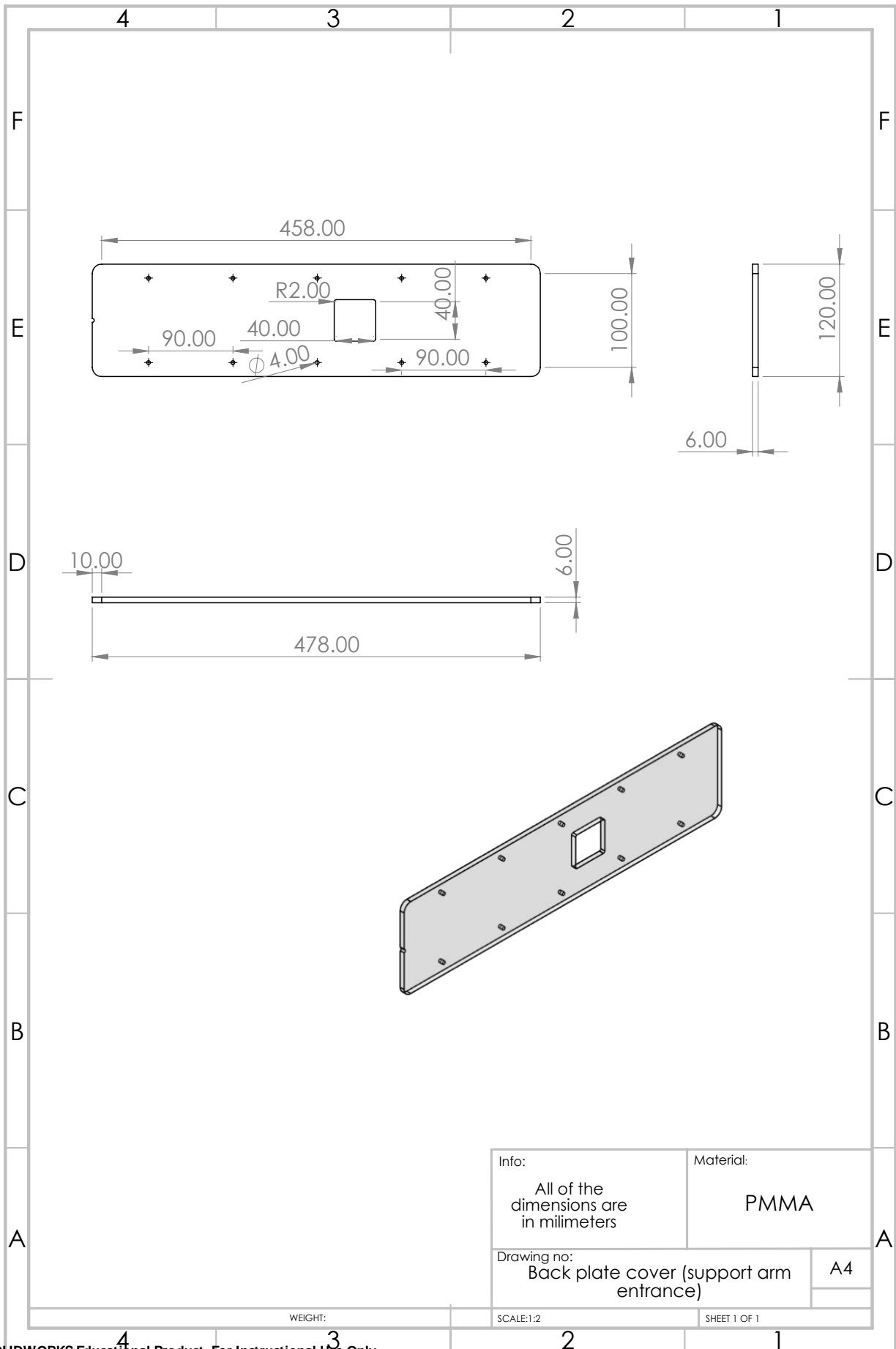


Info: All of the dimensions are in millimeters	Material: PC
Drawing no: Top plate (particle counter entrance)	A4
WEIGHT:	SCALE:1:2
	SHEET 1 OF 1

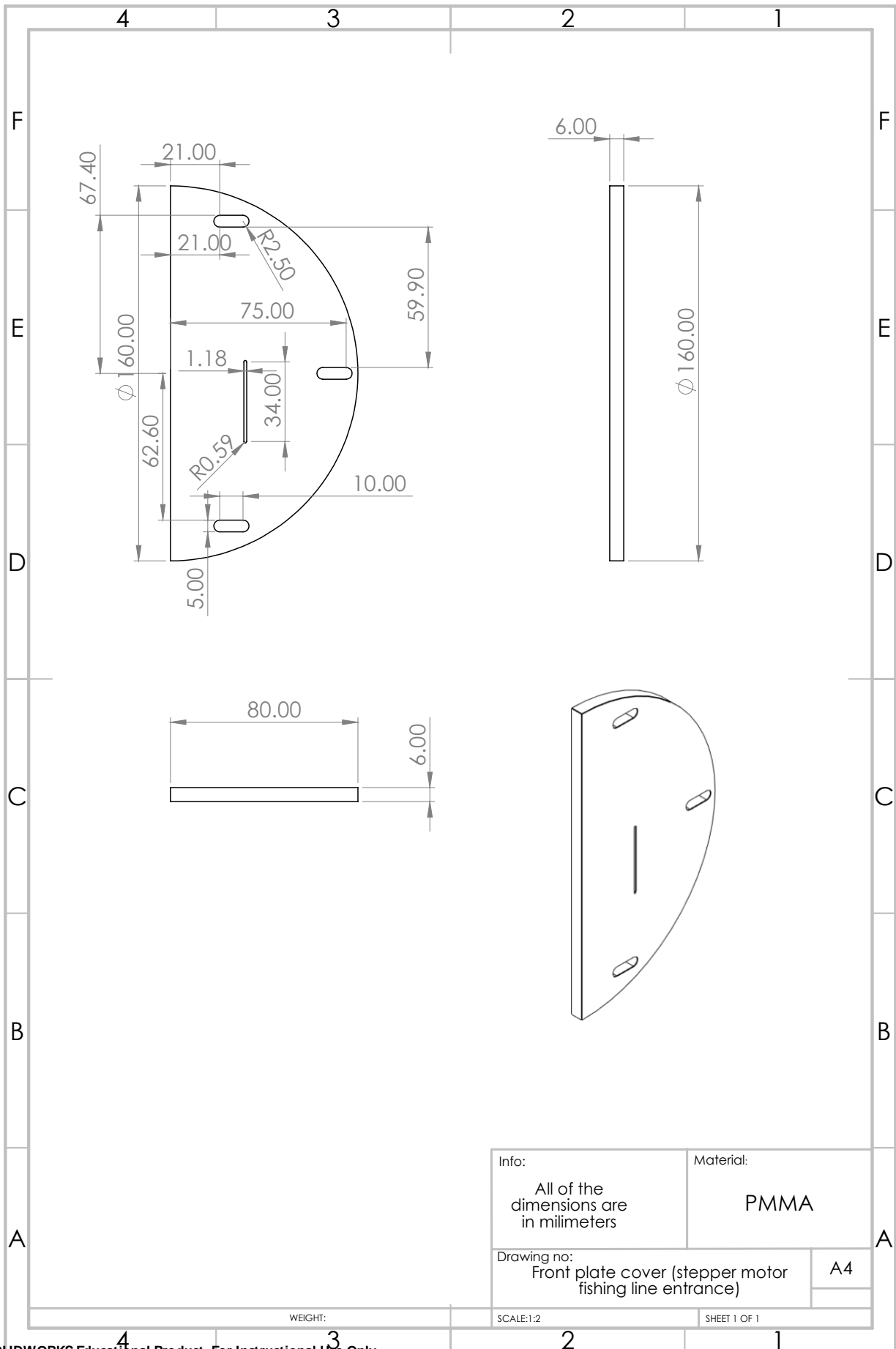




SOLIDWORKS Educational Product. For Instructional Use Only.

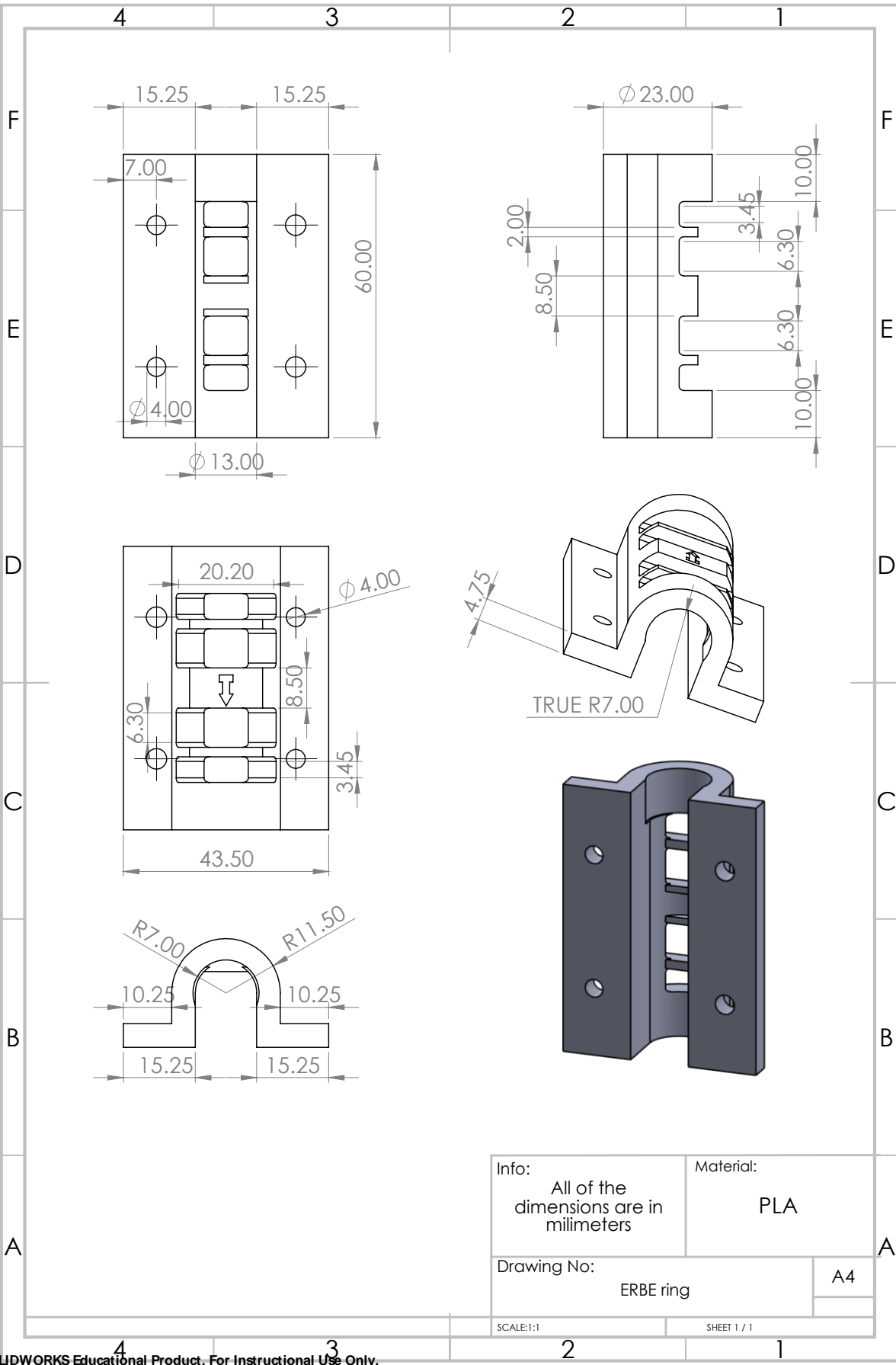


Info: All of the dimensions are in millimeters	Material: PMMA
Drawing no: Back plate cover (support arm entrance)	A4
WEIGHT:	SCALE:1:2
	SHEET 1 OF 1

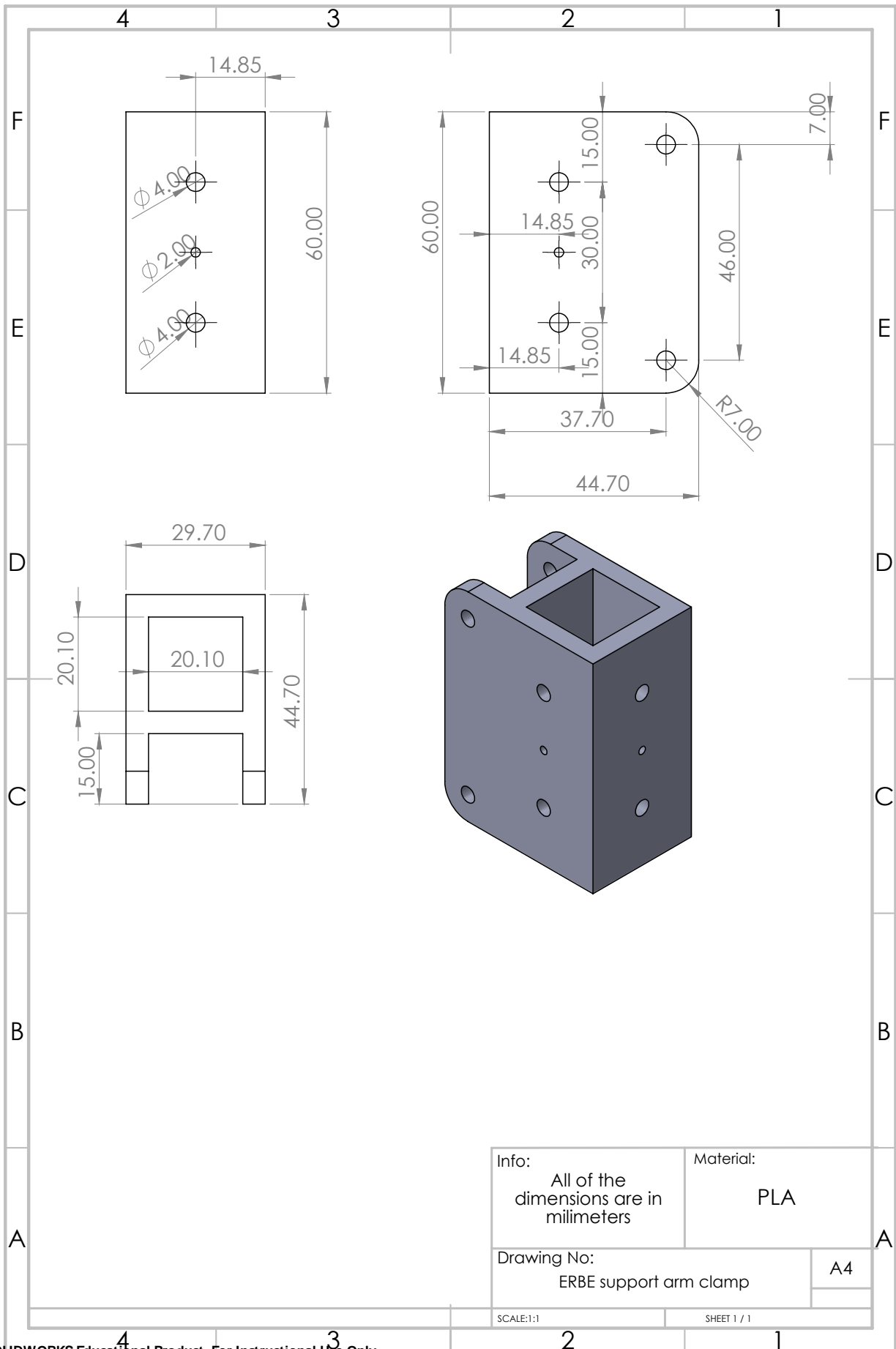


SOLIDWORKS Educational Product. For Instructional Use Only.

ERBE test setup drawings



Info: All of the dimensions are in millimeters	Material: PLA
Drawing No: ERBE ring	A4
SCALE:1:1	SHEET 1 / 1



Info:
All of the
dimensions are in
millimeters

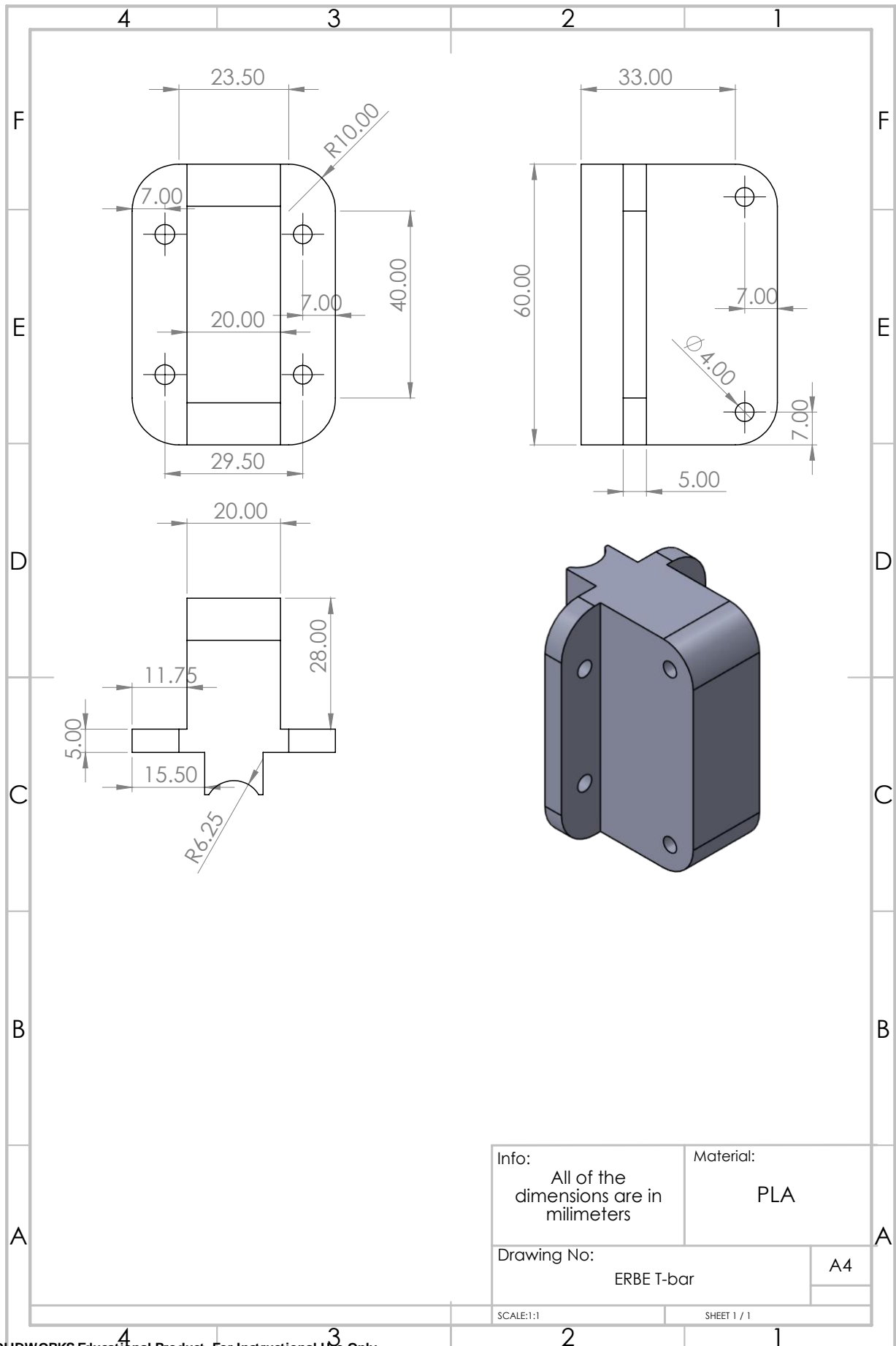
Material:
PLA

Drawing No:
ERBE support arm clamp

A4

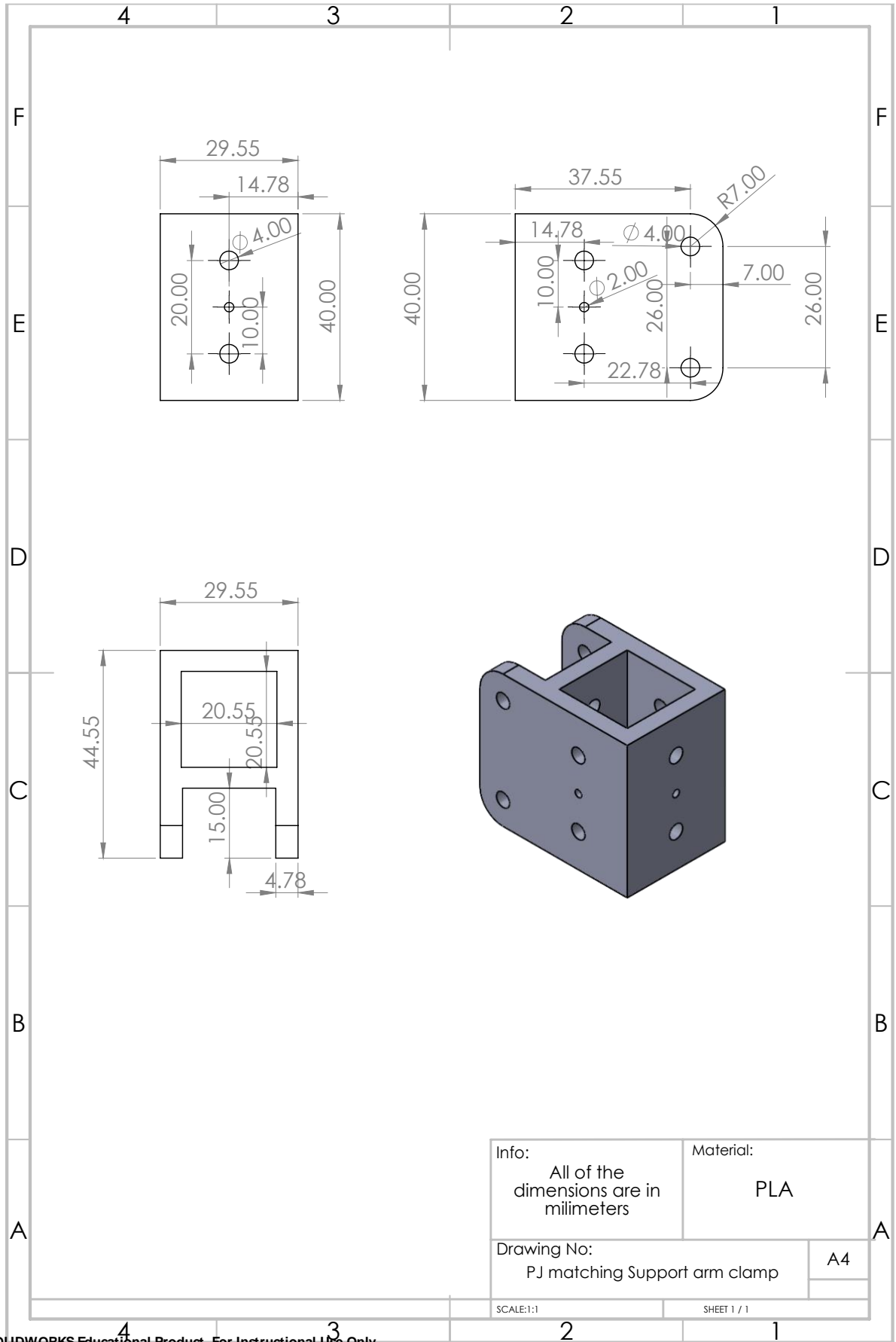
SCALE:1:1

SHEET 1 / 1

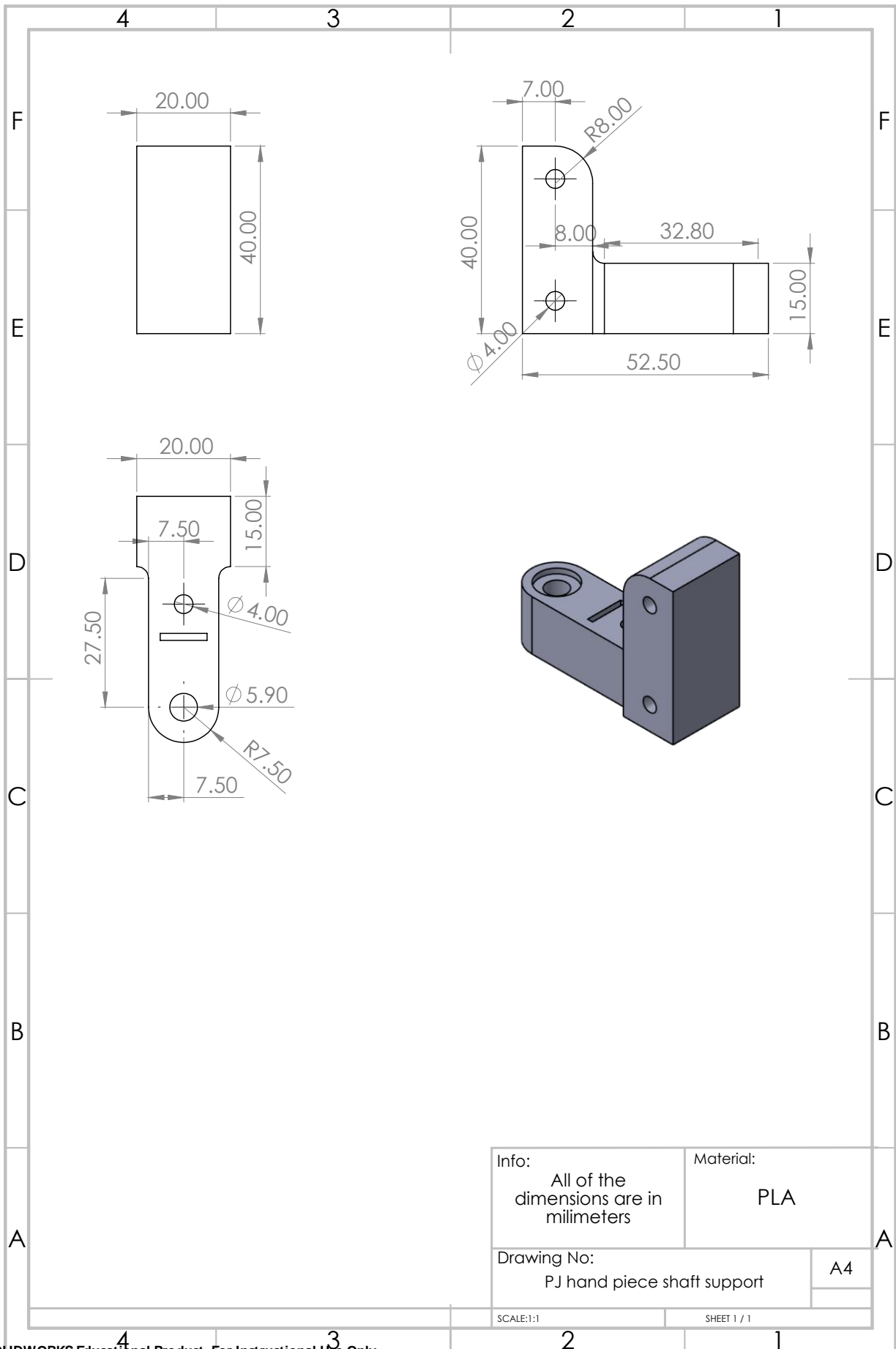


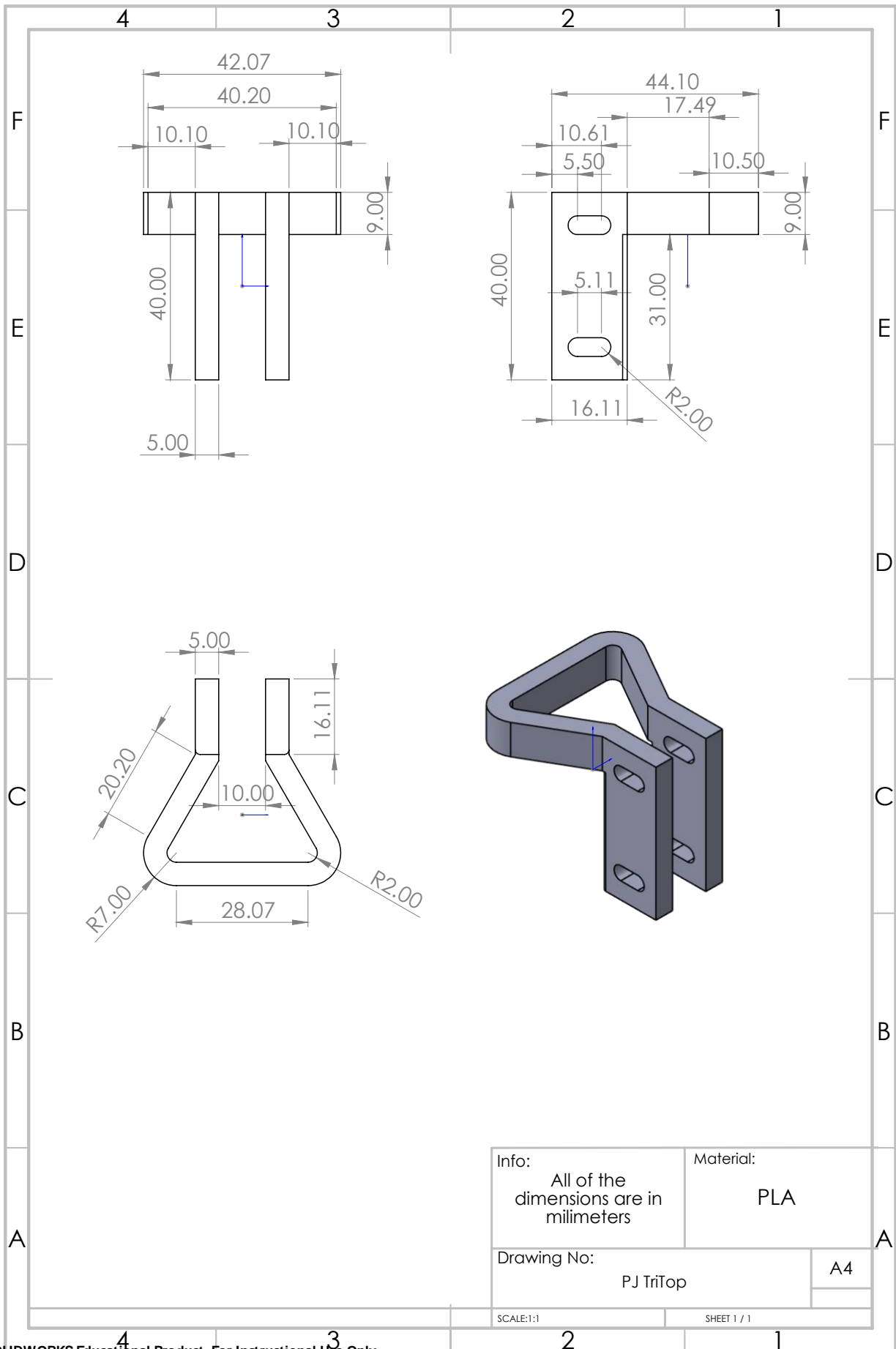
Info: All of the dimensions are in millimeters	Material: PLA
Drawing No: ERBE T-bar	A4
SCALE:1:1	SHEET 1 / 1

PJ test setup drawings

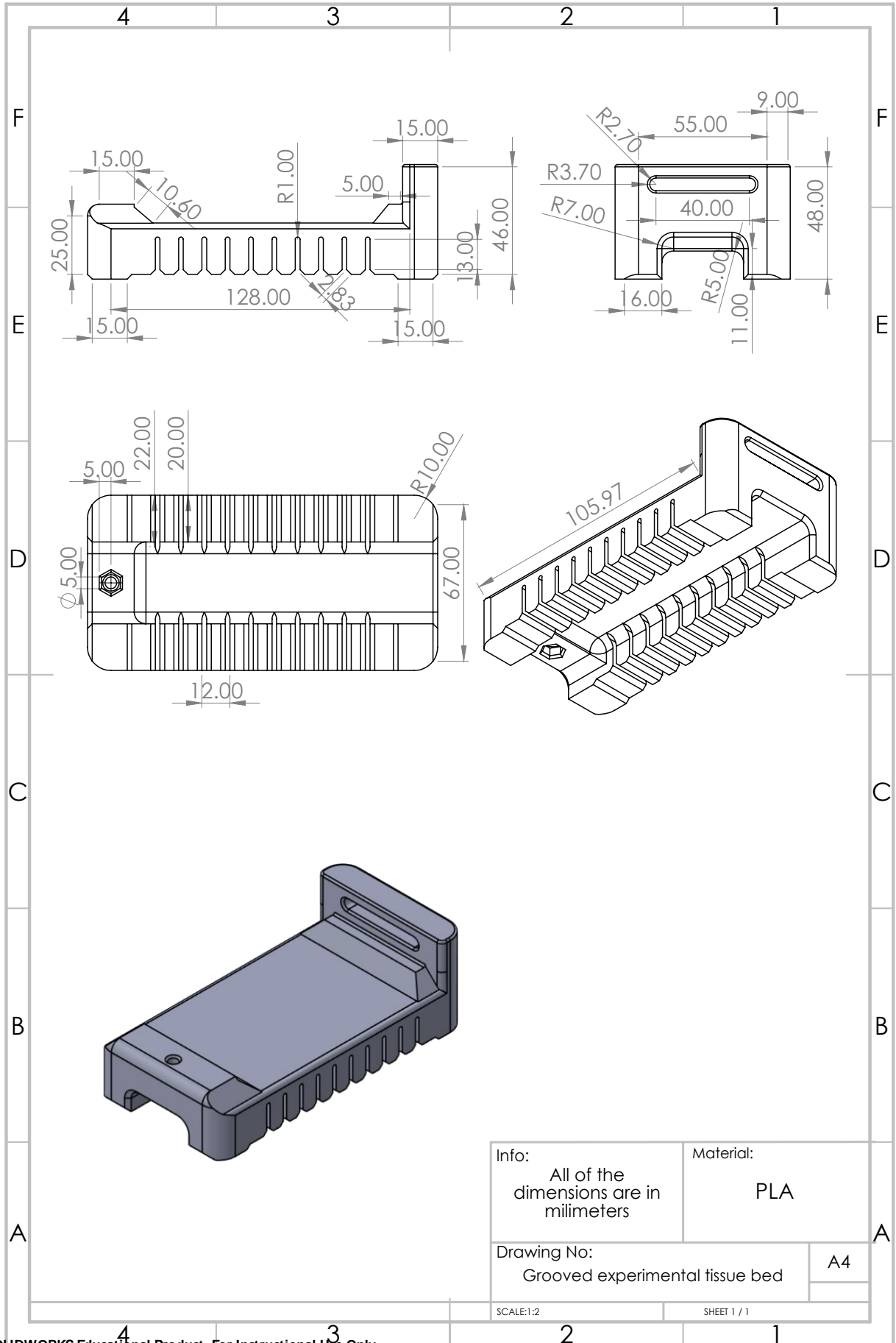


Info: All of the dimensions are in millimeters	Material: PLA
Drawing No: PJ matching Support arm clamp	A4
SCALE:1:1	SHEET 1 / 1

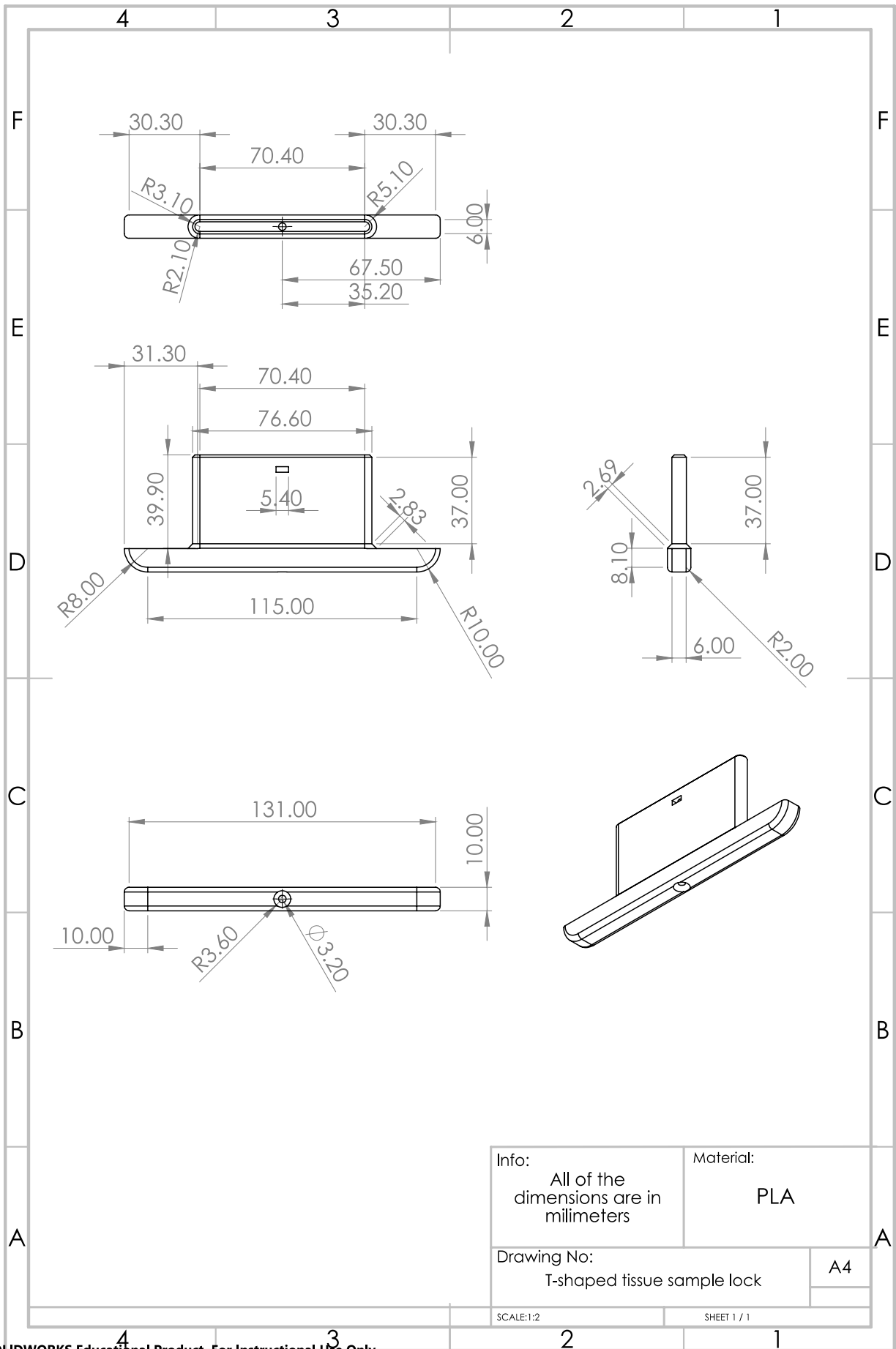




Tissue sample holder drawings



SOLIDWORKS Educational Product. For Instructional Use Only.



Info:
All of the
dimensions are in
millimeters

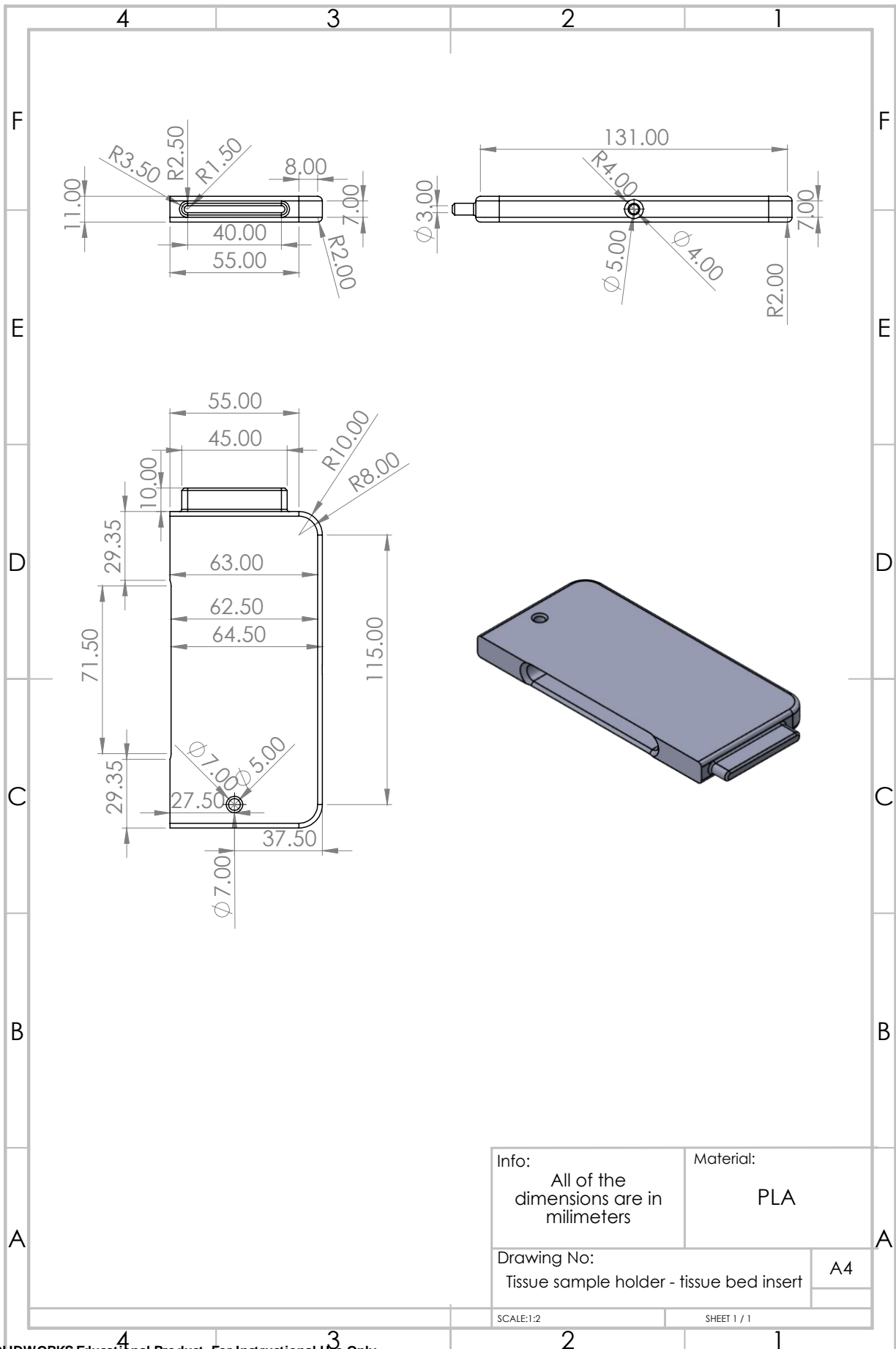
Material:
PLA

Drawing No:
T-shaped tissue sample lock

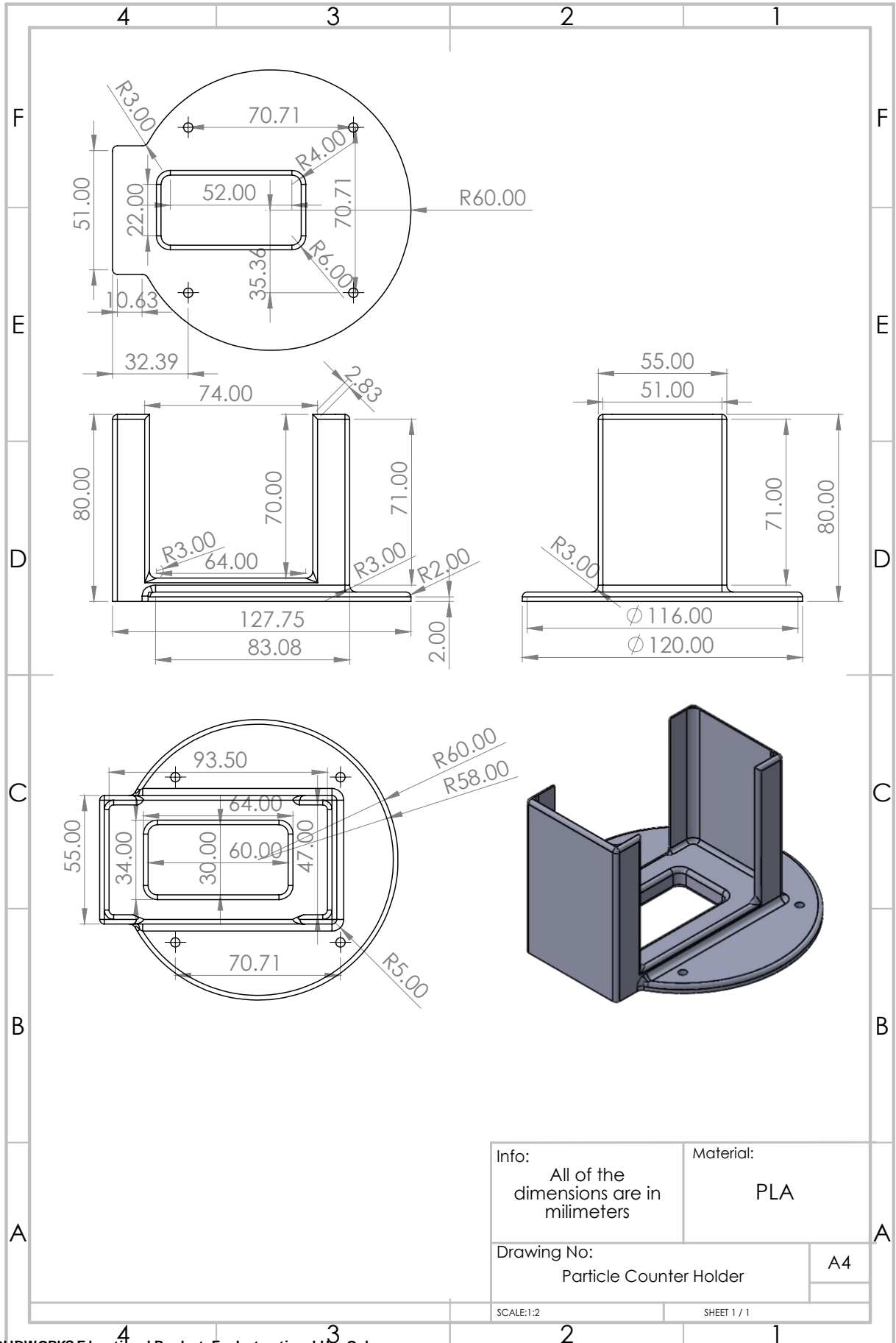
A4

SCALE:1:2

SHEET 1 / 1



Other part drawings



Info:
All of the dimensions are in millimeters

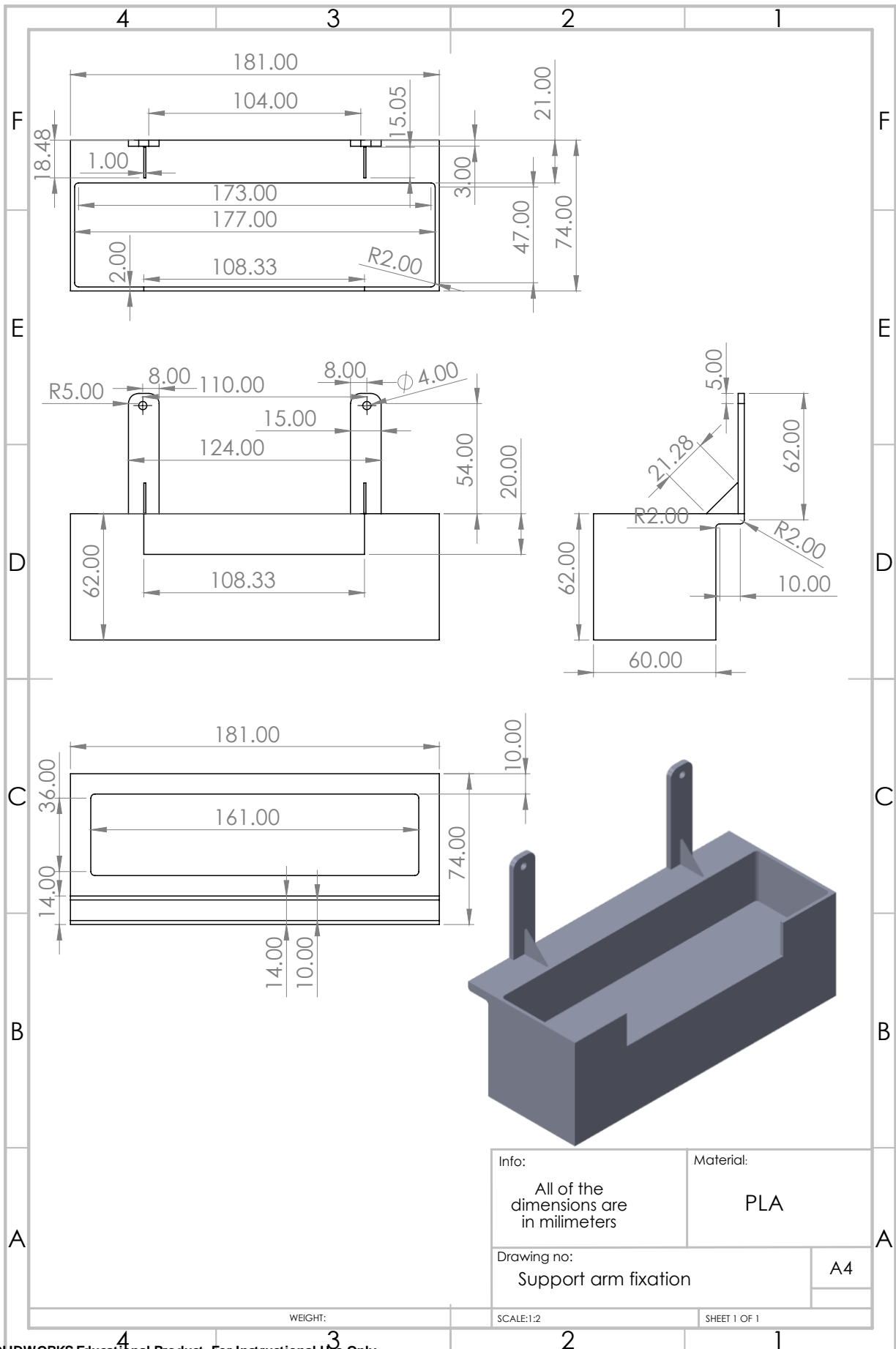
Material:
PLA

Drawing No:
Particle Counter Holder

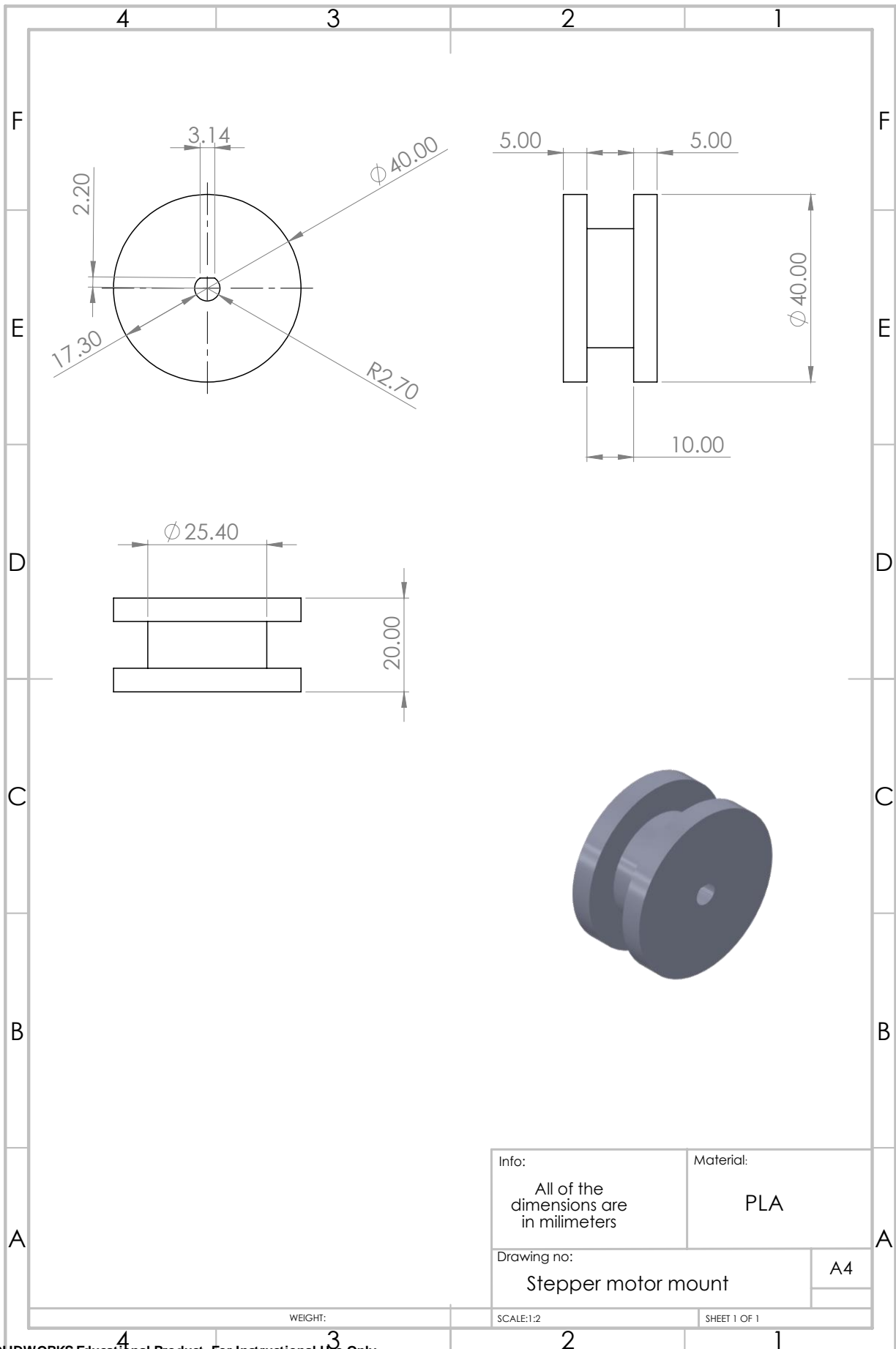
A4

SCALE:1:2

SHEET 1 / 1



SOLIDWORKS Educational Product. For Instructional Use Only.



Info:
All of the dimensions are in millimeters

Material:
PLA

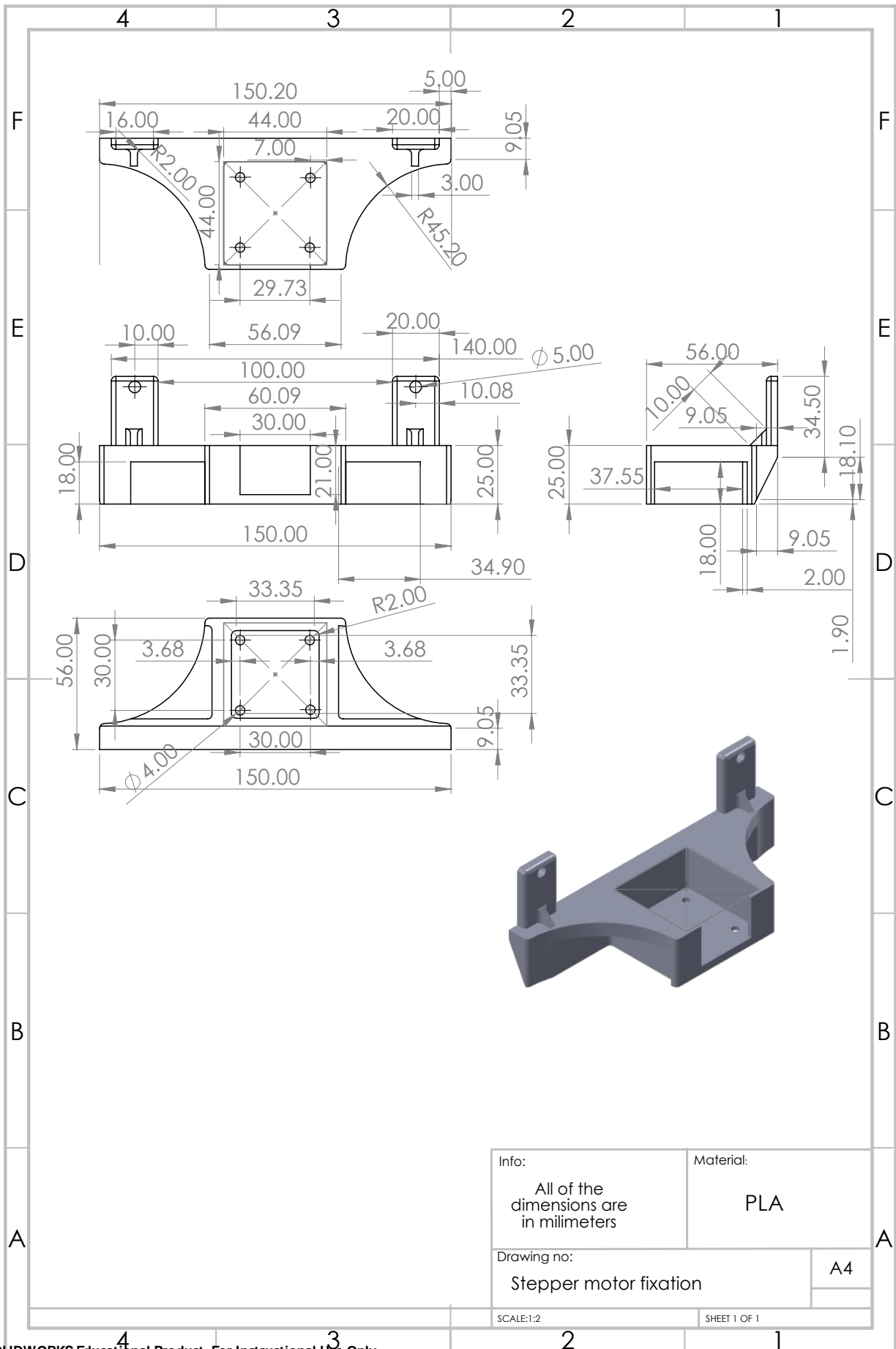
Drawing no:
Stepper motor mount

A4

WEIGHT:

SCALE:1:2

SHEET 1 OF 1



Info:
All of the dimensions are in millimeters

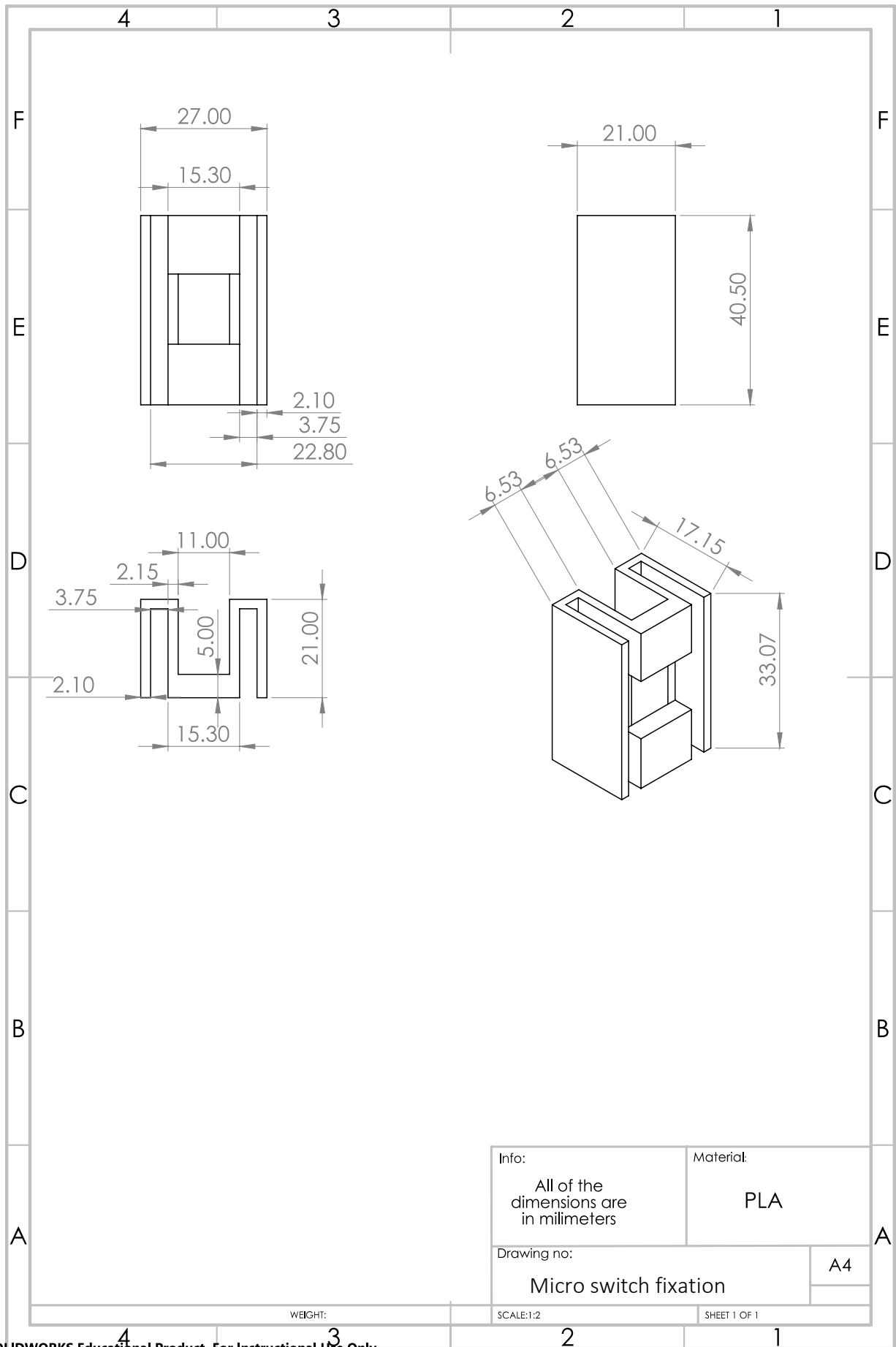
Material:
PLA

Drawing no:
Stepper motor fixation

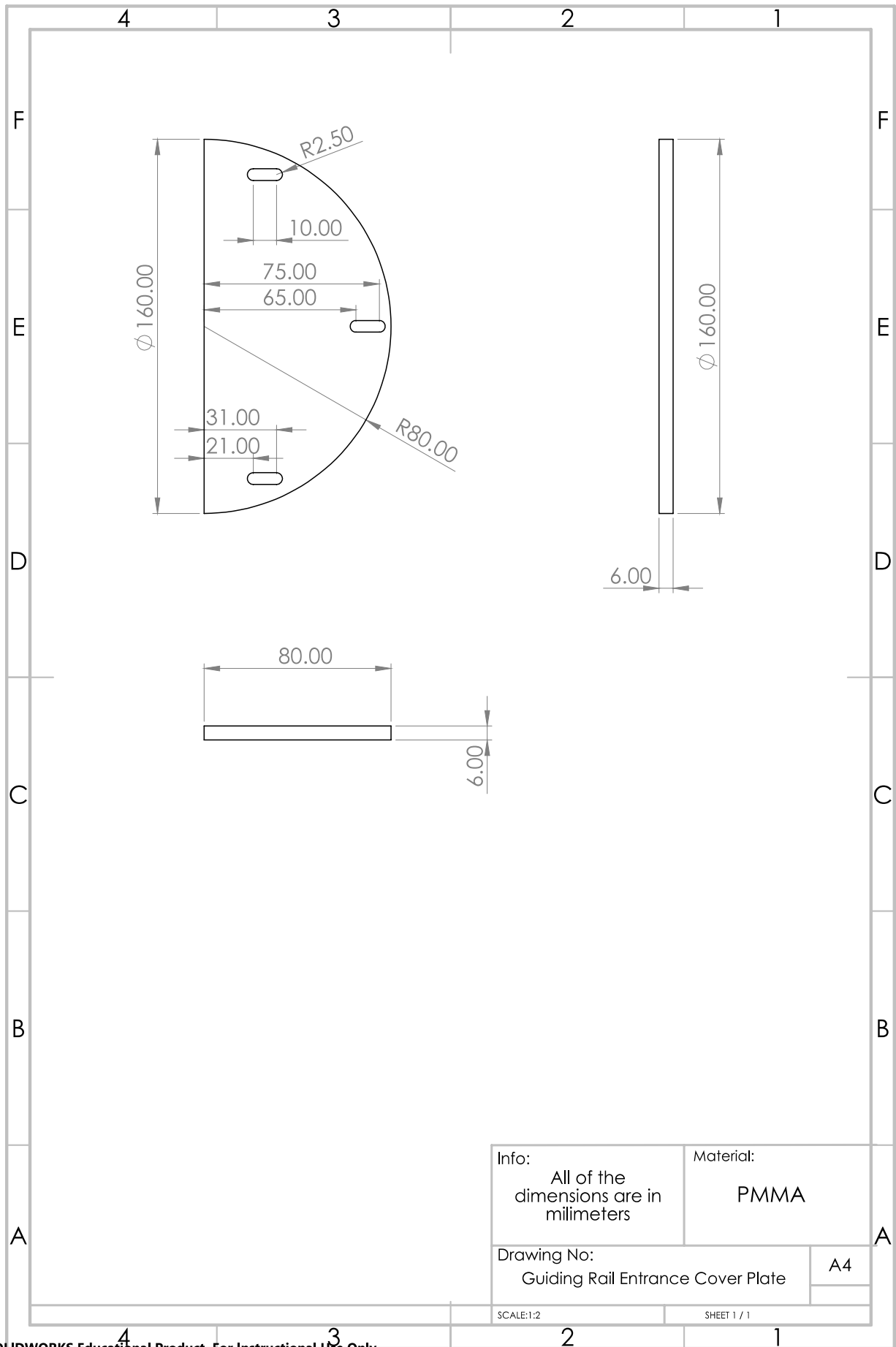
A4

SCALE:1:2

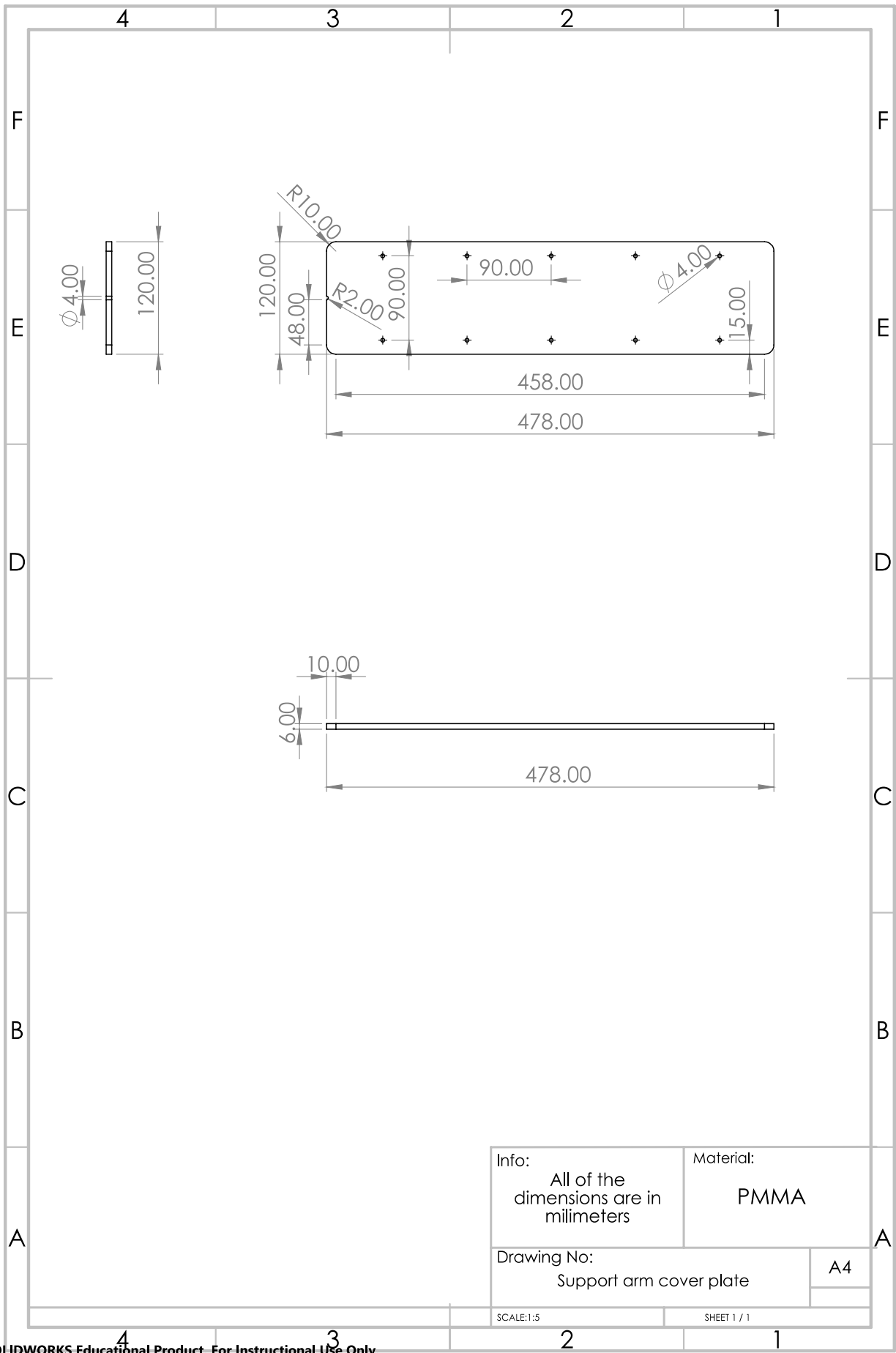
SHEET 1 OF 1



SOLIDWORKS Educational Product. For Instructional Use Only.



SOLIDWORKS Educational Product. For Instructional Use Only.



Info:
All of the
dimensions are in
millimeters

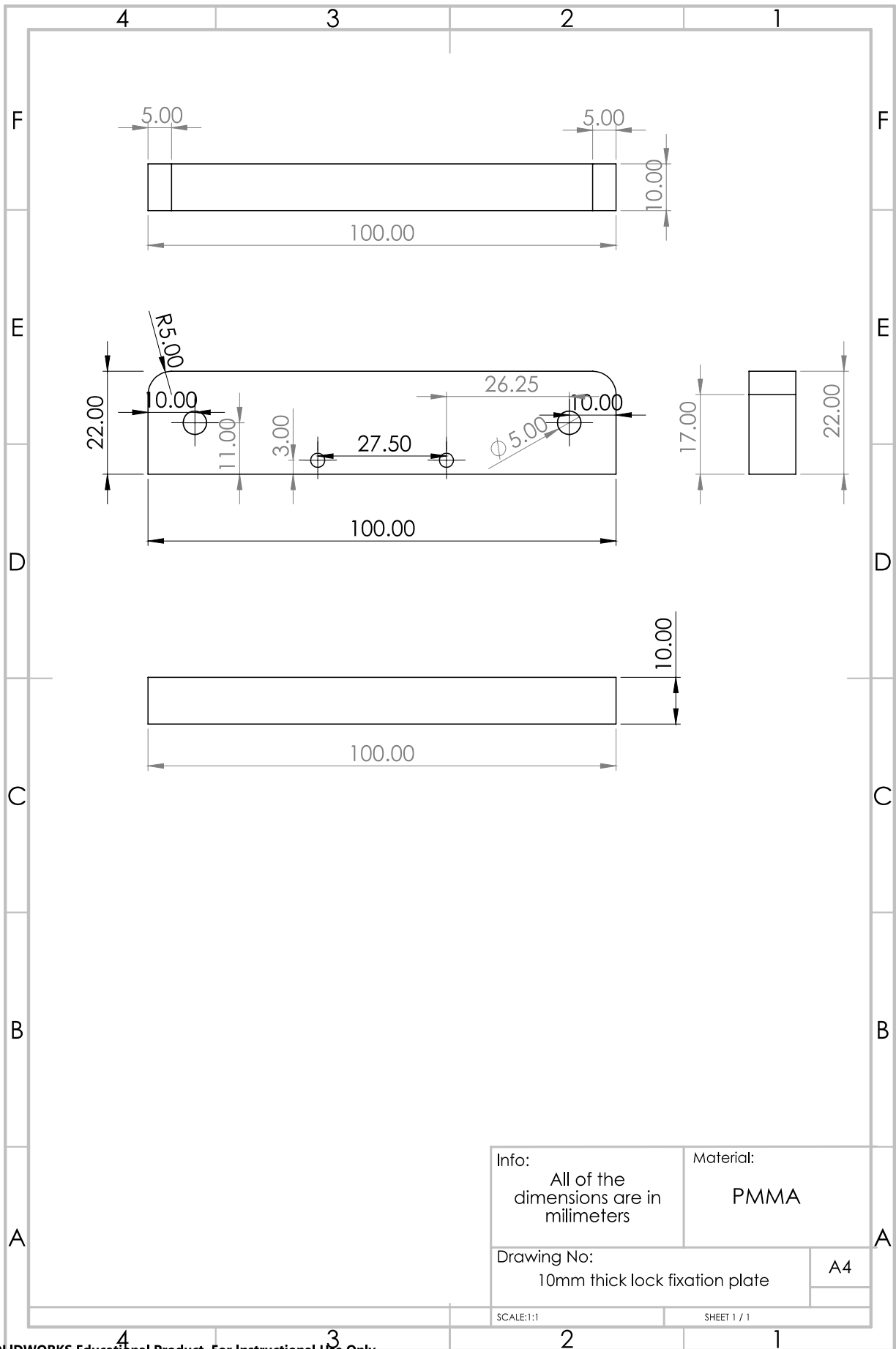
Material:
PMMA

Drawing No:
Support arm cover plate

A4

SCALE:1:5

SHEET 1 / 1



Info:
All of the
dimensions are in
millimeters

Material:
PMMA

Drawing No:
10mm thick lock fixation plate

A4

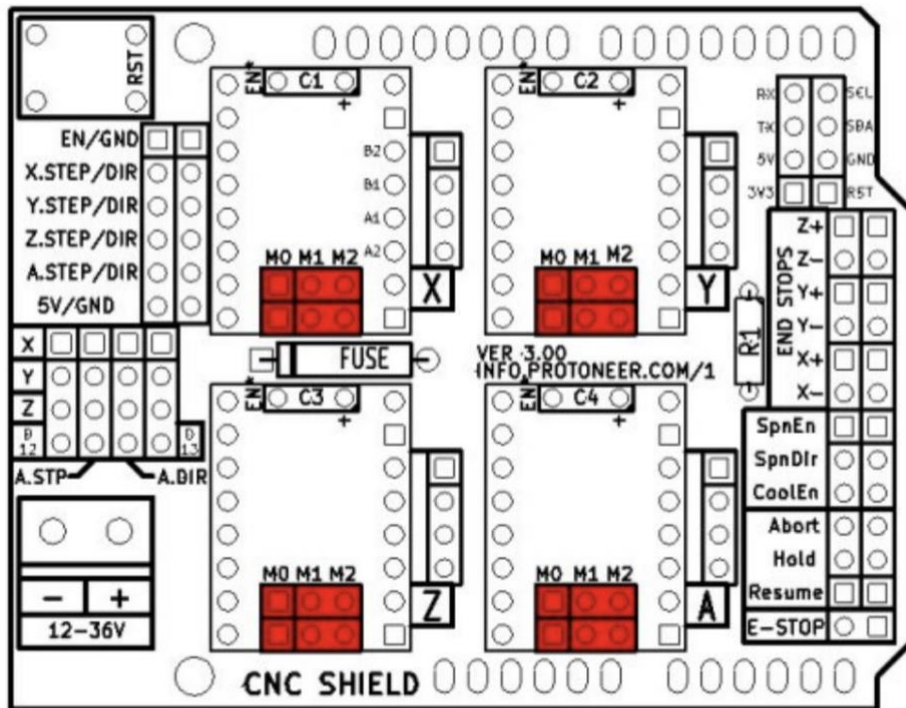
SCALE:1:1

SHEET 1 / 1

Appendix G – Arduino and Gcode settings

An automated pulling motion of the experimental tissue sample was generated with the use of a stepper motor with a stepper motor mount and an Arduino with a CNC shield. The stepper motors can be turned per step size for precise motion.

The required pulling motions were 0.25cm/s and 0.5cm/s for slow and fast cuts respectively. The step size was adjusted on the CNC shield by adding three jumpers for a “high high high” configuration as shown in Figure G.1. This configuration adjusted the stepper motor to 1/16th step (0.1125°) micro-step resolution for the most precise tuning.



A4988 Stepper Driver configuration:

MS0	MS1	MS2	Microstep Resolution
Low	Low	Low	Full step
High	Low	Low	Half step
Low	High	Low	Quarter step
High	High	Low	Eighth step
High	High	High	Sixteenth step

Figure G.1 – The stepper motor micro-step configurations of the Arduino with a CNC shield.

The radius of the stepper motor mount was measured as 1.26 cm and the perimeter was calculated as 7.91 cm. For a 5cm cut, the stepper motor was set to a total of 6.32 turns. Therefore, the step calibration was set to 125 steps per mm displacement as shown in Figure G.2.

The step size was set to 16.8mm for a 10-second run to achieve 0.5cm/s pulling motion. For a 0.25 cm/s cut, the step size was set to 62.5 steps per mm with a 33.6 mm step size. The stepper motor was connected to the X input

of the CNC shield, and the automation was controlled by pressing the X+ button on the UGS program to pull the tissue sample.

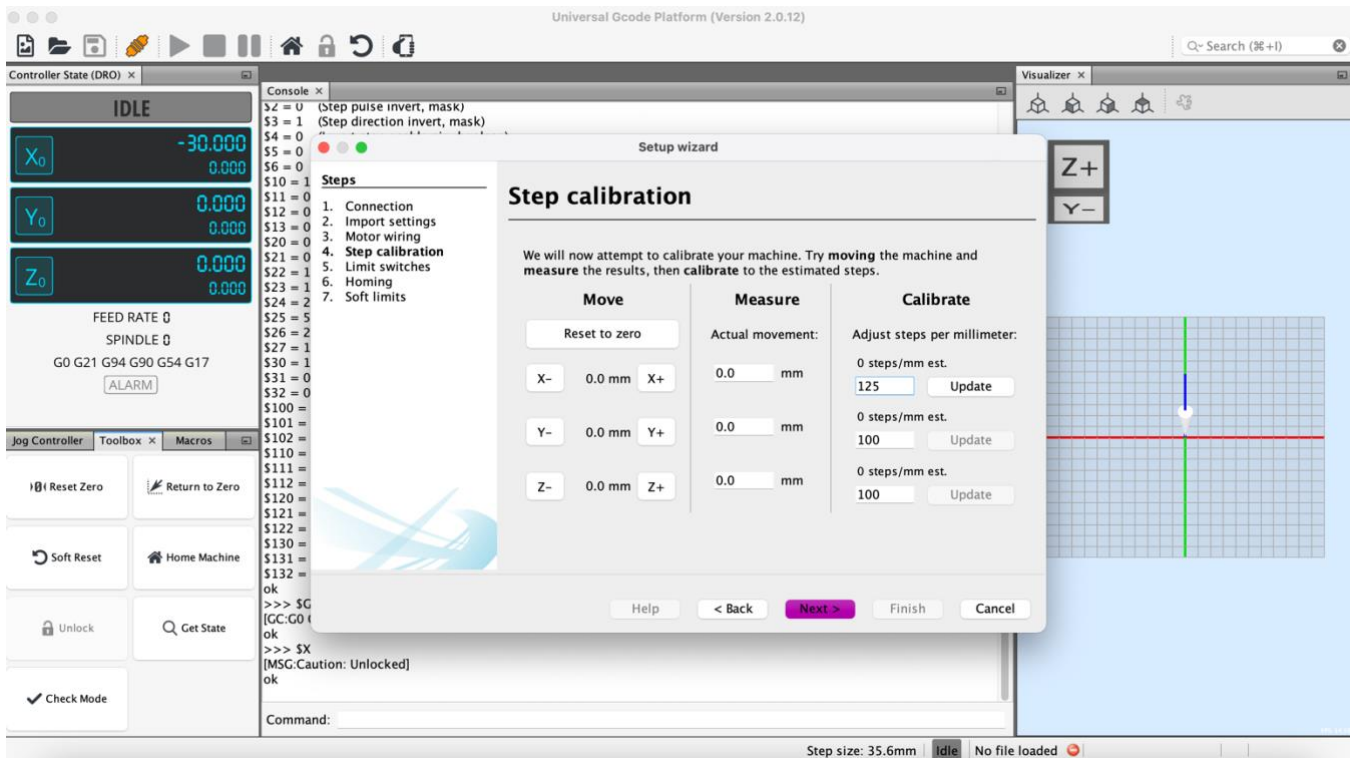


Figure G.2 – The Universal Gcode Platform (UGS) step calibration setup wizard to adjust steps/mm for a 5 cm pulling motion.

To make the machine move, a GRBL code was uploaded to Arduino IDE software. The Universal Gcode Sender (UGS) program was opened and connected to Arduino. Lastly, the Arduino with a CNC shield was connected to the stepper motor as shown in Figure G.3.

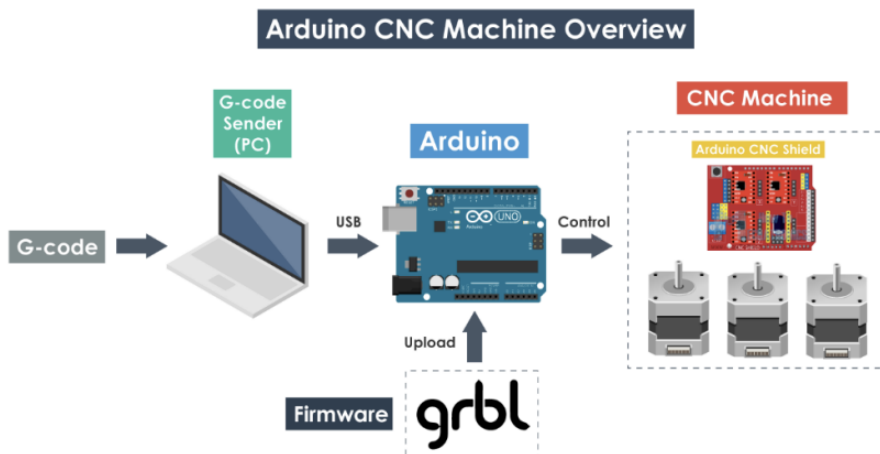


Figure G.3 – Arduino with a CNC shield overview to summarize the steps taken for the connection of the stepper motor.

Appendix H – Off-the-shelf parts

Table H.1 – Product information on off-the-shelf experimental setup parts and utilized devices. The pricing of the already available products was not included in the table.

Product	Brand	Material	Product number	Amount	Price €/Each
Particle counter 985	Fluke	-	095969620321	1	-
PlasmaJet V3+	Plasma surgical	-	PS10-2130-EN	1	-
ERBE icc50	ERBE GmbH elektromedizin	-	10122-041	1	-
Clamps 40x60 mm	RVS Paleis	Stainless Steel	814798240_60	5	2,99
Locks 46 mm	RVS Paleis	Stainless steel	8147922046	4	3,19
Poly-max sealant	Bison	Poly max	6312345	1	10.51
Arduino Uno	Roboter	-	CH340G	1	6.95
Arduino CNC shield	Botland	-	5904422359690	1	13.90
Stepper motor	Nanotec	-	ST4118D3004-A	1	-
Smoke Bomb	Carnavalsland	-	113488	2	2,95
4-6 mm D-Profile rubber sealant	Handson	EPDM	555385	2	4,69
Plant-based ham	Verdino	Pea	45312	8	2,99
				Total	98,27



AUER Packaging Netherlands | Beech Avenue 54-80 | 1119 PW Schiphol-Rijk

Factuuradres

TU Delft
3mE - BME
Leeghwaterstraat 15
2628 CA Delft
Nederland

contactadres

AUER Packaging
Netherlands
Beech Avenue 54-80
1119 PW Schiphol-Rijk

T.: 0800 0224 667
F.: 0800 0224 587

info@auer-packaging.nl
www.auer-packaging.nl

Art. nr	Artikel	Aantal	prijs per stuk	totaal netto
DE 86	Oplegdeksels voor euroboxen	1	€ 13,83	€ 13,83
EG 86/42 HG	Euroboxen gesloten	1	€ 40,65	€ 40,65
Katalog 1.2021-NL/BE		1	€ 0,00	€ 0,00
	Catalogus			












Datum van de uitgevoerde dienst: 20.09.2021
Vrijgesteld van belasting, want intracommunautaire levering.

totaal netto: € 54,48
verzending: € 15,00
totaal bruto: € 69,48

VE: 1 carton
Totaalgewicht: 10,1 kg
Codes (douanetarieven)
DE 86, EG 86/42 HG: 39231090

Aantal	Artikelcode	Artikel		Totaal
1	OM6010600011	Polycarbonaat plaat transparant 6,0 mm	op maat	€ 79.92
<p>Aantal: 2 Lengte: 750 mm Breedte: 400 mm Totaal oppervlak: 0.300000 m2 Stuksprijs: 39.96 Totaalprijs: 79.92</p> <p>Prijs inclusief BTW</p>				
1	OM6010600011	Polycarbonaat plaat transparant 6,0 mm	op maat	€ 59.67
<p>Aantal: 2 Lengte: 560 mm Breedte: 400 mm Totaal oppervlak: 0.224000 m2 Stuksprijs: 29.84 Totaalprijs: 59.67</p> <p>Prijs inclusief BTW</p>				
1	OM6010600011	Polycarbonaat plaat transparant 6,0 mm	op maat	€ 111.89
<p>Aantal: 2 Lengte: 560 mm Breedte: 750 mm Totaal oppervlak: 0.420000 m2 Stuksprijs: 55.94 Totaalprijs: 111.89</p> <p>Prijs inclusief BTW</p>				
			Subtotaal	€ 251.48
			Betalingskosten	€ 0.00
			Verzending	€ 0.00
			Totaal	€ 251.48

Your shopping cart contains 348 products

Product	Description	Unit price	Number of	Total
 A4 m5 / each - hexagon nut A4 article number: 934-4-5_1	€ 0.16	43	€	6.88
 A4 m5 / each - washer A4 item number: 125-4-5_1	€ 0.16	86	€	13.76
 A4 m5x25mm / each - countersunk screw A4 article number: 7991VO-4-5X25_1	€ 0.21	30	€	6.30
 A2 m5x20mm / each - pan head flange screw A2 article number: 9335-2-5 X20_1	€ 0.19	13	€	2.47
 A4 m4 / each - washer A4 item number: 125-4-4_1	€ 0.16	32	€	5.12
 A2 m4x20mm / each - pan head flange screw A2 article number: 9335-2-4 X20_1	€ 0.16	16	€	2.56
 A4 m4 / each - hexagon nut A4 article number: 934-4-4_1	€ 0.16	16	€	2.56
 A2  m3x35mm / each - spherical cylinder screw A2 article number: 7985-2-3 X35_1	€ 0.16	28	€	4.48
 A4 m3 / each - washer A4 item number: 125-4-3_1	€ 0.16	56	€	8.96
 A4 m3 / each - hexagon nut A4 article number: 934-4-3_1	€ 0.16	28	€	4.48

[empty basket](#)

Total products (excl. VAT):	€	57.57
Total (excluding VAT):	€	57.57
Total VAT:	€	12.09
Total (incl. VAT):	€	69.66